

Utilizing Natural Variation and *De Novo* Mutation to  
Understand *Cryptococcus* Evolution

by

Thomas John C Sauters

University Program in Genetics and Genomics  
Duke University

Date: \_\_\_\_\_

Approved:

\_\_\_\_\_  
Paul M. Magwene, Advisor

\_\_\_\_\_  
Andrew Alspaugh

\_\_\_\_\_  
Joseph Heitman

\_\_\_\_\_  
Dennis Ko

Dissertation submitted in partial fulfillment of the  
requirements for the degree of Doctor of Philosophy  
in the University Program in Genetics and Genomics  
in the Graduate School of  
Duke University

2022

ABSTRACT

Utilizing Natural Variation and *De Novo* Mutation to  
Understand *Cryptococcus* Evolution

by

Thomas John C Sauters

University Program in Genetics and Genomics  
Duke University

Date: \_\_\_\_\_

Approved:

\_\_\_\_\_  
Paul M. Magwene, Advisor

\_\_\_\_\_  
Andrew Alspaugh

\_\_\_\_\_  
Joseph Heitman

\_\_\_\_\_  
Dennis Ko

An abstract of a dissertation submitted in partial fulfillment of the  
requirements for the degree of Doctor of Philosophy  
in the University Program in Genetics and Genomics  
in the Graduate School of  
Duke University

2022

Copyright © 2022 by Thomas John C Sauters  
All rights reserved

# Abstract

The evolution of pathogenesis, in many cases, is a story of competition between host and microbe; however, many opportunistic pathogens are primarily found in niches other than the host environment. Such pathogens frequently lack host-to-host transmission, and there may be limited opportunities for an infectious population to be re-dispersed back into the environment. Observations such as these motivate the hypothesis that the evolution of virulence traits in opportunistic pathogens may be primarily driven by environmental selective pressures, rather than the host-environment *per se*.

For *Cryptococcus* the ability to survive interactions with macrophages and the ability to grow at host body temperatures are indispensable to its pathogenic capabilities. The work presented here aims to dissect the genetic underpinnings of these virulence traits using the abundant natural variation of *Cryptococcus* and using the accumulation *de novo* mutations associated with growth under relevant stressors.

An important aspect of the hypotheses surrounding *Cryptococcus* evolution is the predator-prey interactions it has with free-living amoeba. Amoebae are able to consume *Cryptococcus* cells in a manner similar to how macrophages phagocytose and digest infectious cells. This similarity is the basis of the “Amoeboid Predator-Fungal Animal Virulence Hypothesis” which posits that amoeba act as training grounds for environmental fungal pathogens and thus inadvertently select for resistance to immune phagocytes. I tested this hypothesis by using QTL mapping to identify genes and alleles that are involved in amoebae resistance in both *C. neoformans* and *C. de-neoformans*. I identified QTL that contribute to amoeba resistance, and discovered that the largest effect QTL in both species localize to homologous regions of the genome, suggesting a shared mechanism of amoeba resistance. In *C. neoformans*, this QTL also contributes to variation in melanization. I identified a causal vari-

ant for this QTL, a non-coding deletion upstream of a transcription factor, *BZP4*. Contrary to the predictions of the Amoeboid Predator-Fungal Animal Virulence Hypothesis, I did not find an association between the ability to survive amoeba predation and virulence in either *in vitro* or *in vivo* models of infection. These findings suggest a re-evaluation of the amoeba predation model for the evolution of pathogenesis, suggesting that factors other than amoeba may provide the significant selective pressures that underlie virulence ability.

I extended my quantitative analyses of *Cryptococcus* to two important factors involved in both environmental and disease contexts: thermal and low pH tolerance. In doing so, I discovered multiple pleiotropic QTL involved in general growth that also dictate stress tolerance in both high temperature and low pH environments. By fitting growth data to a Gompertz growth model and QTL mapping based on the parameters of this model, I discovered a novel QTL that effects lag, the time it takes for a population of cells to begin growing at an exponential rate. This lag QTL is pleiotropic across growth conditions. I identified a candidate allele for the lag QTL, a 9-bp deletion in *CNAG\_01111*, a gene that has been found to impact growth initiation in other species of fungi.

Finally, taking a complimentary approach to understanding the role of genes in environmental survival, I experimentally evolved a *C. neoformans* strain in conditions of thermal stress and fludioxonil stress. I discovered that strains evolved at high temperatures lose tolerance to fludioxonil and strains evolved in fludioxonil lose temperature tolerance. Furthermore, the loss of fludioxonil tolerance in the high temperature evolved strains can be partially rescued by growing them on media containing fludioxonil. This rescue results in a proportional loss of thermal tolerance. Studying the genomic changes behind the evolved phenotypes I discovered multiple large scale deletions and one multi-gene duplication associated with fludioxonil resistance and a single multi-gene deletion associated with thermal tolerance. There are also a variety

of small scale mutations associated with each evolved condition, including mutations of genes in the HOG and ergosterol pathway that are responsible for fludioxonil resistance. Mutations in uncharacterized multidrug transporters are frequently associated with fludioxonil resistance, suggesting that the evolved strains might also have altered resistance to other antifungals. These findings highlight the polygenic and pleiotropic genetic architecture of adaptation in *C. neoformans* on an ever warming planet with increased use of agricultural antifungals. The trade-offs found may represent a good sign for the use of phenylpyrroles as an agricultural antifungal.

Collectively, my work sheds light on genes and alleles involved in environmental survival while also making important connections back to human disease. It also exhibits the importance of utilizing the natural variation of fungal pathogens to study the evolutionary hypothesis surrounding virulence traits. The studies reported here also provide significant groundwork for many new insights into virulence genes and the origins of *Cryptococcus* pathogenicity.

# Contents

<b>Abstract</b>	<b>iv</b>
<b>List of Tables</b>	<b>x</b>
<b>List of Figures</b>	<b>xi</b>
<b>Acknowledgements</b>	<b>xiii</b>
<b>1 Introduction</b>	<b>1</b>
1.1 Background . . . . .	1
1.1.1 The Origins and Importance of Intraspecific Variation in Environmental Pathogens . . . . .	1
1.1.2 How Phenotypic Variation Contributes to the Evolution of Pathogenesis . . . . .	2
1.1.3 Utilizing Variation to Discover Genotype-Phenotype Connections	3
1.1.4 Generating Variation to Discover Genotype-Phenotype Connections . . . . .	5
1.1.5 Hypotheses Surrounding the Evolution of <i>Cryptococcus</i> Pathogenicity . . . . .	5
1.2 Thesis Outline . . . . .	6
<b>2 An Amoeba Resistance QTL Conserved Across Two Species of <i>Cryptococcus</i> Reveals Novel Insights Into Accidental Pathogenesis</b>	<b>9</b>
2.1 Author Contributions . . . . .	9
2.2 Introduction . . . . .	9
2.3 Results . . . . .	12
2.3.1 Comparison of Amoeba Resistance in Diverse <i>C. neoformans</i> Strains . . . . .	12
2.3.2 Mapping Populations and Genome Sequencing . . . . .	13

2.3.3	Cross Species Amoeba Resistance QTL . . . . .	15
2.3.4	Identification of an Amoeba Resistance Gene . . . . .	18
2.3.5	BZP4 is a pleiotropic QTG for Amoeba Resistance and Melanization . . . . .	19
2.3.6	Gene Expression Differences Associated with <i>BZP4</i> Allelic Variation . . . . .	23
2.3.7	Epistatic QTLs for Amoeba Resistance and Melanization . . .	25
2.3.8	Comparing Amoeba Resistance and Virulence . . . . .	26
2.4	Discussion . . . . .	30
2.5	Materials and methods . . . . .	34
<b>3</b>	<b>Pleiotropy between High Temperature, Low pH, and Antifungal Growth</b>	<b>42</b>
3.1	Author contributions . . . . .	42
3.2	Introduction . . . . .	42
3.3	Results . . . . .	46
3.3.1	Intraspecific Variation in High Temperature and Low pH Growth	46
3.3.2	Pleiotropic QTLs for General, High Temperature, and Low pH Growth . . . . .	47
3.3.3	High Temperature and Low pH Specific QTLs . . . . .	51
3.3.4	QTL Mapping Gompertz Growth Model Parameters Reveals Further Pleiotropy . . . . .	53
3.3.5	The Chromosome 5 Growth QTL is Pleiotropic in YNB Media	60
3.4	Discussion . . . . .	62
3.5	Materials and methods . . . . .	66
<b>4</b>	<b><i>De Novo</i> Mutations Result in Growth Trade-off Between Heat and Fludioxonil Evolved in <i>Cryptococcus neoformans</i></b>	<b>68</b>

4.1	Author Contributions . . . . .	68
4.2	Introduction . . . . .	68
4.3	Results . . . . .	71
4.3.1	Establishing Evolution Parameters . . . . .	71
4.3.2	An Inverse Relationship Between Evolved Fludioxonil and Temperature Tolerance . . . . .	72
4.3.3	Lines Evolved at 39°C Lose Thermal Tolerance During Extended Fludioxonil Challenge . . . . .	74
4.3.4	Variants Associated with Evolved Thermal and Fludioxonil Tolerance . . . . .	76
4.3.5	Multi-gene Deletions in High Temperature and Fludioxonil Evolved Strains Impact Virulence and Drug Tolerance Associated Genes . . . . .	77
4.3.6	A Multi-gene Duplication in A Revertant Strain Impacts Multiple Pleiotropic Stress Response Pathways . . . . .	82
4.4	Discussion . . . . .	83
4.5	Materials and methods . . . . .	89
<b>5</b>	<b>Conclusions</b>	<b>92</b>
5.1	Conclusions . . . . .	92
	<b>Appendix</b>	<b>99</b>
	<b>Bibliography</b>	<b>147</b>
	<b>Biography</b>	<b>163</b>

# List of Tables

2.1	Isolates Used to Study Amoeba Resistance . . . . .	13
3.1	Genes Under the Shared pH 4, 30°C growth QTL . . . . .	51
3.2	Genes Under the pH 4 Growth QTL . . . . .	56
3.3	Genes Under the 37°C Growth QTL . . . . .	57
3.4	Genes Under the Chromosome 5 QTL . . . . .	58
4.1	Experimental Evolution Variant Genes . . . . .	79
4.2	Duplicated Genes . . . . .	83
S1	Genes Under the Chromosome 8 QTL . . . . .	100
S2	Genes Under the Chromosome 7 QTL . . . . .	101
S3	General Growth QTL Genes . . . . .	112
S4	Strain Names for Evolved Lines . . . . .	129
S5	Variant Information for Evolved Lines . . . . .	130

# List of Figures

2.1	Intraspecific variation of amoeba resistance in <i>C. neoformans</i> . . . . .	14
2.2	Amoeba Resistance in <i>C. neoformans</i> and <i>C. deneoformans</i> F <sub>1</sub> Progeny	16
2.3	Amoeba Resistance QTL in <i>C. neoformans</i> and <i>C. deneoformans</i> F <sub>1</sub> Progeny . . . . .	17
2.4	Testing the Connection Between <i>BZP4</i> and Amoeba Resistance . . . . .	20
2.5	The Amoeba Resistance QTL is Pleiotropic for Melanization . . . . .	22
2.6	Differential Expression Between Genes Under the Chromosome 8 QTL	24
2.7	Segregants Tested in Macrophages and Mice . . . . .	27
3.1	<i>C. neoformans</i> Intraspecific Variation for High Temperature and Low pH . . . . .	47
3.2	Bt22 × Ftc555-1 Mapping Population Growth at High Temperature and Low pH . . . . .	48
3.3	Bt22 × Ftc555-1 High Temperature and Low pH Manhattan Plot . . . . .	50
3.4	<i>EIF3k</i> Alignment . . . . .	52
3.5	Gompertz Growth Model Parameter Info-graphic . . . . .	55
3.6	Gompertz Growth Parameter QTLs for High Temperature and Low pH	59
3.7	QTL Mapping YNB Growth . . . . .	61
4.1	High Temperature and Fludioxonil Growth . . . . .	72
4.2	Experimental Evolution Description . . . . .	73
4.3	Post Evolution Phenotyping . . . . .	74
4.4	Revertant Phenotyping . . . . .	75

4.5	Experimental Evolution Variants by Chromosome . . . . .	78
4.6	Deletion on Chromosome 12 . . . . .	80
4.7	Deletion on Chromosome 11 . . . . .	81
4.8	Deletion on Chromosome 14 . . . . .	81
4.9	Duplication on Chromosome 3 in Revertant Background . . . . .	82
S1	Phagocytic Index of Bt22xFtc555-1 Segregants . . . . .	106
S2	Epistatic QTLs for Amoeba Resistance and Melanization . . . . .	107
S3	<i>C. neoformans</i> Strains on L-DOPA . . . . .	108
S4	Segregants Tested in Macrophages and Mice . . . . .	109
S5	<i>C. neoformans</i> Strains on L-DOPA . . . . .	110
S6	Correlations between growth conditions of <i>C. neoformans</i> strains . . .	111

## Acknowledgements

I would like to begin by thanking the members of my committee – Dr. Dennis Ko, Dr. Andrew Alspaugh, and Dr. Joseph Heitman. They were a valuable source of mentorship and encouragement throughout the completion of my graduate studies.

Thank you to the members of the Magwene lab, that I have had the pleasure to work with. Dr. Paul Magwene provided the environment for me to find and grow a passion for microbial evolution. My scientific journey has been forever shaped by his mentorship. Dr. Debra Murray was my rock. Without her to talk to, and receive insight from, my time at Duke would have included less interesting scientific ideas and much more frustration, both inside and outside of the lab. Dr. Cullen Roth played an instrumental role in my understanding of statistical methods and my computational abilities. He has also been a great friend to me over the years.

Thank you to members of the Heitman lab. Dr. Heitman was a consistent source of information and always expressed interest in getting me to my next steps. Dr. Sheng Sun and Anna Floyd-Averette were both instrumental in the work presented here. The members of the Heitman lab also contributed to my enjoyment of conferences and for that, I thank them.

Thank you to members of the Alspaugh lab. Dr. Alspaugh listened to many of my concerns about data reliability and experimental design expressing confidence in my abilities when I was in doubt. Dr. Calla Telzrow was a wealth of information for multiple projects and ideas that I undertook. Talking with her was always a pleasure, and her insights made my scientific life much easier. Dr. Corinna Probst has also been a wonderful colleague to reach out to for ideas and knowledge outside of my field.

To my collaborators in Dr. Robin May's lab, I thank you for your contributions

to this work and for being so willing to discuss ideas unrelated to the collaboration. Our interactions were few, yet enriching.

I would also like to thank my former mentors Dr. Maggie Werner-Washburne and Dr. Irene Salinas. They provided mentorship and the opportunity to become a scientist before I even knew I wanted to be one. Dr. Salinas, instrumentally shaped my thinking as a scientist, preparing me for my graduate studies.

A special thank you goes out to my friends that helped me through the trials and tribulations of life during my graduate studies: Dr. Jeffery Bourgeois, Dr. Rachel Newcomb, Dr. Arielle Fogel, Dr. Korie Busch, Dr. Steven Siecinski, Dr. Katherine Korunes, Dr. George Green, Dr. Lotus Lofgren, Dr. Kieran Samuk, Dr. Marvice Markus, Joshua Sanchez, Joella Sanchez, Wesley Mebust, Mariah Salcedo, and Arpit Bajpai. I could write a second thesis on how each of them has individually enriched my life and enabled me to accomplish my goals.

I would like to finish by thanking my family. The support I have received from my entire family has been a blessing during the course of my graduate work and life. To my father, Brad Sauters, I owe much of my scientific drive and commitment to integrity. He fostered a curiosity for the environment around me from a young age. To my mother Katherine Chavez, I owe my commitment to accomplish the goals set out in front of me. She showed me the strength that it takes to work through adversity to accomplish what I set out to do. To my step-father, Donald Anderson, I owe much of my journey as he pushed me to continue in my goals even when I wasn't sure of my ability to accomplish them. They have all taught me more lessons than one paragraph could ever accomplish. This thesis is, ultimately, a result of their hard work as much as it is mine.

# Introduction

## 1.1 Background

### 1.1.1 The Origins and Importance of Intraspecific Variation in Environmental Pathogens

At its core, the study of trait variation is the study of accumulated genetic adaptations and drift within a population (Warringer *et al.*, 2011; Luo *et al.*, 2015). Generalist species within a population are understood to be drivers of evolution through niche dispersal and subsequent adaptation (Sriswasdi *et al.*, 2017; Xu *et al.*, 2022). The adaptation to diverse niches leads to a high degree of trait variation. Understanding the genetic basis of trait variation then provides insight into the potential selective environments and subsequent adaptations that guided the evolution of a species to its current state.

For opportunistic pathogens, phenotypic variation is a common observation in both clinically and environmentally relevant phenotypes (Macoris *et al.*, 2006; Desjardins *et al.*, 2017; Valdes *et al.*, 2018; Puértolas-Balint *et al.*, 2019). This is in contrast to obligate pathogens that experience reduction in genome size, in comparison to generalist pathogens, leading to reduced phenotypic range (Brown *et al.*, 2012b; Soumana *et al.*, 2017; Stajich, 2017). This variation is, in part, a result of a generalist lifestyle that sees these species occupy a variety of environmental niches, which can include hosts that are opportunistically infected (Kwon-Chung and Sugui, 2013). Adaptation to diverse environments leads to a high degree of genomic and phenotypic variation that not only affects survival in general but also impacts pathogenic potential (Farrer *et al.*, 2015; Robert *et al.*, 2015; Desjardins CA Muñoz JF *et al.*, 2016; Cordero *et al.*, 2018; Cuomo *et al.*, 2018).

Throughout this thesis the term *environmental pathogen* will be used to invoke a specific set of opportunistic pathogens. While commensals such as *Candida albicans* – which can cause disease resultant from a change in hygiene or loss of immune function – are opportunistic pathogens, here I do not consider such species as environmental pathogens. Environmental pathogens are those organisms which may be generally found living within the natural environment, with the capacity to cause disease within hosts (for example *Cryptococcus* species).

### **1.1.2 How Phenotypic Variation Contributes to the Evolution of Pathogenesis**

Environmental pathogens do not possess an easy method of host transmission. This necessitates a host agnostic approach for virulence evolution. This being the case, what adaptations distinguishes a pathogen from a non-pathogen in the environment? There are a number of requirements for a microbe to become a human pathogen. They must be able to survive at human body temperature, resist or evade phagocytic immune cells, survive immune attack from non-phagocytic cells, and acquire nutrients from their environment (Casadevall and Pirofski, 2007). It is hypothesized that the tools required to accomplish these feats evolve from pre-existing variation in traits that contribute to survival in the general environment. From the use of phospholipases to free otherwise unreachable nutrients to the evolution of pigments for thermal tolerance, many phenotypes that evolve to enhance fitness in the non-host environment are believed to contribute to the evolution of pathogenesis (Steenbergen *et al.*, 2001; Cordero *et al.*, 2018).

Across fungal pathogens, it is hypothesized that the virulence phenotypes utilized during infection vary based on selective pressures in the saprophytic niches they oc-

cupy (Paulussen *et al.*, 2017). For example, *Aspergillus fumigatus* is able to evade phagocytosis during infection by growing hyphae, making it impossible for cells to be phagocytosed (Heinekamp *et al.*, 2015). Alternatively, *Cryptococcus neoformans* evades phagocytosis through the production of extracellular polysaccharide capsule and increases in cell size and ploidy (O’Meara and Alspaugh, 2012). Both species employ hyphae for increased access to nutrients (Paulussen *et al.*, 2017; Watkins *et al.*, 2017); however, the environmental niches they occupy reflect why only one of them utilizes hyphae during infection. *Aspergillus* species penetrate compostable environments with their hyphae, necessitating hyphae that are active at higher temperatures (Kwon-Chung and Sugui, 2013). *Cryptococcus* hyphal growth is used on the surface of their saprophytic environment to facilitate mating and nutrient acquisition (Botts and Hull, 2010). Reflecting this difference in selective environment, hyphal growth in *Cryptococcus* is actually blocked by increased temperatures with hyphal cells being avirulent in animal models (Sia *et al.*, 2000; Wang *et al.*, 2012).

### **1.1.3 Utilizing Variation to Discover Genotype-Phenotype Connections**

The importance of studying the intraspecific variation of environmental pathogens is illustrated by findings in *Aspergillus fumigatus* and *Saccharomyces cerevisiae*. The reference strains for these fungi were found to poorly represent the common phenotypic and genotypic states of their respective species. (Warringer *et al.*, 2011; Jason E. Stajich Lotus A. Lofgren, 2022). The reference strains are, in fact, genotypically atypical for both species, leading to concerns of the generalizeability of phenotype–genotype connections found using these strains.

As I will illustrate in this thesis, the most studied strain in *C. neoformans*, H99,

is also phenotypically anomalous with respect to multiple traits. The decision to use these strains as references occurred before the data sets existed to vet their use as references. Now that the information is available, the genotypic and phenotypic diversity of a population is an important consideration in determining genotype–phenotype relationships. To fully study the ability for environmental pathogens to cause disease, and to ask why they cause disease, it is necessary to examine the variation of the phenotypic and genotypic determinants of disease.

Looking at within genus variation, the pathogenic species within *Cryptococcus* display a great deal of genotypic and phenotypic variation (Farrer *et al.*, 2015; Rossi *et al.*, 2016; Desjardins *et al.*, 2017; Roth *et al.*, 2021). Major virulence factors such as, capsule, melanin, thermal tolerance, the ability to produce giant cells (referred to as titan cells), and resistance to major antifungals have all been found to vary between and within species (Martinez *et al.*, 2001; Chen *et al.*, 2013; Cordero *et al.*, 2018; Desjardins *et al.*, 2017; Roth *et al.*, 2021; Sun *et al.*, 2022). Virulence factor variation also results in differences in the ability to cause disease (Litvintseva and Mitchell, 2009; Rossi *et al.*, 2016). This intraspecific variation has been exploited through quantitative trait locus (QTL) mapping and genome wide association study (GWAS). These studies yielded many important insights into the regulation of the aforementioned phenotypes by the HOG pathway, copper regulatory pathway, melanin synthesis pathway, and multiple G-coupled transcription factors (Lin *et al.*, 2006; Desjardins *et al.*, 2017; Roth *et al.*, 2021; Sun *et al.*, 2022). The success of these studies provides the basis to ask fundamental questions about the relationship between environmental stress response and virulence in *Cryptococcus* through further quantitative genetic investigation.

### 1.1.4 Generating Variation to Discover Genotype-Phenotype Connections

Instead of utilizing standing variation, experimental evolution studies exploit *de novo* variation to connect genotype and phenotype. Experimental evolution has been used to uncover the polygenic route to extreme thermal tolerance in *S. cerevisiae* (Huang *et al.*, 2018), azole resistance through the increased expression of multidrug transporters and duplications of *ERG11* in *C. neoformans* and *C. albicans* (Tso *et al.*, 2018), and for virulence attenuation in *C. albicans* mediated by mutations in the cyclic AMP pathway (Handelman and Osherov, 2022). Discovering the genes and pathways where *de novo* mutations accrue during experimental selection informs the potential evolutionary strategies pathogens utilise for stress resistance in natural environments. In a world that is experiencing increases in global temperature and increased use of agricultural antifungals, understanding the routes fungal pathogens take to achieve resistance to these and other environmental stressors is growing in importance.

### 1.1.5 Hypotheses Surrounding the Evolution of *Cryptococcus* Pathogenicity

Many outstanding questions exist regarding the evolution of *Cryptococcus* virulence. The inability for *Cryptococcus* strains to be transmitted between hosts indicates a mechanism for evolving and maintaining virulence related phenotypes in the environment. To this end, the role of many virulence factors have been viewed through the lens of environmental adaptations. The capsule's ability to resist desiccation and aid in resistance to environmental phagocytes, the ability for melanin to thermo-regulate and resist UV radiation, and the capacity for multiple secreted enzymes to aid in nu-

trient acquisition have all been hypothesized as potential origins of these individual virulence factors (Steenbergen *et al.*, 2003; Casadevall, 2006; Kwon-Chung and Sugui, 2013). It has also been suggested that passage at 37°C is necessary for the maintenance of *C. neoformans* virulence, displaying some need for thermal passaging from either an environmental or non-mammalian host source (Xu, 2004). Collectively the hypothesized origins of these virulence factors are known as the “Accidental Pathogen Hypothesis” (Casadevall and Pirofski, 2007). This hypothesis posits that, for environmental pathogens, stressors within the environment drive the selection of traits that also resist the immune systems of mammalian hosts. Many studies exist that compare the role of individual genes or specific phenotypes between environmental stressors and virulence (Zaragoza *et al.*, 2008; Chrisman *et al.*, 2010; Watkins *et al.*, 2018). While these studies provide insight into potential interrelatedness between virulence genes and their role in the environment, they lack context of what is naturally being selected for by environmental stressors. Without this context, it is difficult to make evolutionary connections between virulence genes and their environmental origins. Through studying the natural variation of genes involved in environmental stress resistance, comparisons between virulence and the environment can be more accurately drawn.

## 1.2 Thesis Outline

The goal of my thesis was to dissect the genetic basis of phenotypic traits integral to the survival of *Cryptococcus* in the environment that are also required for pathogenesis. To accomplish this, I utilized a combination of quantitative genetics and experimental evolution to identify both existing and *de novo* genetic variation that underlies phenotypic traits that are critical for fungal survival both in the external environment and in the context of pathogenesis.

Chapter two describes my efforts to test a key tenet of the accidental pathogen hypothesis – that selection of traits important for surviving encounters with microbial predators may also contribute to virulence potential. I employed QTL mapping to identify genomic regions and alleles that contribute to *Cryptococcus* survival when challenged with the phagocytic amoeba, *Acanthamoeba castellanii*. Using mapping populations derived from both *C. neoformans* and *C. deneoformans* crosses, I identified a cross-species QTL region. For the *C. neoformans* cross, I subsequently identified a specific causal variant underlying this amoeba resistance QTL. I demonstrate that this QTL region also effects melanization, an important virulence trait.

In chapter three, I map QTL for thermal tolerance and growth at low pH, using the same *C. neoformans* cross as in chapter two. I discover three QTLs that govern general growth, two unique QTLs linked to temperature tolerance, and two unique QTLs underlying acid tolerance. A pleiotropic QTL on chromosome 5 is revealed through QTL mapping based on Gompertz growth parameters. I also describe the impact of nutrient composition on stress QTL presentation.

Chapter four utilizes experimental evolution to characterize mutations, genes, and pathways involved in the adaptation of *Cryptococcus* to high temperature and the antifungal drug, fludioxonil. An interesting trade-off is found between these evolved resistances. Namely, I find thermal tolerance and fludioxonil resistance to be inversely related; however, thermal tolerant strains produce spontaneous mutants that are able to grow on fludioxonil, after losing the ability to do so. Mutation analysis reveals several interesting *de novo* mutations, deletions encompassing multiple genes (referred to here as multi-gene deletions), and a duplication associated with fludioxonil tolerance. There is potential for pleiotropic alterations in antifungal tolerance and virulence for many of the mutations is discovered.

The final chapter situates my findings into the current literature and describes

future avenues of research that are likely to complement the findings I report.

# An Amoeba Resistance QTL Conserved Across Two Species of *Cryptococcus* Reveals Novel Insights Into Accidental Pathogenesis

## 2.1 Author Contributions

Additional data and results not previously presented in Roth *et al.* are included. The genetic crosses and associated genome sequence data used in this chapter were generated by my co-authors, Sheng Sun and Joseph Heitman. Progeny and genome sequence data from *C. neoformans* crosses were produced by my collaborator Debra Murray. Variant calling and alignments were performed by Paul Magwene. Segregant filtering was performed by Cullen Roth. QTL analysis was performed in collaboration with Cullen Roth. All mouse husbandry was performed by Anna Floyd-Averette in the Heitman lab. Macrophage experiments were completed by my collaborator Chinaemerem (Uju) Onyishi in Robin May's lab at the University of Birmingham.

Research reported in this chapter was supported by the National Institute of Allergy and Infectious Diseases of the National Institutes of Health under award number R01AI133654. The content is solely the responsibility of the authors and does not necessarily represent the official views of the National Institutes of Health.

## 2.2 Introduction

For many free-living pathogens, there is no host-to-host transmission and infection of a host is not an obligatory stage of their life cycle. Pathogenesis in these cases is considered opportunistic, and key traits that facilitate virulence are not likely to have evolved due to adaptation to the host directly (Brown *et al.*, 2012b; Lanzas

*et al.*, 2020). Rather, the ability to cause disease is hypothesized to be an unintentional byproduct of evolving in a varied, stressful environment (“accidental virulence”; Casadevall (2008)). This raises the question, “What environmental interactions contribute to the evolution of virulence?”

A prominent hypothesis proposed for many environmental pathogens suggests that predator-prey interactions between microbes drive the evolution of traits advantageous to pathogenesis (Adiba *et al.*, 2010). Chief among the predators that have been suggested as relevant to the evolution of virulence traits are amoebae. For example, bacterial pathogens such as *Bordetella*, *Legionella*, and *Pseudomonas*, as well as the fungal pathogens *Paracoccidioides*, *Cryptococcus*, and *Aspergillus*, are all preyed upon by phagocytic amoebae (Taylor-Mulneix *et al.*, 2017; Best and Kwaik, 2018; Siddiqui *et al.*, 2015; Albuquerque *et al.*, 2019; Steenbergen *et al.*, 2001; Fan *et al.*, 2021; Waeyenberghe *et al.*, 2013). Amoebae share many similarities with macrophages and other primary immune cells that microbial pathogens encounter during infection of mammalian hosts. These similarities include the use of receptors to identify targets, actin mediated phagocytosis, acidification, nitrosative stress, and metallo-ion toxicity in the phagosome. (Yan *et al.*, 2004; Escoll *et al.*, 2013; Davies *et al.*, 1991; German *et al.*, 2013). In light of this, it has been proposed that amoebae may serve as “training grounds” for intracellular pathogens (Smith *et al.*, 2013). For fungi in particular, the idea that interactions with amoebae in the environment drives the selection of fungal traits necessary for survival during mammalian infection has been termed the “Amoeboid Predator-Fungal Animal Virulence Hypothesis” (Casadevall *et al.*, 2019).

For the fungal pathogen *Cryptococcus neoformans*, interactions with free-living amoebae have been documented for nearly 100 years (Castellani, 1930). Amoebae are found in many of the same niches that *C. neoformans* inhabits, and *C. neoformans* is actively consumed by amoebae isolated from pigeon guano (Ruiz *et al.*, 1982).

*C. neoformans*, and the amoebae that consume it, are globally distributed (Rajasingham *et al.*, 2017; Siddiqui, 2012). *C. neoformans* is a saprophytic fungus; however, it has the ability to cause disease in vulnerable human populations, primarily infecting individuals with reduced immunity due to factors such as HIV/AIDS or patients receiving immunosuppressive drug treatments (Brown *et al.*, 2012a; Voelz and May, 2010; May *et al.*, 2016; Dromer *et al.*, 2007). *C. neoformans* infections in mammals are facilitated by a variety of traits including: a polysaccharide capsule (O’Meara and Alspaugh, 2012; Leon-Rodriguez *et al.*, 2018; Zaragoza *et al.*, 2008), the ability to grow at high temperatures (Leach and Cowen, 2013; Findley *et al.*, 2009), the production of melanin (Cordero, 2017; Liu *et al.*, 2021), and a battery of secreted phospholipases (Djordjevic, 2010; Cox *et al.*, 2001) and ureases Cox *et al.* (2000); Kappaun *et al.* (2018). These same virulence factors act as defense mechanisms against amoebae (Chrisman *et al.*, 2010; da S. Derengowski *et al.*, 2013; Zaragoza *et al.*, 2008). Passaging *C. neoformans* strains with amoebae increases virulence factor presentation and results in enhanced pathogenicity in mammalian tissue culture, insects, and mouse models of infection (Rizzo *et al.*, 2017; Steenbergen *et al.*, 2003). These findings support the hypothesis that amoebae may play a key role in the evolution of *C. neoformans* virulence factors. However, most studies that characterize the similarities between *Cryptococcus*’s interactions with amoebae and with animal immune systems have targeted known virulence genes, primarily through gene deletion studies. Furthermore, these studies used a small number of *Cryptococcus* strain backgrounds. Focusing on previously identified genes, in a limited number of strains, may bias or obscure other genes and pathways important for amoeba resistance.

In this study we ask, “Do alleles important for fungal survival with amoeba correspond to known virulence genes?” To answer this question, we employed quantitative trait locus (QTL) mapping to identify genomic regions and allelic variants

that contribute to resistance against amoeba predation in two pathogenic species of *Cryptococcus*, *C. neoformans* and *C. deneoformans*. For both species we identified major effect QTL. Surprisingly, we found these QTL regions are homologous between the species. For *C. neoformans*, the amoeba resistance QTL we identified is also a melanization QTL. Using a combination of comparative genomics and genetic engineering we identified a likely causal variant for this QTL region, a 1.8 kb deletion upstream of the transcription factor gene *BZP4*. We show that disruption of this region leads to altered transcription of *BZP4* and other genes, and these transcriptional differences are in turn associated with reduced amoeba resistance and melanization capacity. Despite alterations in amoeba resistance and melanization associated with dysregulation of *BZP4*, our comparative analysis suggests that *BZP4* is not required for virulence in mice or macrophages. In addition, we find no relationship between genetic variation in the ability to resist amoeba predation and virulence in mouse models of infection. Our findings both advance the understanding of the genetic architecture of virulence traits, but also suggest the need for a more nuanced perspective on the evolutionary and ecological interactions that have shaped microbial pathogenesis.

## 2.3 Results

### 2.3.1 Comparison of Amoeba Resistance in Diverse *C. neoformans* Strains

We developed a plate-based assay to quantify *Cryptococcus* resistance to predation by the amoeba, *Acanthamoeba castellanii* (Fig. 2.1A; Lin *et al.* (2015)). Briefly, an established lawn of *Cryptococcus* cells is inoculated with a drop of amoeba. After a defined period of time, the cleared (consumed) portion of the lawn is quantified and

**Table 2.1:** Genetically diverse *C. neoformans* strains surveyed for amoeba resistance.

Strain	Lineage	Site	Source
Bt102	VNBI	clinical	Litvintseva et al. (2003)
Bt22	VNBI	clinical	Litvintseva et al. (2003)
Bt45	VNBI	clinical	Litvintseva et al. (2003)
Ftc192-1	VNBI	environmental	Chen et al. (2015)
Ftc267-1	VNBI	environmental	Chen et al. (2015)
FTC555-1	VNBI	environmental	Chen et al. (2015)
Bt1	VNBII	clinical	Litvintseva et al. (2003)
Bt103	VNBII	clinical	Litvintseva et al. (2003)
Bt206	VNBII	clinical	Litvintseva et al. (2003)
Bt65	VNBII	clinical	Litvintseva et al. (2003)
Bt75	VNBII	clinical	Litvintseva et al. (2003)
AD1-7a	VNI	clinical	Dromer et al. (2007)
Bt130	VNI	clinical	Litvintseva et al. (2003)
H99	VNI	clinical	Perfect et al. (1980)
KN99a	VNI	laboratory	Nielsen et al. (2015)

used as a measure of resistance. The larger the clearance area, the less resistant the cells are to amoeba consumption.

We applied this amoeba resistance assay to a diverse set of *C. neoformans* strains that represent major sub-lineages within this species (Table 2.1). This assay revealed extensive variation in amoeba resistance between strain backgrounds (Fig. 2.1C). Notably, there is no simple relationship between the site of collection and amoeba resistance; clinical strains isolated from patient samples exhibit both resistant and sensitive amoeba phenotypes.

### 2.3.2 Mapping Populations and Genome Sequencing

From our collection of genetically diverse strains, we identified strains of opposite mating type ( $MAT\mathbf{a}$ - $MAT\alpha$ ) that differed in their resistance to amoeba. We carried out pairwise mating tests to identify strain pairs with sporulation and germination efficiency suitable for establishing a large genetic mapping population. The *C. neoformans* strains Bt22 and Ftc555-1 were chosen for further analysis based on spore

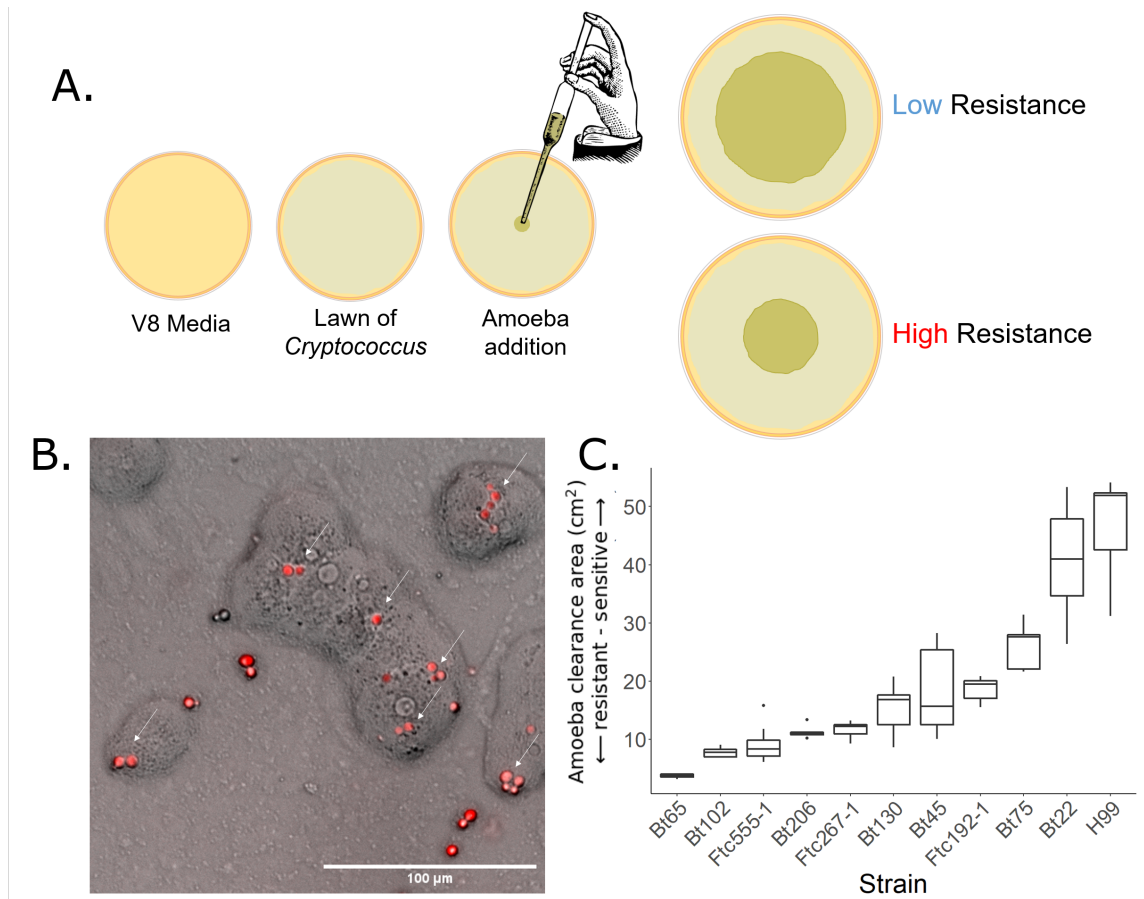


**Figure 2.1: Amoeba resistance varies between strains of *C. neoformans*.** **A.** A schematic overview of the amoeba resistance assay. A lawn of *Cryptococcus* is grown on V8 media for 60 hours. *A. castellanii* are added to the center of the lawn. *A. castellanii* consume the cells across the plate for a period of 12 or 18 days (based on amoeba activity). *Cryptococcus* strains able to resist amoeba have smaller areas of consumption when imaged. **B.** *A. castellanii* in co-culture with *C. neoformans* expressing RFP on solid V8 media. White arrows indicate examples of phagocytosed *C. neoformans* cells. **C.** Boxplots representing amoeba resistance phenotypes for a diverse set of *C. neoformans* strains after 18 days of amoeba co-culture. The x-axis displays the strains assayed. The y-axis represents the area the amoeba consumed. Smaller clearance areas indicate greater resistance to amoeba.

viability and differences in their amoeba resistance. The low-resistance strain Bt22 (MAT $\alpha$ ) is a clinical isolate while the high-resistance strain Ftc555-1 (MAT $\alpha$ ) is an environmental isolate collected from a mopane tree; both strains were collected in Botswana (Chen *et al.*, 2015b). Using manual spore dissection, we generated 384 progeny from a cross between these two strains. The genomes of these progeny were then sequenced on the Illumina NovaSeq 6000 platform to an average depth of  $\sim 15\times$ . Based on the resulting sequence data, the progeny were filtered based on criteria including sequencing depth, read quality, elevated ploidy, and clonality. After filtering, the final mapping population was composed of 304 recombinant progeny. 46,670 variable sites were identified between the parental strains that were collapsed into 4,943 haploblocks.

### 2.3.3 Cross Species Amoeba Resistance QTL

The F<sub>1</sub> segregants generated from the Bt22  $\times$  Ftc555-1 cross exhibited a diverse response to amoeba predation (mean of predation area 23.46 cm<sup>2</sup> and SD 14.99 cm<sup>2</sup>). There is a substantial amount of transgressive segregation – 16.9% of the segregants exhibited resistance higher than Ftc555-1, and 38.4% of segregants exhibited lower resistance than Bt22 (Fig. 2.2B). Substantial transgressive segregation suggests that epistatic interactions between parental alleles contribute to both increased and decreased resistance beyond the parental phenotypes. Segregant genotypes and phenotypes were combined to carry out QTL mapping based on a marker regression approach Roth *et al.* (2021). Our QTL analysis revealed that genetic variation for amoeba resistance in our mapping population is dominated by a single, major effect locus on chromosome 8 (Fig. 2.3A). Segregants with Bt22 haplotypes at the chromosome 8 QTL peak exhibited significantly larger zones of amoeba clearance than those offspring with the Ftc555-1 haplotype (Fig. 2.3B). The QTL on chromosome 8

explains an astonishing 62% of variation in amoeba resistance.

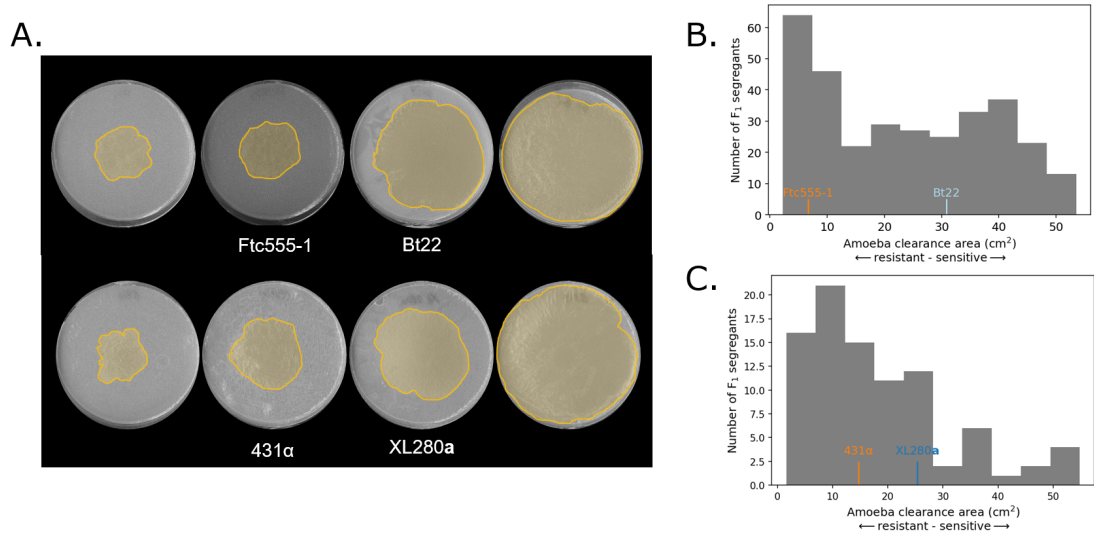


**Figure 2.2: Phenotypic variation in amoeba resistance in mapping populations derived from both *C. neoformans* and *C. deneoformans* crosses.** **A.** Representative images of plates from amoeba resistance assays. On the plates, the area consumed by amoeba are highlighted in yellow. Parental strains are shown in the middle panels, and transgressive segregants are on the left and right. **B.** A histogram displaying amoeba resistance of segregants in the *C. neoformans* cross. The x-axis represents the amoeba clearance area. Phenotypes of the two parental strains are indicated in orange (Ftc555-1) and blue (Bt22). **C.** A histogram of the *C. deneoformans* cross amoeba phenotypes. Phenotypes of the two parental strains are indicated in orange (431) and blue (XL280)

To determine if there are similarities in the genetic architecture of amoeba resistance between sister species of *Cryptococcus*, we carried out a similar analysis using a mapping population derived from a *C. deneoformans* cross described in Roth *et al.* (2021). This cross, between strains XL280a and 431 $\alpha$ , consists of 90 recombinant progeny. XL280a and 431 $\alpha$  have only modest differences in amoeba resistance, but similar to what we describe above, the *C. deneoformans* offspring exhibited a high degree of transgressive segregation for this trait. 15.4% of offspring displayed negative transgressive segregation (segregants with lower amoeba resistance than XL280a), 54.8% positive transgressive segregation (segregants with lower amoeba resistance

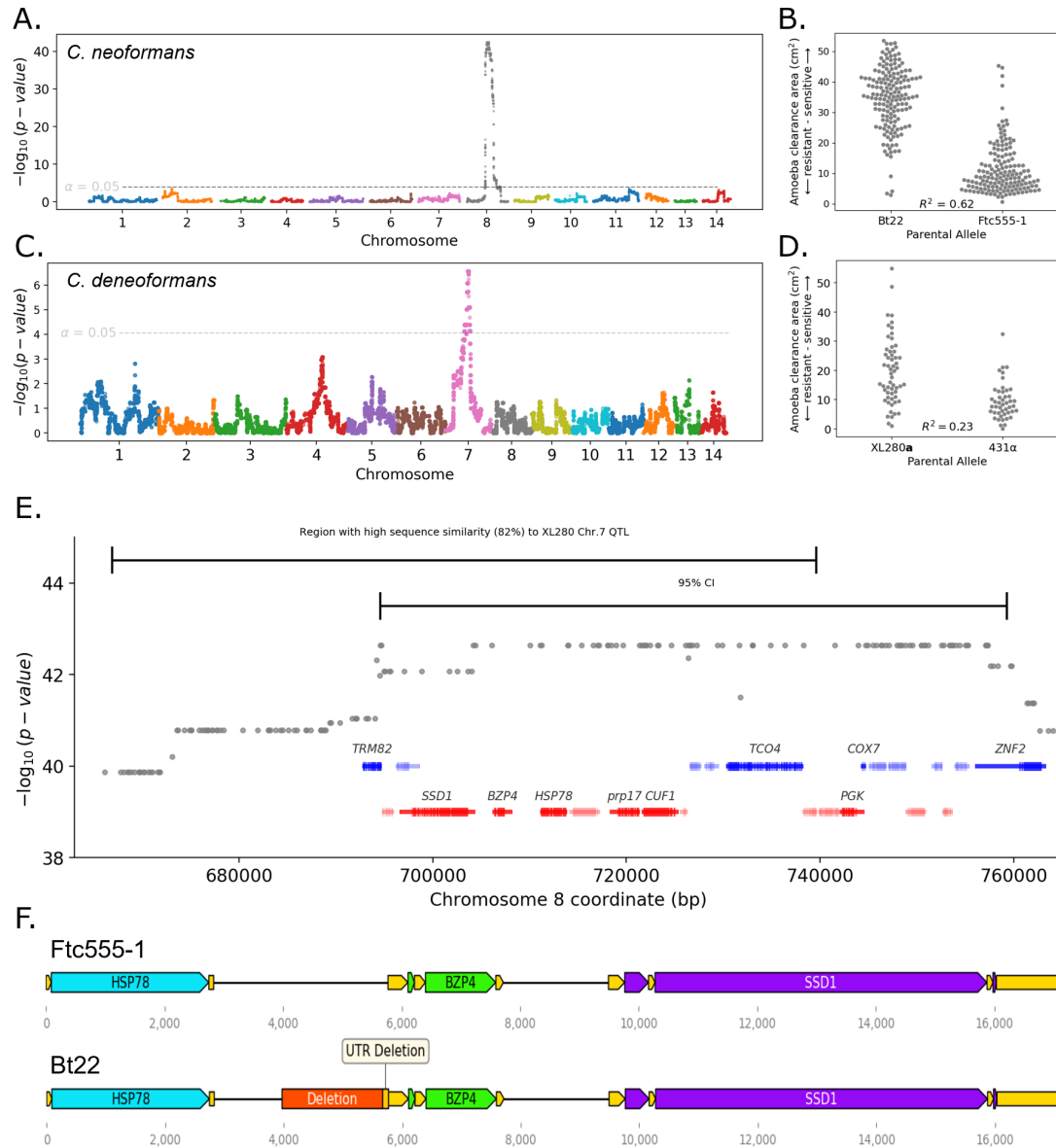


**Figure 2.3: Amoeba resistance QTL for *C. neoformans* and *C. deneoformans*.** **A.** Manhattan plot representing the association between genotype and amoeba resistance in the *C. neoformans* mapping populations. The dotted line indicates the significance threshold determined by permutation. **B.** Distributions of segregant phenotypes associated with the QTL peak on chromosome 8 for *C. neoformans*. The x-axis represents allelic state at the QTL peak. **C.** Manhattan plot for amoeba resistance in the *C. deneoformans* mapping population. **D.** Segregant phenotypes by chromosome 7 genotype for *C. deneoformans*. **E.** A magnified view of the 95% confidence interval of the *C. neoformans* QTL for amoeba resistance. Barred lines at the top are the 95% confidence intervals for the *C. deneoformans* and *C. neoformans* amoeba resistance QTL. **F.** Gene diagrams for the region around *BZP4* for Ftc555-1 and Bt22. UTRs are shown in yellow.

than 431 $\alpha$ ), and 29.8% non-transgressive (Fig. 2.2A,D). QTL analysis using this population identified a significant peak on chromosome 7 that explains 23% of the variance of amoeba resistance (Fig. 2.3C). Strains with the 431 $\alpha$  allele on chromosome 7 have a higher average resistance to amoeba (Fig. 2.3D). By examination of the genes under the QTL peak on chromosome 7, we found this region is orthologous to the *C. neoformans* QTL peak on chromosome 8. These two regions share 82% nucleotide sequence identity and conserved synteny (Fig. 2.3E), suggesting there are conserved genes required for amoeba resistance within the *Cryptococcus* species complex.

### 2.3.4 Identification of an Amoeba Resistance Gene

To identify candidate causal variants for the QTL region on chromosome 8 in the *C. neoformans* cross, we analyzed the predicted effect of nucleotide sequence differences on annotated features in this region (Table S1). We identified 25 genes within the 64 kb region that comprises the 95% confidence interval for this QTL. Ten of those genes have an annotated function or have homology to annotated genes in other fungal species. Across all the genes in the QTL region, we identified 31 synonymous mutations, 29 non-synonymous mutations, and two indels. The two indels both result in nonsense mutations but these genes have no characterized function, no known gene deletion phenotype, and the mutations are in the opposite direction than we would predict for the QTL effect (i.e. they were present in the resistant strain, suggesting gene deletion would improve resistance). Further characterization of non-coding regions in the QTL region led to the identification of a large sequence difference between Bt22 and Ftc555-1, a 1789 bp deletion occurs in the Bt22 background in the intergenic region between the genes *BZP4* and *HSP78*. The Bt22 variant truncates 100 bp of the annotated *BZP4* 5' UTR and 1689 bp further upstream (Fig. 2.3F).

Using *C. neoformans* phylogenetic data and short-read sequence data from Des-

Desjardins *et al.* (2017), we identified a strain, Bt45, that is nearly genetically identical to Bt22 (~200 SNP differences) but does not share the deletion upstream of *BZP4* (Fig. 2.4A). We measured the amoeba resistance of Bt45 and found that it exhibits significantly greater resistance than Bt22 (pairwise t-test  $P < 0.0005$ ), though not to the level observed for Ftc555-1 (Fig. 2.4B). This comparison between these two nearly genetically identical strains is akin to an “allele swap” experiment and provides strong evidence that the non-coding variant we identified upstream of *BZP4* is the likely causal variant underlying the Chromosome 8 QTL.

To provide further evidence of *BZP4*'s contribution to amoeba resistance, we used CRISPR-Cas9 editing to delete *BZP4* in the Ftc555-1 background (Lin *et al.*, 2020; Huang *et al.*, 2022). We constructed two independent *bzp4* $\Delta$  mutants and measured their amoeba resistance phenotypes. Both mutants exhibited a significant reduction in amoeba resistance (pairwise t-test  $P < 0.0005$ ) and melanization (Fig. 2.4B, S3).

In sum, multiple lines of evidence suggest that the 1789 bp deletion we identified upstream of *BZP4* is the causal variant for the large effect amoeba resistance QTL we identified on chromosome 8. For the sake of conciseness, in the text that follows we will refer to the two allelic states at this locus as *BZP4*<sup>B</sup> (Bt22 allele) and *BZP4*<sup>F</sup> (Ftc555-1 allele).

### 2.3.5 *BZP4* is a pleiotropic QTG for Amoeba Resistance and Melanization

*BZP4* is a transcription factor that has been shown to play a role in regulation of the melanin synthesis pathway under nutrient deprivation conditions (Lee *et al.*, 2019a). Variation at the *BZP4* locus was previously identified in a genome wide association study (GWAS) for melanization (Desjardins *et al.*, 2017). In that study, *bzp4* loss-of-function mutations, found exclusively in clinical isolates, were found to correlate

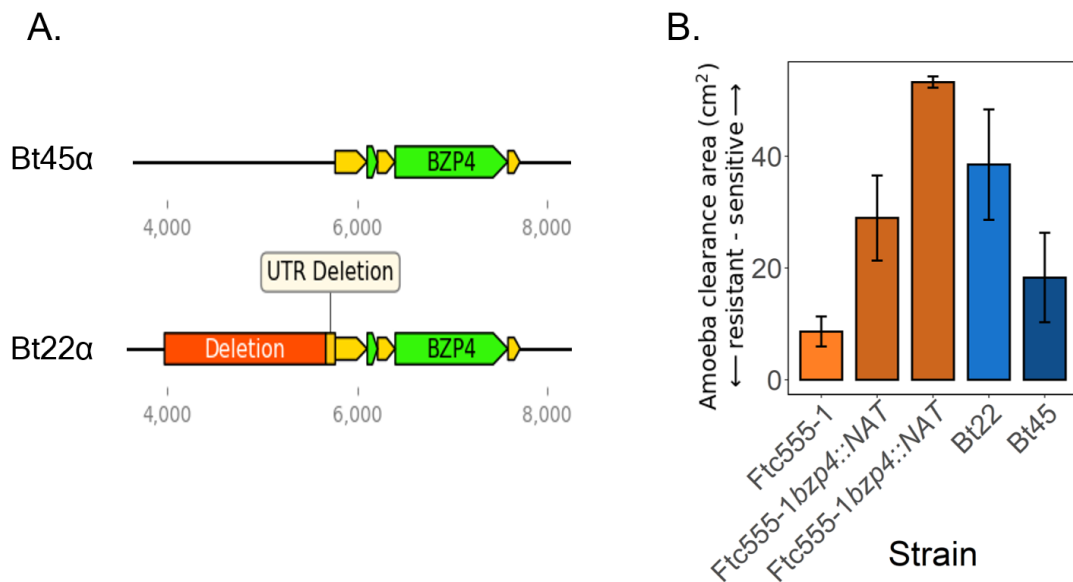


**Figure 2.4: Disruption of *BZP4* reduces amoeba resistance.** **A.** Models of the genomic regions surrounding *BZP4* in Bt22 and Bt45. **B.** Amoeba resistance assay for two independent gene deletions of *BZP4* in the Ftc555-1 background and a closely related strain of Bt22, Bt45. Bars are colored for comparison between closely related strains. The x-axis represents the strain tested. The y-axis represents the area amoeba consumed.

with reduced melanization. A later study found that decreased expression of *BZP4* is correlated with decreased melanization in VNI clinical isolates (Yu *et al.*, 2020).

Based on the role of *BZP4* in the regulation of melanin synthesis, we reasoned that the *BZP4* variant we identified in our amoeba resistance mapping might also result in differences in the ability to produce melanin. While neither of the parent strains in our cross lacks melanin, Bt22 exhibits less melanin pigmentation than Ftc555-1 when grown under the same inductive conditions (Fig. 2.5A). We assayed our *C. neoformans* mapping population for the ability to produce melanin when grown on L-DOPA plates. Segregants in the cross ranged from completely white (devoid of melanin) to a deep ebony color accompanied by melanin leaking into the surrounding media (Fig. 2.5A). Across the segregants, 23.45% of the segregants displayed positive transgressive segregation (more melanized than Ftc555-1) while 24.43% displayed negative transgressive segregation (less melanized than Bt22). We examined the joint distribution of amoeba resistance and melanization phenotypes among the offspring, finding a positive but non-linear relationship between them (Fig. 2.5D).

QTL mapping based on the melanization phenotypes identified a major peak on chromosome 8 nearly identical in location to the QTL for amoeba resistance (Fig. 2.5C). This QTL explains a remarkable 50.2% of the phenotypic variation for melanization (Fig. 2.5B). Based on the similarity of the QTL for amoeba resistance and melanization (Fig. 2.5C), as well as the previously demonstrated role of *BZP4* in the regulation of melanin synthesis, we propose that the non-coding deletion upstream of *BZP4* has pleiotropic effects on both of these traits.

In contrast to our findings in *C. neoformans*, the chromosome 7 QTL for amoeba resistance in the *C. deneoformans* cross does not appear to have a pleiotropic effect on melanization. Instead, a nonsense mutation in the gene *RIC8* is primarily responsible for variation in melanization for this cross as described in an earlier study from our

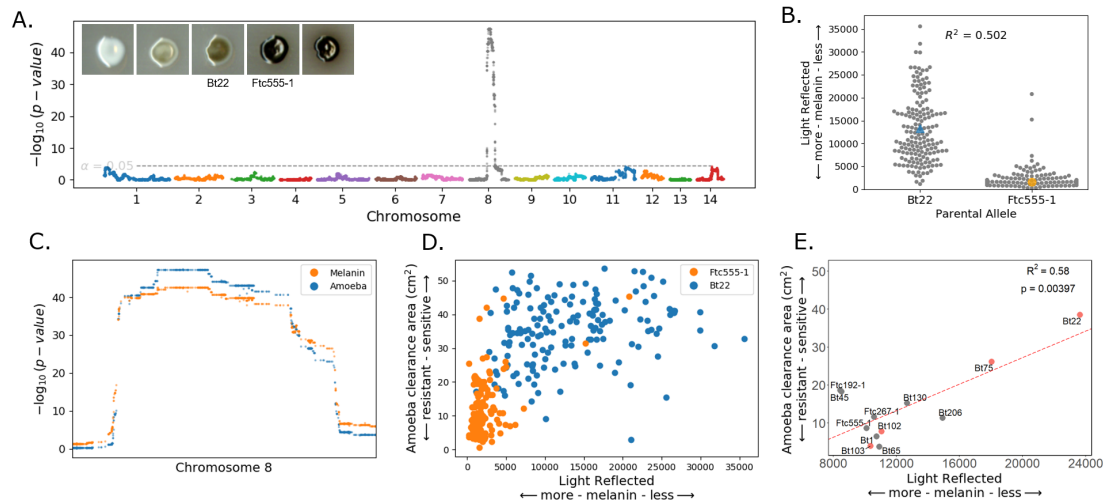


**Figure 2.5: Melanization and amoeba resistance share the same QTL.** **A.** Manhattan plot representing the association between genotype and melanization in the *C. neoformans* plot. The y-axis represents the strength of the association between genotype and light reflected (the degree of melanization). The x-axis represents the genomic location of the haploblocks used in the associations. The dotted line represents a significance threshold determined by a permutation test. Representative images of parents and segregants on L-DOPA media are also included. Each colony is from the randomized plates used for QTL mapping. Images are brightened 30% to better display the difference in pigmentation. **B.** Segregant phenotypes at the maximum significance value of the QTL on chromosome 8. The x-axis represents the segregant allele at the maximum significance of the QTL. The y-axis represents the light reflected off of the colony when melanized. Parental strains are indicated in orange (Ftc555-1) and blue (Bt22). **C.** A magnified view of the chromosome 8 QTL peaks for amoeba resistance and melanization illustrating the QTL overlap. **D.** Plot comparing amoeba resistance and melanization phenotypes. The x-axis represents melanization and the x-axis represents amoeba resistance. Each dot represents a single segregant. Segregants are colored by their allele at the chromosome 8 QTL. **E.** Correlation between amoeba resistance and melanization in natural isolates, with the strain H99 removed.  $p < 0.005$

research groups (Roth *et al.*, 2021).

To test whether the relationship we observed between amoeba resistance and melanization in our *C. neoformans* mapping population holds more broadly, we again employed the genetically diverse collection of *C. neoformans* strains described above. We supplemented this collection with additional strains that have predicted *BZP4* loss-of-function mutations, and we measured amoeba resistance and melanization for each isolate. All strains, including those with predicted *BZP4* loss-of-function mutations, are capable of producing melanin given sufficient incubation time (Fig. S3). However, we observed large differences in the rate of melanization between strains and used images taken at two days of growth as a measure of the variation. When comparing amoeba resistance and melanization across the diverse strain set, the reference strain H99 is notable as an outlier in terms of the bivariate relationship among these traits (Fig. S4). With H99 excluded, there is a strong linear relationship between amoeba resistance and melanization ( $R^2 = 0.58$ ) (Fig. 2.5E). A notable trend among strains with predicted *BZP4* loss-of-function mutations is that those that melanize more readily (Bt103 and Bt102) are more resistant to amoeba than those that melanize slowly (Bt22 and Bt75) (Fig. 2.5E).

### **2.3.6 Gene Expression Differences Associated with *BZP4* Allelic Variation**

Since the *BZP4* allele we identified involves a deletion of a large upstream non-coding region, we hypothesized that the phenotypic effects of this allele are mediated by a reduction in the expression of the *BZP4* gene, with consequent effects on the downstream targets of this transcription factor. To test this hypothesis we carried out gene expression profiling using RNAseq. Using six offspring with each *BZP4* genotype (6 for Bt22 and 6 for Ftc555-1; 12 strains in total) we compared transcriptional

responses when grown on V8 plates with or without the addition of amoeba.

*BZP4* was significantly differentially expressed between strains with the *BZP4<sup>B</sup>* and *BZP4<sup>F</sup>* alleles, in both amoeba and non-amoeba conditions (Fig. 2.6A, B). *BZP4<sup>B</sup>* strains exhibited an average 1.83-Log<sub>2</sub>fold decrease in expression relative to *BZP4<sup>F</sup>* strains when co-cultured with amoeba and a 2.06-Log<sub>2</sub>fold decrease when amoeba were absent (Fig. 2.6A). No other gene under the chromosome 8 QTL showed statistically significant differences in expression. While there are differences in *BZP4* expression between genotypes, no significant change in the expression of *BZP4* was observed between control and amoeba conditions (Fig. 2.6A). This suggests that the effect of the *BZP4* allelic differences we identified is not specific to the amoeba challenge conditions of our assay.

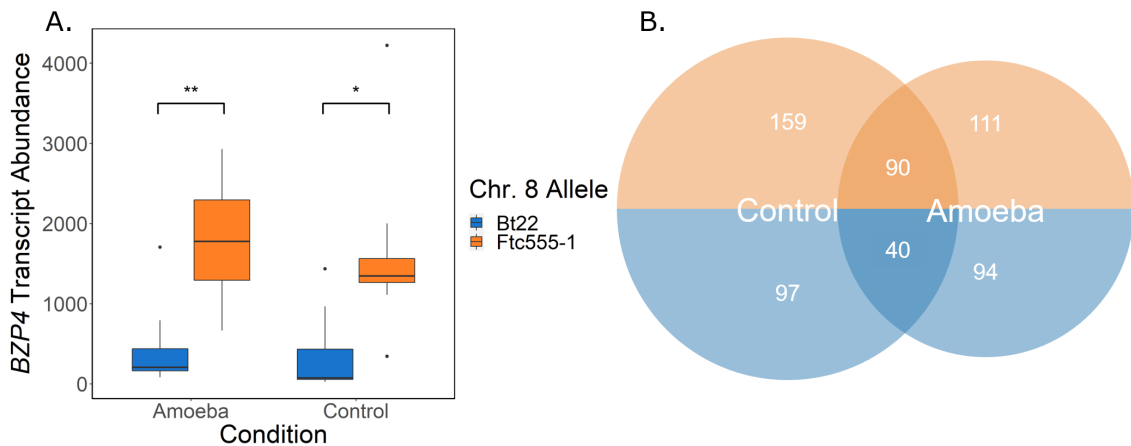


**Figure 2.6: *BZP4* expression is significantly different between genotypes.** **A.** Boxplots representing the difference in transcript abundance between conditions with each parental allele under the chromosome 8 QTL. The y-axis represents the total transcript counts. Boxplots are colored by parental allele. Significance is determined by ANOVA. “\*\*” p < 0.005; “\*” p < 0.05 **B.** A Venn Diagram displaying the number of genes with increased and decreased expression for amoeba and control conditions based on the parental allele. Genes with decreased expression are colored in orange and increased expression is colored in blue.

Given that *BZP4* was identified as a candidate QTL for melanization, and the

transcription factor it encodes has been previously implicated in the regulation of melanin synthesis genes, we predicted that such genes would also exhibit differences in expression as a function of *BZP4* genotype. Contrary to our prediction, we found that no major melanin synthesis genes were significantly differentially expressed between genotypes, when measured on the V8 growth media used in our amoeba experiments.

Investigating genome wide expression differences, we observe 589 genes with a greater than 2-fold difference between genotypes in either amoeba and control conditions. Of the 589 differentially expressed genes, 130 are shared between conditions, 255 are specific to the control conditions, and 204 are amoeba specific. Using GO term analysis for the 90 shared gene that have increased expression when *BZP4* expression is reduced, we find transmembrane transporter activity, oxidoreductase activity, and transition metal ion binding to increase in activity with reduced *BZP4* expression. Interestingly, there is a paucity of GO predictions for the 40 shared genes that are decreased in expression with reduced *BZP4* expression, as many of the genes are hypothetical or poorly characterized. The number of genes that have an inverse transcriptional relationship with *BZP4* expression indicates a role in gene repression. GO terms specific to amoeba conditions further display transmembrane transporter activity and oxidoreductase activity. Hydrolase activity is represented in control specific conditions.

### **2.3.7 Epistatic QTLs for Amoeba Resistance and Melanization**

While the pleiotropic chromosome 8 QTL we identified in the *C. neoformans* cross explains a very large portion of variation for both amoeba resistance and melanization, both traits show continuous rather than bimodal distributions and there is a large degree of transgressive segregation. These observations suggested that there are likely

additional alleles, perhaps interacting epistatically with the major effect allele on chromosome 8, that contribute to phenotypic differences in both of these traits. To test for epistatic interactions, we subdivided our mapping population based on the chromosome 8 genotype, and reanalyzed the mapping models for each subpopulation (Fig S2). For amoeba resistance, we find a single epistatic QTL on chromosome 5, exclusive to the segregants with the Ftc555-1a allele on chromosome 8 (Fig S2A). This epistatic chromosome 5 QTL explains 19% of the variation within that subgroup and it increases the overall variance explained for amoeba resistance to 64%. We identified two epistatic QTL for melanization, one in the segregants that have the Bt22 allele on chromosome 8 and the second in those that have the Ftc555-1 allele (Fig S2B). The epistatic QTL in the Bt22 background is found on chromosome 1 and explains 26% of the variation within that subgroup. The epistatic allele in the Ftc555-1 background occurs on chromosome 7 and accounts for a more modest 7.8% of variance. With these epistatic interactions included, the variance in melanization explained by all the QTL we identified increases to 56.4%. Evidence of epistasis for amoeba resistance and melanization highlights the importance of strain background and the impact of individual allelic differences on traits of interest.

### **2.3.8 Comparing Amoeba Resistance and Virulence**

The accidental pathogen hypothesis is based on the similarities between amoeba and macrophage interactions with *Cryptococcus*. Both amoeba and macrophages employ similar methods of detecting, phagocytosing, and degrading fungal cells but the question remains, does survival when challenged with one phagocyte relate to success with the other? To answer this question, we measured the internal proliferation rate (IPR) in macrophages of offspring from the Bt22  $\times$  Ftc555-1 cross. Offspring strains were chosen to represent opposite extremes in terms of their amoeba resistance phe-

notypes. These low and high resistance strains were assayed alongside the parental strains. J774A.1 murine macrophages were infected with *C. neoformans* cells and the internal proliferation rate of yeast cells was measured using time lapse microscopy as described in the Methods. All offspring assayed, regardless of *BZP4* genotypes and amoeba resistance phenotypes, showed similar macrophage internal proliferation rates (Fig. 2.7A). Phagocytic index, another measure of yeast-macrophage interactions, also showed no association with *BZP4* allelic variation or amoeba resistance (Fig. S1). Thus, in contrast to the predictions of the accidental pathogen hypothesis, we do not observe a relationship between amoeba resistance alleles and survival in macrophages.

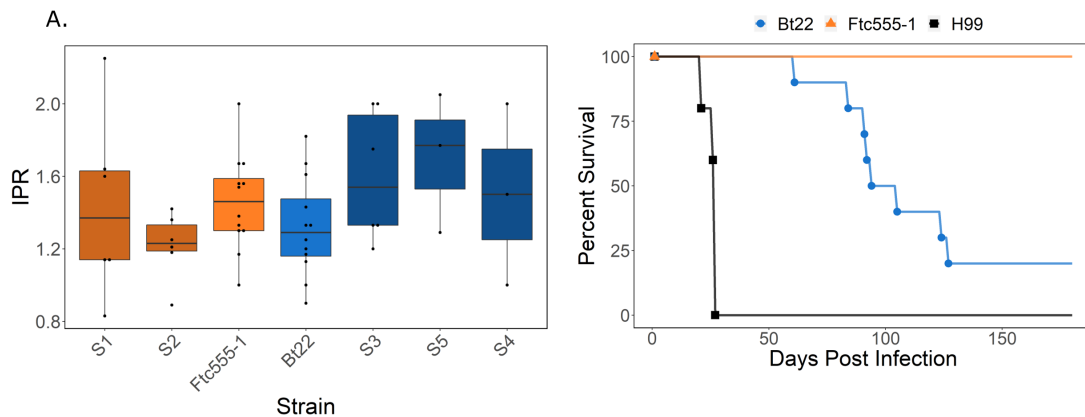


**Figure 2.7: Amoeba resistance and virulence tests do not correlate A.** Barplots representing the internal proliferation rate of parental strains and segregants. Boxplots are colored by the chromosome 8 allele. Orange boxes have the Ftc555-1 allele and blue have the Bt22 allele, darker colors indicate segregants. Dots represent individual measurements. Strains are oriented in rank order of amoeba resistance (highest to lowest resistance). Significance determined by ANOVA  $p = 0.29$   $F = 1.28$ . **B.** Mouse survival curves for the parental strains and a group of segregants. H99 is in black, Ftc555-1 is in orange, and Bt22 is in blue.

In order to explore the relationship between amoeba resistance and the ability to cause disease in animal models, we intranasally infected an equal number of 4-5 week old male and female A/J mice with offspring from the *C. neoformans* cross,

the parental strains, and the reference strain H99. Mouse survival was monitored for a period of 179 days, with mice sacrificed based on disease progression symptoms (Fig. 2.7B). Though our analysis involve only a modest number of strains, we observed no relationship between *BZP4* genotype and virulence in mice. The virulence of the parental strains, Bt22 and Ftc555-1, is in the opposite direction of their amoeba resistance phenotypes. Bt22, which exhibits low resistance to amoeba predation, has modest virulence with a time to 50% lethality (LT50) of ~92 days. This is in stark contrast to Ftc555-1, which is highly resistant to amoeba, but is completely avirulent in the mouse model of infection we employed. The reference strain, H99, is strongly virulent (LT50 ~21 days) but has very low amoeba resistance. Furthermore, we detected no association between LT50 estimated from mouse survival curves and the *BZP4* genotype of a small number of segregants (Fig. 2.7B, Fig. S5B).

Finding a lack of correlation between amoeba resistance and virulence for strains from our mapping population, we broadened our analyses to include an additional nine, genotypically diverse *C. neoformans* strains. Using the same intranasal mouse infection model described above, we found that virulence was highly variable among strains, but again we found no correlation between amoeba resistance and LT50 measures of mouse survival (Fig. S5A) (Farrer *et al.*, 2016).

We then sought to understand if amoeba success predicts the ability to cause disease in animal models. We intranasally infected an equal number of 4-5 week old male and female A/J mice with a select group of segregants and the parental strains. We allowed the experiment to run for 179 days, sacrificing mice based on disease progression symptoms. We find that the chromosome 8 QTL does not correlate with virulence in mice. The virulence of the parent strains, Bt22 and Ftc555-1, was in the opposite direction of amoeba resistance, and we detected no association between LD50 values estimated from mouse survival curves and *BZP4* genotype in segregants

(Fig. 2.7B). Bt22 is not a highly virulent strain in relation to H99; however it will kill mice if given enough time. This is in stark contrast to Ftc555-1, which is highly resistant to amoeba, but is completely avirulent in the mouse model of infection we employed.

Finding a lack of correlation between amoeba resistance and virulence for strains from our mapping population, we broadened our analyses to include an additional nine, genotypically diverse *Cryptococcus neoformans* strains. Using the same intranasal mouse infection model described above, we found that virulence was highly variable among strains, but similar to the analyses of segregants from the Bt22  $\times$  Ftc555-1 cross, there was no correlation between amoeba resistance and LD50 measures of mouse survival (Fig. 2.7C).

## 2.4 Discussion

Our findings provide novel insights into the genetic architecture of fungal-amoebal interactions and the potential impact of selection for amoeba resistance on *Cryptococcus* virulence. Using QTL mapping, we identified a transcription factor, *BZP4*, that is important for *C. neoformans* survival in the presence of amoeba. This gene also affects melanization, a classical virulence trait that is considered important for the pathogenic abilities of *Cryptococcus* (Fan *et al.*, 2005; Nosanchuk *et al.*, 1999; Doering *et al.*, 1999; Liu *et al.*, 2021). Despite its role in mediating interactions with amoeba and the production of melanin, allelic variation at *BZP4* is not predictive of proliferation rates in macrophages or virulence in mouse models of infection. This suggests that the relationship between resistance to amoeba and virulence potential may be more complex than the accidental pathogen hypothesis predicts.

Another striking outcome of our study is the discovery of an amoeba resistance QTL in homologous genomic regions for both *C. neoformans* and *C. deneoformans*. Cross species QTLs are rare, but they have been found for drought resistance between species of legume (Chai *et al.*, 2017), a cardiovascular disease marker between humans and baboons (Tejero *et al.*, 2008), and gravitropism in corn and *Arabidopsis* (Yoshihara *et al.*, 2022). Our study marks the first detection of cross species QTL in fungi and it suggests that the amoeba survival mechanisms we discovered may be conserved between different pathogenic species of *Cryptococcus*. We have not, as yet, identified the specific causal variant for the amoeba QTL in *C. deneoformans*, though non-coding variants in the vicinity of *BZP4* are among the top candidates we intend to pursue in future work.

The importance of strain background prompted us to further investigate the results of a prior GWAS analysis that implicated *BZP4* loss-of-function mutations with

reduced melanization capacity (Desjardins *et al.*, 2017). In our re-analysis of the large set of sequenced genomes from this study, we noted that *BZP4* loss of function is found only in strains isolated in clinical settings. This corroborates a similar finding that reduced expression of *BZP4* is unique to clinical strains (Yu *et al.*, 2020). Furthermore, each of the candidate *BZP4* loss-of-function mutations we identified appears to be both independent and recent based on comparison to closely related strains. These observations lead us to speculate that *BZP4* loss-of-function mutations may actually be advantageous during human infection. If this is true, this would further call into question the connection between amoeba resistance and virulence.

Our findings share a mix of both similarities and differences to a recent study by Fu *et al.* that employed experimental evolution to identify phenotypes and mutations selected for during *Cryptococcus* co-culture with amoeba (Fu *et al.*, 2021). A reduction in melanization was one of the phenotypic changes they observed that was most consistent across the three genetic backgrounds studied. This is in opposition to our findings, where we found that melanization was correlated with *higher* resistance to amoeba. However, similar to what we report here, their study failed to detect an association between amoeba resistance and macrophage challenge or virulence in mice. A particularly interesting genotypic change that Fu *et al.* identified in three independently evolved populations, derived from the H99 strain background, was duplications of chromosome 8. In light of our current study, the effect of a duplication of *BZP4*, which is located on chromosome 8, cannot be ignored as a potential positive effect of this duplication on amoeba resistance.

In our *C. neoformans* mapping population, we observed a positive, but non-linear relationship, between amoeba resistance and melanization, and *BZP4* is a candidate QTG for both of these traits. This begs the question, "Do differences in melanization mediate variation in amoeba resistance?" Several lines of evidence suggest that this

may only be part of the story. We found that *BZP4* is differentially expressed, as a function of *BZP4* genotype, in both control and amoeba conditions. *BZP4* is a transcriptional activator of *LAC1*, the gene responsible for the enzyme laccase that catalyzes the reaction of dopamine to melanin in *Cryptococcus* (Zhu and Williamson, 2004); however, *LAC1* expression, and the expression of other key genes in the melanin synthesis pathway, do not vary as a function of *BZP4* genotype in the V8 media conditions used to co-culture amoeba and *Cryptococcus*. In addition, we did not observe melanization of *Cryptococcus* on V8 media, regardless of the presence or absence of amoeba. This is in contrast to our finding that amoeba resistance broadly correlates with melanization, and the observation that *BZP4* loss-of-function strains that rapidly melanize have increased amoeba resistance. This lead us to propose a model in which *BZP4* affects amoeba resistance through both melanin dependant and melanin independent mechanisms. Among the pathways that *BZP4* could affect amoeba resistance outside of melanin synthesis, *BZP4* has been found to positively regulate thiol-dependent ubiquitinyl hydrolase activity and negatively regulate aldo/keto reductase activity (Lee *et al.*, 2019b). Future studies that characterize the transcriptional targets of *BZP4*, such as through ChIP-seq analysis, will be critical to weigh these alternate hypotheses and reconcile the relative contribution of melanin synthesis and other process to amoeba resistance.

Our discovery of QTLs for amoeba resistance in homologous genomic regions in both *C. neoformans* and *C. deneoformans*, suggests that amoeba resistance mechanisms may be conserved in the *Cryptococcus* genus. If the transcription factor *BZP4* is a key player in mediating escape from amoeba, as our evidence supports, an interesting question is whether *BZP4* function is an absolute requirement. Two clinical isolates, Bt102 and Bt103, suggest that this is not the case. These strains have predicted *bzp4* loss-of-function mutations, but were highly resistant to killing by amoeba.

This could be due to allelic variation acting either downstream of *BZP4* or in a pathway parallel to *BZP4* that also helps to regulate amoeba resistance. This further emphasizes the importance of strain background in understanding the broader implications of gene function.

In summary, the transcription factor *BZP4* is important for the survival of *Cryptococcus* when exposed to phagocytic amoebae. Despite the importance of *BZP4* in amoeba resistance, *BZP4* function is not correlated with survival in macrophages nor is it predictive of virulence in mice. Furthermore, *BZP4* function may be selected against in some clinical isolates of *Cryptococcus*, which would suggest that amoebae and mammalian hosts are competing, rather than complementary, selective environments. While interactions with amoebae cannot be ruled out as a contributing factor to the evolution of *Cryptococcus* virulence, our findings suggest that phagocytic amoebae and phagocytic immune cells, despite their many parallels, are distinct niches from the perspective of fungal survival.

## 2.5 Materials and methods

### Strains, Laboratory Crosses and Isolation

All strains were maintained on yeast peptone dextrose (YPD) plates grown at 30°C for 48 hours from -80°C stocks. Overnight cultures for amoeba assays, melanin assays, and RNA isolation were made in liquid YPD at 30°C on a rotor drum. Melanization was assayed by growing strains on minimal media plates with L-DOPA (7.6 mM L-asparagine monohydrate, 5.6 mM glucose, 10 mM MgSO<sub>4</sub>, 0.5 mM 3,4-dihydroxy-L-phenylalanine, 0.3 mM thiamine-HCl, and 20 nM biotin) for 72 hours. Plates were then scanned on an Epson Expression XL Flatbed Scanner in reflective mode at 300 dpi. ImageJ was used to calculate greyscale intensity of the colonies. Each sample was measured in triplicate.

### Amoeba Resistance Assay

*C. neoformans* and *C. deneoformans* strains were grown overnight in 3 mL of liquid YPD on a roller drum before being diluted down to OD 0.6. 100 µL of diluted culture was spread on solid V8 media petri dishes using glass beads. Plates were grown at 30°C for 60 hours before being removed from the incubator. *Acanthamoeba castellanii* (ATCC 30234) were grown in ATCC 712 in a 75 mL tissue culture flask. Amoeba were harvested, between passage 5 and 15, from flasks and suspended at a concentration of 10<sup>6</sup> cells/mL before 50 µL of amoeba culture were pipetted onto the center of the *Cryptococcus* lawn. Plates were allowed to dry at room temperature on the bench top for 10 minutes and then placed in a 25°C incubator for 12 - 18 days. Measurements were taken at days 1, 12, and 18. Area of clearance was calculated by subtracting the day 1 measurement from the final day measurement as the day 1 measurement represented the initial spread of the amoeba culture on the plates. Two

final time points were used (12 and 18 days) based on amoeba replication rate and activity. Rank order of amoeba affect was conserved between days 12 and 18.

### **Spore Dissection**

Meiotic progeny were recovered by microdissection of random basidiospores as previously described (Sun *et al.*, 2019). Briefly, cells from the two parental strains were each resuspended in sterile water to a density of OD600=1.0. Equal volumes of cell suspensions were mixed, and 5  $\mu$ L of the mixture, as well as the two parental strains (serving as negative controls of mating), were spotted onto MS solid medium. The MS plates were incubated in the dark at room temperature ( 23°C for two weeks, at which time robust hyphae, basidia, and basidiospore chains were produced by the spots from the mixture of the two parental strains. Basidiospores from a large number of basidia in one location along the edge of the mating spot were picked directly from the MS plates using the needle of a dissection microscope each time, then transferred and separated onto YPD solid medium. To reduce the chances of sampling clones from the same basidia, we only separated limited numbers of basidiospores from one location (<5%), and sampled multiple locations, as well as from multiple mating spots.

### **DNA extraction, Library Preparation, and Sequencing**

DNA was extracted with MasterPure Yeast DNA Purification kit and cleaned up the Zymo Research Genomic Clean and Concentrator kit (following manufacturer's instructions) followed by quantification with PicoGreen. After quantifying the DNA with PicoGreen, samples were prepped for genomic sequencing using seqWell's plexWell 96 kit to prepare the libraries. Briefly, samples were individually bar-coded in sets of 96 using randomly inserted transposons, pooled, and then purified. Next,

each pooled sample was bar-coded, enriched, and finally size-selected purified. Libraries were sequenced at Duke University’s Sequencing and Genomic Technologies Facility on the NovaSeq 6000 S-Prime with 150 basepair paired end reads. Reads were aligned to the H99 *C. neoformans* reference genome using BWA. Variant calling was carried out using SAMtools and Freebayes.

### **Segregants Filtering and SNP Filtering**

Segregants were filtered to remove aneuploidy and clonality described in detail in Roth *et al.* (2018). Of the original 384 segregants we were left with 304 after filtering. Variant sites were filtered based on read depth, allelic read depth ratio, quality scores, and minor allele frequency as described in Roth *et al.* (2021). Total number of bi-allelic variant sites prior to filtering was 59,430 that were reduced down to 46,670 after filtering.

### **QTL Mapping**

The 46,670 genetic variants were combined into 4,943 haploblocks, defined by linkage, using methods described previously by Roth *et al.* (Roth *et al.*, 2021). For association testing of amoeba resistance and melanization, a Mann-Whitney U test was used across these 4,943 haploblocks to associate phenotype and genotype, coding the Bt22 and Ftc555-1 genotypes as zero and one respectively. The  $-\log_{10}$  (p-value) from the Mann-Whitney U tests was monitored to identify QTL and 95% confidence intervals were calculated using permutation testing, a thousand times with replacement (Visscher *et al.*, 1996).

## Permutation Testing

Permutation testing was carried out as described in Churchill and Doerge (1994) and Roth *et al.* (2021) for establishing significance thresholds for QTL mapping. A thousand permutations were used for the melanin and amoeba phenotypes. Random assignments of genotype and phenotype were held constant for every condition tested to preserve autocorrelation between phenotypes. The 95<sup>th</sup> percentile of the permuted null distribution were used as the threshold for significance.

## RNA Isolation and Sequencing

12 segregants and duplicates of the parental strains were used for the analyses comprising 16 individual samples. Samples were grown overnight in liquid YPD on a rollerdrum and were added to V8 petri dishes. V8 cultures were grown at 30°C for 60 hours. Amoeba cultures were collected and suspended at a concentration of  $1 \times 10^6$  cells/mL. 450  $\mu$ L of amoeba culture was added to the center of the *Cryptococcus* lawn with slight agitation to aid in the spread of the culture. Plates were allowed to dry on the benchtop for 30 minutes before being incubated at 25°C for 48 hours. A consistent area of 30 cm<sup>2</sup> was cut from the plates and then scraped to collect cells. Collected cells were resuspended in 1 mL of PBS and were placed in dry ice for 10 minutes. Samples were then lyophilized for 12 - 18 hours. Whole RNA was extracted using the RNeasy Plant Mini Kit (Qiagen 74904).

Control samples did not have amoeba added to them, but were handled in a similar fashion in every other aspect of the protocol.

Libraries were prepared and sequenced by the Duke sequencing core using the Illumina NextSeq 500 High Output Kit producing 150-basepair paired end reads.

## **RNAseq Analysis**

Reads were aligned using the CNA3 of H99 *C. neoformans* var. *grubii* (accession GCA\_000149245.3). from the Ensemble Fungi database. Reads were aligned using Kallisto.

Analysis of RNA sequences was performed using Deseq2 in R. Briefly, transcript abundance was normalized using a built in median of ratios method. Samples were normalized based on condition (amobea or control). GO term analysis was performed using the fungidb GeneByLocusTag tool.

## **Tissue Culture**

The J774A.1 macrophage cell line was cultured in T-75 flasks [Fisher Scientific] in Dulbecco's Modified Eagle medium, low glucose (DMEM) [Sigma-Aldrich], supplemented with 10% live fetal bovine serum (FBS) [Sigma-Aldrich], 2mM L-glutamine [Sigma-Aldrich], and 1% Penicillin and Streptomycin solution [Sigma-Aldrich] at 37°C and 5% CO<sup>2</sup>.

## **Phagocytosis Assay**

To measure the phagocytosis of various *Cryptococcus* segregants by macrophages, J774A.1 cells were seeded at a density of  $1 \times 10^5$  cells per well of a 24-well plate [Greiner Bio-One], then incubated overnight at 37°C and 5% CO<sup>2</sup>. At the same time, an overnight culture of *C. neoformans* parental strains or segregants was set up by picking a fungal colony from YPD agar plates (50g/L YPD broth powder [Sigma-Aldrich], 2% Agar [MP Biomedical]) and resuspending it in 3mL liquid YPD broth (50 g/L YPD broth powder [Sigma-Aldrich]). The culture was then incubated at 25°C overnight under constant rotation (20rpm).

On the day of the assay, macrophages were activated using 150ng/mL phorbol 12-myristate 13-acetate (PMA) [Sigma-Aldrich] for 1 hour at 37°C. PMA stimulation was performed in serum-free media to eliminate the contribution of complement proteins during phagocytosis. To prepare *C. neoformans* for infection, overnight *C. neoformans* cultures were washed two times in 1X PBS, counted using a hemacytometer, and fungi was incubated with macrophages at a multiplicity of infection (MOI) of 10:1. The infection was allowed to take place for 2h at 37 °C and 5% CO<sup>2</sup>. After 2h infection, as much extracellular *Cryptococcus* as possible was washed off using 1X PBS.

### **Fluorescent Microscopy Imaging**

The number of phagocytosed fungi was quantified from images from a fluorescent microscope. To distinguish between phagocytosed and extracellular *C. neoformans*, wells were treated with 10 g/mL calcofluor white (CFW) [Sigma-Aldrich] for 10mins at 37°C. The wells were washed again with PBS to remove residual CFW. Fluorescent microscopy images were acquired at 20X magnification using the Nikon Eclipse Ti inverted microscope [Nikon] fitted with the QICAM Fast 1394 camera [Hamamatsu]. Images were analysed using the Fiji image processing software [ImageJ]. To quantify the number of phagocytosed *Cryptococcus* from the resulting images, the total number of ingested *C. neoformans* was counted in 200 macrophages, then the values were applied to the following equation: ((number of phagocytosed *C. neoformans*/number of macrophages) \* 100).

### **Intracellular Proliferation Rate Assay and Time-lapse Imaging**

To investigate the intracellular proliferation rate (IPR) of *Cryptococcus* strains within macrophages, infected macrophages were captured at a regular interval over an ex-

tended period. Time-lapse imaging was performed by running the phagocytosis assay as usual, then after washing off extracellular *Cryptococcus* with 1X PBS, serum-free culture media was added back into the wells before imaging. Images were captured using the Nikon Eclipse Ti microscope at 20X magnification. Images were acquired every 5 minutes for 18 hours at 37 °C and 5% CO<sub>2</sub>.

The resulting video was analysed using Fiji [ImageJ] and IPR was determined by quantifying the total number of internalised fungi in 200 macrophages at the ‘first frame’ (time point 0 (T0)) and ‘last frame’ (T10). The resulting values were used in the following equation: ((number of phagocytosed *C. neoformans*/number of macrophages) \* 100). Next, the number of phagocytosed fungi at T10 was divided by the number of phagocytosed fungi at T0 to give the IPR (IPR = T10/T0).

## **Mouse Infections**

Mouse Infections *Cryptococcus* strains for inoculation were grown overnight in 5 ml of YPD broth at 30°C in a roller drum. Cells were pelleted by centrifugation and washed twice with sterile PBS. The cell pellet was resuspended in PBS, diluted, and counted by hemocytometer. The final inoculum was adjusted to a cell density of 4 x 10<sup>6</sup> CFU/ml. Test groups consisting of five male and five female A/J mice aged 4-5 weeks were purchased from Jackson Labs (stock #000646) and infected via intranasal instillation. Mice were anesthetized using isoflurane administered with a calibrated vaporizer. 25 µl of the prepared inoculum was pipetted into the nares one drop at a time until the full volume containing 10<sup>5</sup> CFU was inhaled. Mice were observed until fully recovered from anesthesia. Following infection, mice were monitored daily for symptoms of disease progression including weight loss, labored breathing, lack of grooming, social isolation, and any signs of pain or distress. Mice were euthanized upon reaching humane endpoints according to guidelines set forth by Duke’s Animal

Care and Use Program. Survival curves were plotted using GraphPad Prism version 8 and analyzed using log-rank (Mantel-Cox) statistical test.

### **Ethics Statement**

Animal experiments were performed under Duke protocol number A148-19-07, in accordance with guidance issued by Duke's Institutional Animal Care and Use Committee and the U.S. Animal Welfare Act. Animals were housed in facilities managed by veterinary staff with Duke Lab Animal Research (DLAR) and accredited by the Association for Assessment and Accreditation of Laboratory Animal Care (AAALAC).

# Pleiotropy between High Temperature, Low pH, and Antifungal Growth

## 3.1 Author contributions

Genetic progeny and raw sequencing data were generated by my collaborators Sheng Sun and Debra Murray. Variant calling and alignments were performed by Paul Magwene. Genome assemblies and curve fitting were performed by Cullen Roth. QTL analysis was performed in collaboration with Cullen Roth. Experiments in YNB were performed by Debra Murray.

Research reported in this chapter was supported by the National Institute of Allergy and Infectious Diseases of the National Institutes of Health under award number R01AI133654. The content is solely the responsibility of the authors and does not necessarily represent the official views of the National Institutes of Health.

## 3.2 Introduction

Chapter two concentrated on biotic factors involved in the accidental pathogen hypothesis. In this chapter I aim to understand two important stress response mechanisms involved in both biotic and abiotic environments, thermal and low pH tolerance.

Thermal tolerance, specifically for high temperatures, is an integral virulence phenotype for fungal pathogens (Robert and Casadevall, 2009; Bergman and Casadevall, 2010). Endothermy close to or above human body temperature is restrictive for fungal growth. This is illustrated by the reduction in the number of fungal pathogens that are able to infect animals with body temperatures above 35°C (Robert *et al.*, 2015). Within the genus *Cryptococcus*, the ability to grow at human body temperature sep-

arates non-pathogenic species from those that are pathogenic (Findley *et al.*, 2009). High temperature growth has been hypothesized to facilitate long distance dispersal of *Cryptococcus*, through passage in birds, which have average body temperatures close to 40°C (Johnston *et al.*, 2016); however, it is also possible that thermal tolerance evolved entirely independent of animal interaction. *C. neoformans* and *C. deneoformans* are both globally distributed organisms, and the ability to withstand varying temperatures is vital to their environmental persistence (May *et al.*, 2016).

Loss of genes responsible for high temperature growth results in attenuated virulence (Findley *et al.*, 2009; Perfect, 2006). This loss of virulence is both related to temperature intolerance and the loss of other virulence factors, because thermal tolerance is a highly polygenic trait involving many stress response pathways (and Joseph Heitman Yong-Sun Bahn, 2005; Stempinski *et al.*, 2021). Key stress signalling pathways, including the high osmolarity glycerol (HOG), calcineurin, Rim101, and Ram pathways, are all thermo-regulated (Yang *et al.*, 2017). These pathways influence virulence as well as mating and environmental survival.

Thermal tolerance is an ideal candidate phenotype for quantitative genetic studies. The polygenic nature of thermal tolerance offers the potential to find a multitude of associated genes (Perfect, 2006). Concurrently, pathways that modulate thermal tolerance are often pleiotropic, offering the potential to discover genes involved in multiple important virulence traits (and Joseph Heitman Yong-Sun Bahn, 2005; Chen *et al.*, 2013). Thermal tolerance is also variable in *Cryptococcus* (Martinez *et al.*, 2001; Cordero *et al.*, 2018; Roth *et al.*, 2021). Variation in thermal tolerance has been linked to latitude, providing a clear role for environmental selection for different traits in regulating temperature (Cordero *et al.*, 2018). Exploiting this variation will provide links between thermal tolerance and other clinically relevant traits of interest.

In a previous study from the Magwene lab, allelic variation in the gene *RIC8*

was identified as contributing to variation in thermal tolerance in *C. deneoformans* (Roth *et al.*, 2021). *RIC8* is an activator of cyclic-AMP – Protein Kinase A (cAMP-PKA) signalling. Roth *et al.* identified a *RIC8* stop gain allele resulting in impaired thermal tolerance, melanization, capsule size, and H<sub>2</sub>O<sub>2</sub> resistance, exemplifying the pleiotropic nature of genes involved in thermal tolerance.

Similar to high temperature stress, growth in acidic conditions (< pH 5) negatively impacts the growth of *C. neoformans* (DeLeon-Rodriguez and Casadevall, 2016). Low pH resistance is facilitated by a number of virulence factors, including ureases, capsule, and melanin (Fu *et al.*, 2018; Leon-Rodriguez *et al.*, 2018; Wang *et al.*, 1995). During pathogenesis, *C. neoformans* cells are engulfed by macrophages where they are exposed to pH in the range of 4.2 – 5 in the phagolysosome (Levin *et al.*, 2016; Fu *et al.*, 2018; DeLeon-Rodriguez and Casadevall, 2016). Survival in macrophages is integral to the survival and spread of *C. neoformans* during infection; thus the expression of virulence factors that reduce pH and increase pH tolerance are indispensable. When engulfed by amoeba *Cryptococcus* experience similarly acidified phagolysosomes as in macrophages necessitating the use of similar tools to de-acidify the compartment (Aubry *et al.*, 1993; Akya *et al.*, 2009; Rayamajhee *et al.*, 2022). In the environment, *C. neoformans* is also exposed to a wide range of acidic and basic conditions. Bird guano, a favored environment of *Cryptococcus*, exhibits pH values in the range 4 – 8 (Spennemann *et al.*, 2017). These observations suggest that without the ability to resist acidic conditions, *C. neoformans* would not be able to cause disease or persist in its preferred environmental niches.

Temperature tolerance and pH resistance are, genetically, quite closely related. The calcineurin pathway regulates both stress responses, and the polysaccharide capsule and melanization characteristic of *Cryptococcus* contribute to resistance to both (Odom *et al.*, 1997; Chen *et al.*, 2012; Leon-Rodriguez *et al.*, 2018; Wang *et al.*, 1995).

Studying these pathways together has the added benefit of providing a window into the naturally occurring genetic variation that is both shared and specific to these phenotypes.

In this study, I employ quantitative trait locus (QTL) mapping to identify genomic loci that contribute to growth variation in high temperature and low pH. Using the same mapping population described in chapter two, I identified pleiotropic “general growth QTL” on chromosomes 3 and 6. I also identified thermal tolerance specific QTL on chromosomes 2 and 11, and QTL specific to low pH growth on chromosomes 1 and 10. By characterizing population growth by fitting growth curves to the Gompertz growth model, I gained additional insights into the genetic architecture of stress responses. Gompertz growth analysis revealed that the thermal tolerance QTL on chromosome 5 impacted lag time for every condition. I identify a candidate gene for the chromosome 5 QTL, *CNAG\_01111* a subunit of the *EIF3* translation initiation factor known to impact replication rate and replication initiation in other fungal species. The findings here illustrate that genes involved in general growth are both involved and predictive of success in stressful environments.

## 3.3 Results

### 3.3.1 Intraspecific Variation in High Temperature and Low pH Growth

Having shown in chapter two that neither amoeba resistance, nor melanization, impacted virulence in this mapping population, I decided to study other important phenotypes involved in environmental survival and virulence. High temperature growth and survival in acidic conditions, mimicking phagolysosomal pH, are beneficial to both environmental growth and are indispensable to pathogenesis. Using the same diverse set of strains that represent 3/4 of the *C. neoformans* lineages from chapter two, I assayed growth at 30°C, 37°C, and pH 4. Strains were grown over 72 hours in liquid YPD using a 96 well plate reader with OD measurements taken every 15 minutes. The mean growth curves are reported in figure 3.1. Total growth was determined by calculating the area under the curve for each strain.

Comparing all three conditions, the 30°C and pH 4 conditions were significantly correlated ( $R^2= 0.8986$ ) while growth at 37°C did not correlate with either of the other conditions (Fig. S6). Despite the correlation between growth at 30°C and pH 4, strains grown at pH 4 clustered into three distinct patterns of growth, displaying different dynamics in achieving a similar AUC to 30°C. The strains, Bt1, Bt65, and Bt22 all displayed an increased lag phase followed by growth that reached a higher final OD than the rest of the strains (Fig. 3.1). H99 was slow growing throughout the assay never reaching saturation. Similarly, H99 grew poorly at 30°C. Growth at 37°C was noticeably reduced compared to the other conditions also displaying increased variation between strains.

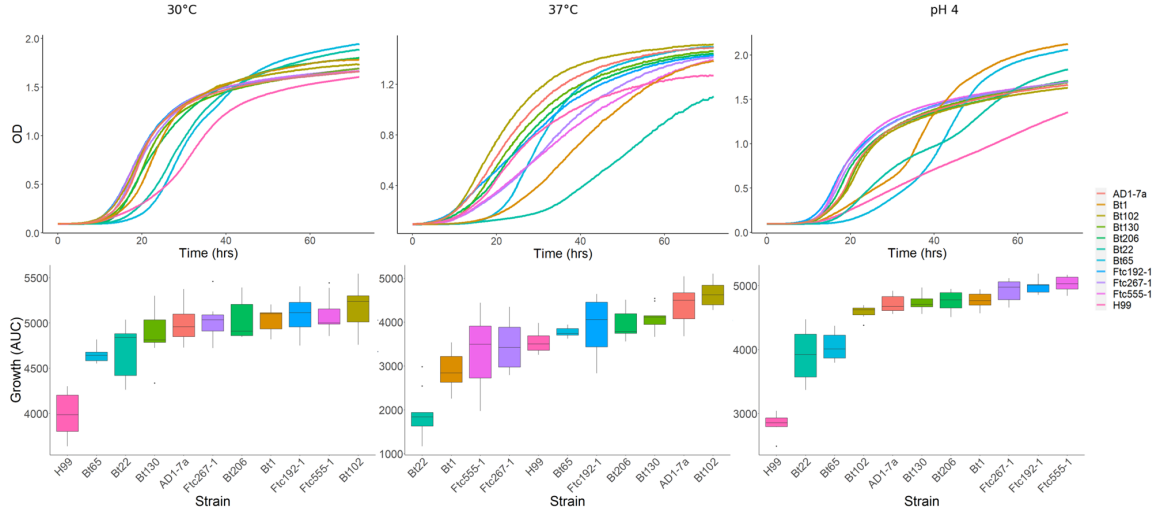


**Figure 3.1: Varying levels of intraspecific variation between diverse *C. neoformans* strains.** (Top) Growth curves for *C. neoformans* strains growth at 30°C, 37°C, and pH 4 in YPD media. Growth was carried out over 72 hours. (Bottom) Quantifications of the area under the curve (AUC) for the growth of the assayed strains. Y-axis are not held constant in this depiction to better display the diversity of 37°C growth.

### 3.3.2 Pleiotropic QTLs for General, High Temperature, and Low pH Growth

Using the same mapping population from the Bt22  $\times$  Ftc555-1 cross described in chapter two, I assayed the growth of each segregant at 30°C, 37°C, and in pH 4 (Fig. 3.2). At 30°C and in pH 4, 57% and 44% of the segregants respectively exhibited phenotypes intermediate of the parental phenotypes, indicating substantial transgressive segregation. A subset of the segregants grown at pH 4 displayed the slow start, high final OD phenotype that some of the strains, including Bt22, displayed in the initial assay. Surprisingly, 47% of the segregants grown at 37°C exhibited positive transgressive segregation. Many of the segregants that outgrew Ftc555-1 at 37°C grew close to the same max OD as those growing at 30°C (Fig. 3.2).

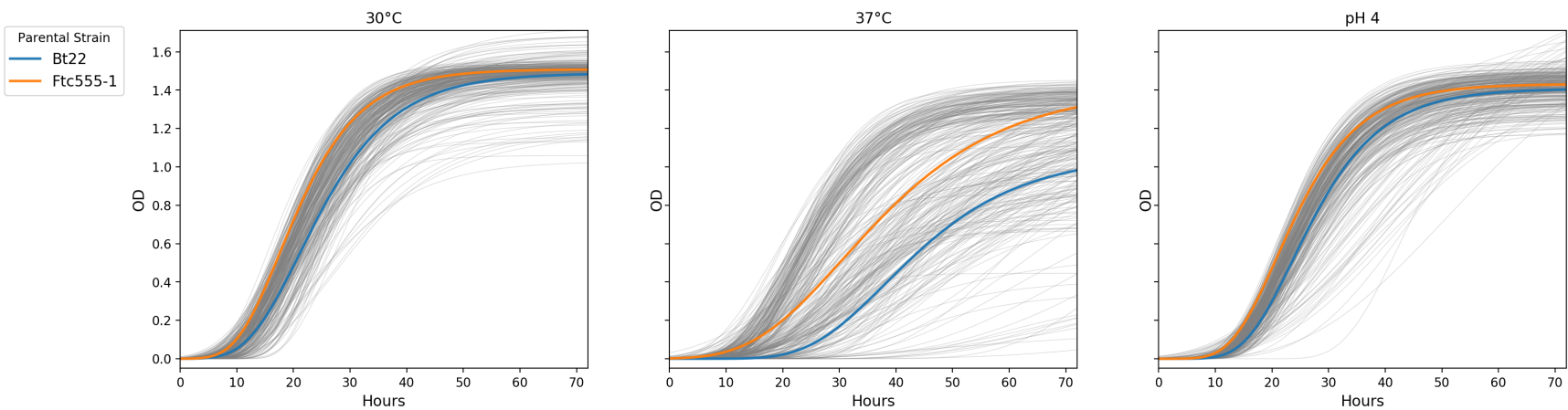


**Figure 3.2: Varying levels of transgressive segregation for segregants of the Bt22 × Ftc555-1 cross.** Mean growth curves for the Bt22 × Ftc555-1 mapping population grown at 30°C, 37°C, and pH 4. Parental growth curves are in orange for Ftc555-1 and blue for Bt22. Segregant phenotypes are in gray.

Utilizing the same marker based QTL mapping approach from chapter two, I identified six unique QTL across the three phenotypes. The QTL identified on chromosomes 3 and 6 were determined to be “general growth QTL” as they contribute to variation across conditions (Fig. 3.3). The chromosome 3 and 11 general growth QTL are actually the same QTL, both residing on chromosome 3. This is a result of using H99 as the reference genome for alignment. H99 has a translocation that occurs between chromosome 3 and 11, and this QTL falls within that translocation area (Morrow *et al.*, 2012). The chromosome 3 QTL explains between 10% (pH 4) and 12% (37°C) of the variance in growth. Based on 95% confidence intervals the chromosome 3 QTL is 291 kb and it contains 254 genes, 98 of which have a characterized function (Table S3). The other 156 genes under the peak are hypothetical. The chromosome 6 general growth QTL explains between 6% (30°C) and 10% (37°C) of the growth variance. Notably, the 95% confidence interval for 37°C growth is 20 kb upstream of the other phenotypes. The chromosome 6 QTLs overlap in all three phenotypes, however I cannot rule out the possibility that the pleiotropic effect I observed may be the result of two causal QTL in linkage. Fine mapping, either by creating mapping populations with additional recombination in this region or through functional assessment of knockouts and/or allele swaps, will be needed to distinguish between these possibilities. In table 3.1 the genes are presented in separate groups based on the separate confidence intervals. For 30°C and pH 4 the 95% confidence intervals cover 11kb that contains 3 characterized genes.

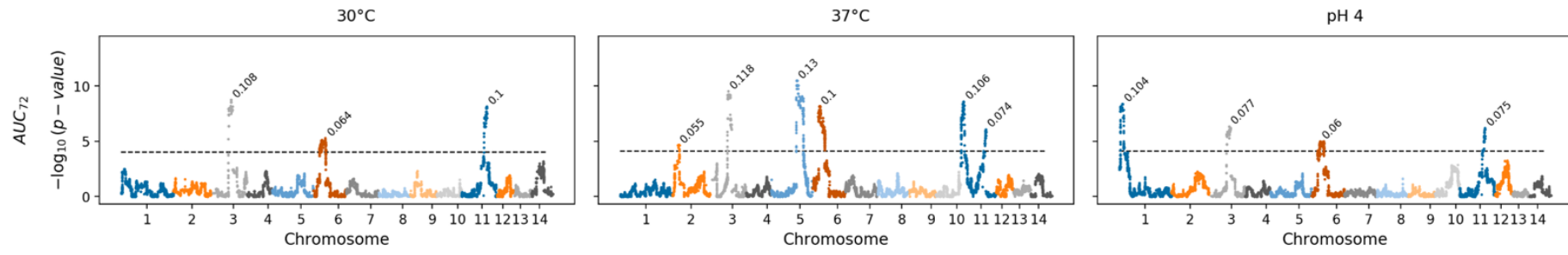


**Figure 3.3: Pleiotropic and condition specific QTL for growth in differing growth conditions.** Manhattan plots representing the association between growth in the indicated growth condition and genotype. The x-axis represents the chromosomal haploblocks and the y-axis represents the strength of association. The dotted line indicates the significance threshold  $\alpha = 0.05$  calculated using permutation testing.  $R^2$  values for maximum p-values of the peak are displayed above each QTL calculated using a one-way ANOVA.

Genes under the shared pH 4, 30°C growth QTL					
Gene ID	Phenotype	Chromosome	Gene Name	Transcript	Description
CNAG_02353	30°C, pH 4	6		CNAG_02353-t26_1	betaine lipid synthase
			CNAG_02353-t26_2	betaine lipid synthase, variant	
CNAG_02354			CNAG_02354-t26_1	large subunit ribosomal protein L2	
CNAG_02355			CNAG_02355-t26_1	solute carrier family 35 (UDP-xylose/UDP-N- acetylglucosamine transporter), member B4	
CNAG_07634			CNAG_07634-t26_1	hypothetical protein	
CNAG_12536			CNAG_12536-t26_1	unspecified product	
CNAG_12537			CNAG_12537-t26_1		
CNAG_12556			CNAG_12556-t26_1		

**Table 3.1:** Genes Under the Shared pH 4, 30°C Growth QTL

37°C growth revealed three unique QTL on chromosomes 2, 5, and 11. The QTL on chromosome 2 and 11 explain a modest 5.5% and 7.4% of growth variance. The chromosome 2 95% confidence interval is centered on the hypothetical gene CNAG\_06709. *CNAG\_06709* is homologous to the *S. cerevisiae* gene *TTI1*, a subunit of the chromatin remodelling and telomere length regulating ASTRA complex. The chromosome 11 QTL 95% confidence interval contains 65 genes, 20 of which are characterized, in a 138kb region. The gene *CNAG\_01507*, which encodes Cig121p, is the only gene with characterized function relating to temperature, in other species (Tóth *et al.*, 2018; Li and Deed, 2021). In the Ftc555-1 background *CNAG\_01507* has an early stop gain resulting in the loss of the last fourth of the protein. Notably, the metallo-beta-lactamase *CNAG\_01521* has a stop loss in the Ftc555-1 background. This gene does not have a characterized role in thermal tolerance, however.

### 3.3.3 High Temperature and Low pH Specific QTLs

The QTL on chromosome 5 for 37°C growth is in the same approximate regions as the epistatic QTL found for amoeba resistance in chapter two. This QTL has the highest effect size of the QTLs identified explaining 13% of the growth variance at 37°C. The 95% confidence interval covers 10 kb; however, the peak of the QTL covers 89 kb. I elected to survey the 39 genes under the maximal peak area despite the smaller

area of the confidence interval (Table 3.4). The confidence interval implies a smaller area than is feasible for a prediction from this  $F_1$  cross based on the recombination that I see in this region. Of the 38 genes that are under the peak, there are 15 genes with characterized function (Table 3.4). There are very few differences between alleles for genes under this peak. The one gene that stands out as a candidate QTL is *CNAG\_01111*. *CNAG\_01111* has a 9 bp deletion in Bt22 that leads the last third of the protein to have a dramatically altered amino acid sequence (Fig. 3.4). *CNAG\_01111* encodes eukaryotic translation initiation factor 3 subunit K (*EIF3k*), a non-essential subunit of the *EIF3* translation initiation factor that, when lost, often leads to noticeably reduced replication rate and initiation in some fungi (Smith *et al.*, 2013; Lin *et al.*, 2021).

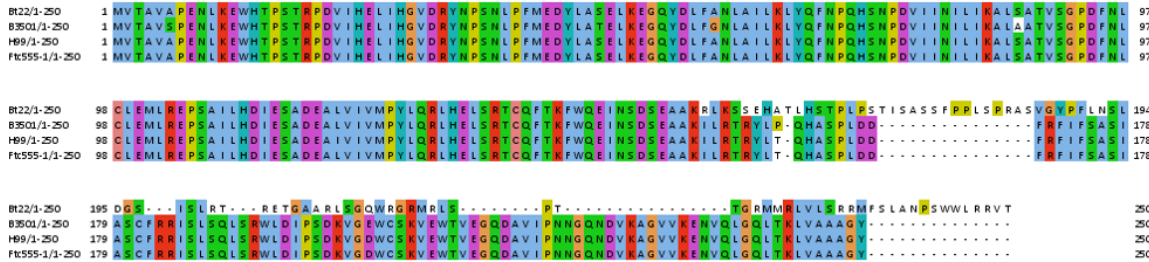


**Figure 3.4:** The *EIF3k* frameshift dramatically alters amino acid coding. An alignment of *EIF3k* between the reference strain H99, Bt22, Ftc555-1, and *Cryptococcus deneoformans* strain B3501 depicts conservation of amino acid sequence and the affects of the Bt22 frameshift.

Growth in pH 4 media revealed a unique QTL on chromosome 1 (Fig. 3.3). This QTL overlaps with the melanin epistatic QTL in the Bt22 background described in chapter two. The 95% confidence interval for the chromosome 1 QTL spans 107kb that contains 49 genes and explains 10.4% of the variance for growth at pH 4 (Table 3.2). There are a number of hypothetical genes under this peak that have frameshift mutations resulting in either early stop codons or dramatically altered amino acid coding. Of the 30 characterized genes under the peak, *ZFC6* stands out as a candidate QTL

despite not having well characterized function. It is activated by Hapx in iron limiting conditions; however, the result of this activation is unknown. Segregants with the Bt22 allele have an early stop gain that results in a loss of the last quarter of its amino acid sequence.

### 3.3.4 QTL Mapping Gompertz Growth Model Parameters Reveals Further Pleiotropy

By fitting the data to the Gompertz growth model, I sought to gain insight into the dynamics of growth in the tested conditions, seeing as growth at pH 4 displays multiple growth strategies. The Gompertz growth model describes population growth using an asymptotic logistic regression curve that represents population growth as slow at the beginning and end of a given time period (Winsor, 1932; Xu, 1987). The model provides estimates of lag, maximum growth rate, and the population maximum. QTL mapping based on the Gompertz growth model was used to identify loci involved in root development and genomic breeding estimations (Campbell *et al.*, 2020; Podisi *et al.*, 2013). I QTL mapped the Gompertz growth parameters, lag and maximum growth rate ( $\mu$ ).

Using this approach, I identified many of the same QTL found when mapping AUC (Fig. 3.6). These repeat QTL display different effect sizes than I originally found, indicating they have different relationships with growth rate and lag than AUC.

QTL mapping based on maximum growth rate revealed the chromosome 3 QTL for 30°C growth, QTL on chromosomes 2, 3, 5, 6, and 11 for 37°C growth, and QTL on chromosomes 10 and 3 for pH 4 growth. The 37°C maximum growth rate mapping revealed the same QTL as the AUC mapping. This is in stark contrast to the other conditions, as they both have fewer associated QTL for maximum growth

rate than for AUC. The effect sizes for the 37°C maximum growth rate QTL are also dramatically different to the AUC QTL. The chromosome 3, 5, and 6 QTL all explain less variance than they do for AUC. Interestingly, the thermal tolerance specific QTL on chromosome 2 and 11 increase in effect size when mapping maximum growth rate. The QTL on chromosomes 2 and 11 gained 3.4% and 3.1% variance explained respectively when mapped using maximum growth rate (Fig. 3.6). These QTL are not present when mapping lag, indicating a role in growth acceleration post initiation.

QTL mapping maximum growth rate revealed a new QTL on chromosome 10 unique to pH 4 (Fig. 3.6). This QTL has a modest effect size of 5% variance explained; however, it serves to highlight the potential to find new QTL by fitting growth data to classical models. Genes under this peak are included in table 3.2).

Interestingly, mapping based on lag time revealed QTL on chromosome 5 for 30°C growth, chromosomes 3, 5, and 6 for 37°C growth, and chromosomes 1, 3, and 5 for pH 4 growth. The consistently seen chromosome 5 QTL is the same locus found when mapping 37°C AUC, making it a “general lag QTL.” It also increases in affect size dramatically for 37°C explaining 17% of the lag time variance, increasing from 13% for AUC (Fig. 3.6). This indicates a role in growth initiation which is consistent with the function of *CNAG\_01111* in other fungal species (Smith *et al.*, 2013; Lin *et al.*, 2021). This finding also displays the utility of QTL mapping parameters of model fit data. The pleiotropy of chromosome 5 would have been lost if not for this additional analysis.

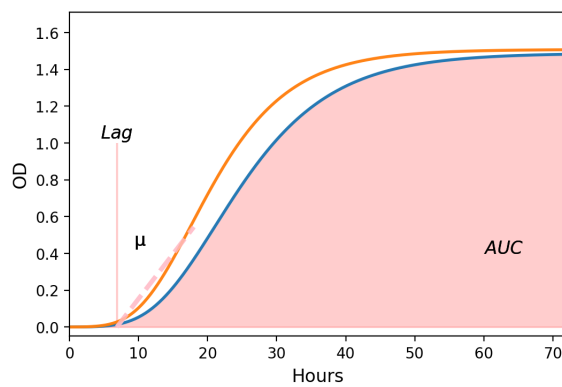


Figure 3.5: A visualization of the growth parameters used for QTL mapping.

				Genes under the pH 4 growth QTL			
Gene ID	Phenotype	Chromosome	Gene Name	Transcript	Description		
CNAG_00027	pH 4	1		CNAG_00027-126_1	transcriptional activator		
CNAG_00028				CNAG_00028-126_1	high-affinity nicotinic acid transporter		
				CNAG_00028-126_2	high-affinity nicotinic acid transporter, variant		
CNAG_00029				CNAG_00029-126_1	D-3-phosphoglycerate dehydrogenase		
CNAG_00030				CNAG_00030-126_1			
				CNAG_00030-126_2	D-3-phosphoglycerate dehydrogenase, variant		
CNAG_00031				<i>MLR1</i>	CNAG_00031-126_1	hypothetical protein, variant	
					CNAG_00031-126_2	hypothetical protein	
CNAG_00032					CNAG_00032-126_1	2,4-dihydroxyhept-2-ene-1,7-dioic acid aldolase	
CNAG_00033					CNAG_00033-126_1	hypothetical protein	
CNAG_07306					CNAG_07306-126_1		
CNAG_07307					CNAG_07307-126_1		
CNAG_07308					CNAG_07308-126_1		
CNAG_00034					CNAG_00034-126_1	large subunit ribosomal protein L9e	
CNAG_00035					CNAG_00035-126_1	hypothetical protein	
CNAG_00036					<i>SEC14-2</i>	CNAG_00036-126_1	SEC14 cytosolic factor
CNAG_00038					CNAG_00038-126_1	Alcohol dehydrogenase	
CNAG_00039					<i>ZFC6</i>	CNAG_00039-126_1	hypothetical protein
CNAG_00040					<i>ERG11</i>	CNAG_00040-126_1	cytochrome P450, family 51 (sterol 14- demethylase)
CNAG_00043						CNAG_00043-126_1	hypothetical protein
						CNAG_00043-126_2	hypothetical protein, variant
						CNAG_00044-126_1	ribosome assembly protein 1
CNAG_00044						CNAG_00044-126_1	hypothetical protein
CNAG_00045						CNAG_00045-126_1	26S proteasome regulatory subunit N8
CNAG_00046						CNAG_00046-126_1	pyruvate dehydrogenase kinase
CNAG_00047					<i>PKP1</i>	CNAG_00047-126_1	Sugar transporter
CNAG_00048						CNAG_00048-126_1	hypothetical protein
CNAG_00049						CNAG_00049-126_1	hypothetical protein
CNAG_00050						CNAG_00050-126_1	putative set3c deacetylase complex subunit
CNAG_00051					<i>SNT1</i>	CNAG_00051-126_1	
						CNAG_00051-126_2	
CNAG_00052						CNAG_00052-126_1	hypothetical protein
CNAG_00053						CNAG_00053-126_1	
CNAG_00054						CNAG_00054-126_1	
CNAG_00055						CNAG_00055-126_1	
CNAG_00056						CNAG_00056-126_1	
CNAG_00057					<i>FPP1</i>	CNAG_00057-126_1	fructose-1,6-bisphosphatase I
CNAG_00058						CNAG_00058-126_1	T-complex protein 1 subunit epsilon
CNAG_00059						CNAG_00059-126_1	hypothetical protein
CNAG_00060						CNAG_00060-126_1	chaperone regulator
				CNAG_00060-126_2	chaperone regulator, variant		
CNAG_00061			<i>CIT1</i>	CNAG_00061-126_1	citrate synthase, mitochondrial		
CNAG_00062				CNAG_00062-126_1	26S proteasome regulatory subunit N3		
CNAG_00063			<i>CSE4</i>	CNAG_00063-126_1	Histone H3		
CNAG_00064				CNAG_00064-126_1	COPII-coated vesicle protein		
CNAG_00065				CNAG_00065-126_1	ran-binding protein 1		
CNAG_00066				CNAG_00066-126_1	membrane protein		
CNAG_00067			<i>SSS1</i>	CNAG_00067-126_1	protein translocase SEC61 complex gamma subunit		
CNAG_00068				CNAG_00068-126_1	specific RNA polymerase II transcription factor		
CNAG_12006				CNAG_12006-126_1	unspecified product		
CNAG_12007				CNAG_12007-126_1			
CNAG_12008				CNAG_12008-126_1			
CNAG_12009				CNAG_12009-126_1			
CNAG_12010				CNAG_12010-126_1			
CNAG_12011				CNAG_12011-126_1			
CNAG_12012				CNAG_12012-126_1			
CNAG_12005				CNAG_12005-126_1			
CNAG_04633		10		CNAG_04633-126_1	hypothetical protein		
CNAG_04634				CNAG_04634-126_1			
CNAG_04635				CNAG_04635-126_1	endopeptidase		
CNAG_04636				CNAG_04636-126_1	metacaspase-1		
CNAG_04637			<i>MBF1</i>	CNAG_04637-126_1	multiprotein-bridging factor 1		
CNAG_04638				CNAG_04638-126_1	hypothetical protein		
CNAG_04639				CNAG_04639-126_1			
CNAG_04640			<i>ACL1</i>	CNAG_04640-126_1	ATP-citrate synthase subunit 1		
CNAG_04641				CNAG_04641-126_1	general transcription factor 3C polypeptide 3 (transcription factor C subunit 4)		
CNAG_04642			<i>TSP2</i>	CNAG_04642-126_1	tetraspanin Tsp2		
CNAG_04646				CNAG_04646-126_1	hypothetical protein		
CNAG_04647				CNAG_04647-126_1	Glutathione synthetase		
CNAG_04648				CNAG_04648-126_1	sisler chromatin cohesion protein pds5		
CNAG_04649				CNAG_04649-126_1	peptide alpha-N-acetyltransferase		
CNAG_04650				CNAG_04650-126_1	actin-like protein arp6		
CNAG_04651				CNAG_04651-126_1	hypothetical protein		
CNAG_04652				CNAG_04652-126_1	enoyl reductase		
CNAG_04653				CNAG_04653-126_1	hypothetical protein		
CNAG_04654				CNAG_04654-126_1	UNC-50 family protein		
CNAG_04655				CNAG_04655-126_1	rab family protein		
CNAG_04656				CNAG_04656-126_1	arginine-tRNA-protein transferase		
CNAG_04656				CNAG_04656-126_2	arginine-tRNA-protein transferase, variant		
CNAG_04657				CNAG_04657-126_1	Short-chain dehydrogenase		
CNAG_04658				CNAG_04658-126_1	hypothetical protein		
CNAG_04659			<i>PDC1</i>	CNAG_04659-126_1	Pyruvate decarboxylase		
CNAG_04662			<i>CTF4</i>	CNAG_04662-126_1	chromosome transmission fidelity protein 4		
CNAG_04663				CNAG_04663-126_1	hypothetical protein		
CNAG_04664			<i>MRPL37</i>	CNAG_04664-126_1	large subunit ribosomal protein L37		
CNAG_04665				CNAG_04665-126_1	hypothetical protein		
CNAG_04666				CNAG_04666-126_1	26S protease regulatory subunit 8		
CNAG_04667				CNAG_04667-126_1	hypothetical protein		
CNAG_04668			<i>UBC12</i>	CNAG_04668-126_1	ubiquitin-conjugating enzyme E2 M		
CNAG_04669				CNAG_04669-126_1	mitochondrial matrix protein import protein		
CNAG_04670				CNAG_04670-126_1	hypothetical protein		
CNAG_04671				CNAG_04671-126_1			
CNAG_04673				CNAG_04673-126_1	NAD dependent epimerase/dehydratase		
CNAG_04674			<i>ADA3</i>	CNAG_04674-126_1	transcriptional adapter 3		
CNAG_04675				CNAG_04675-126_1	hypothetical protein		
CNAG_07857				CNAG_07857-126_1			
CNAG_07999				CNAG_07999-126_1			
CNAG_08000				CNAG_08000-126_1			
CNAG_12929				CNAG_12929-126_1	unspecified product		
CNAG_12930				CNAG_12930-126_1			
CNAG_12931				CNAG_12931-126_1			
CNAG_12932				CNAG_12932-126_1			
CNAG_12933				CNAG_12933-126_1			
CNAG_12934				CNAG_12934-126_1			
CNAG_12935				CNAG_12935-126_1			
CNAG_12936				CNAG_12936-126_1			
CNAG_12937				CNAG_12937-126_1			

Table 3.2: Genes Under the pH 4 Growth QTL

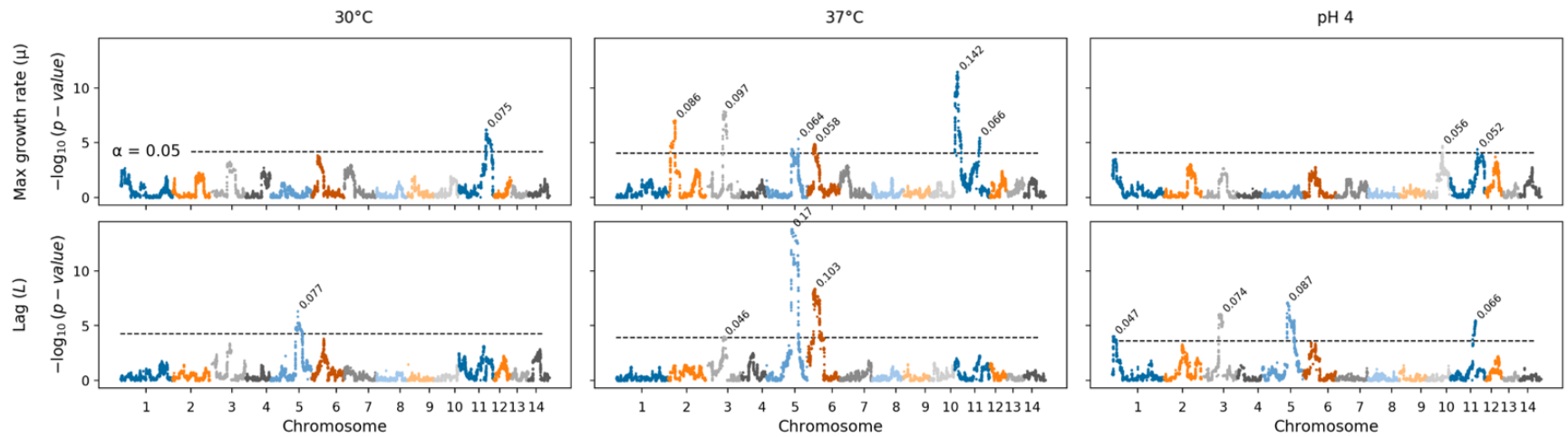
Genes under the 37°C growth QTL					
Gene ID	Phenotype	Chromosome	Gene Name	Description	
CNAG_01130	37°C	9	CNAG_01130	hypothetical protein	
CNAG_01131			CNAG_01131	hypothetical protein	
CNAG_01132			CNAG_01132	nucleolar protein 6	
CNAG_01133			CNAG_01133	mitochondrial protein	
CNAG_01134			CNAG_01134	hypothetical protein	
CNAG_12462			CNAG_12462	unspecified product	
CNAG_12463			CNAG_12463	unspecified product	
CNAG_02439			6	CNAG_02439	hypothetical protein
CNAG_02440				CNAG_02440	hypothetical protein, variant
CNAG_02441				CNAG_02441	catenin transcription 3/like
CNAG_02442	CNAG_02442	hypothetical protein			
CNAG_02443	CNAG_02443	NADH dehydrogenase			
CNAG_02444	CNAG_02444	hypothetical protein			
CNAG_02445	CNAG_02445	Phosphoenolpyruvate mutase			
CNAG_02446	CNAG_02446	response regulator receptor protein			
CNAG_02447	CNAG_02447	hypothetical protein			
CNAG_02448	CNAG_02448	hypothetical protein			
CNAG_02449	CNAG_02449	long chain fatty acid CoA ligase			
CNAG_02450	CNAG_02450	hypothetical protein			
CNAG_02451	7/FFS	CNAG_02451	unspecified product		
CNAG_02452		CNAG_02452	hypothetical protein		
CNAG_02453		CNAG_02453	unspecified product		
CNAG_02454		CNAG_02454	HAICA ribonucleoprotein complex non-core subunit NAF1		
CNAG_02455		CNAG_02455	choline transporter		
CNAG_02456		CNAG_02456	importin beta-2 subunit		
CNAG_02457		CNAG_02457	unspecified product		
CNAG_02458		CNAG_02458	GTPase activating protein		
CNAG_02459		CNAG_02459	transcription initiation factor 3 subunit C		
CNAG_02460		CNAG_02460	endonuclease		
CNAG_02461	EPP1	CNAG_02461	unspecified product		
CNAG_02462		CNAG_02462	12.5 small nuclear ribonucleoprotein B/N4		
CNAG_02463		CNAG_02463	unspecified product		
CNAG_12685		CNAG_12685	unspecified product		
CNAG_12686		CNAG_12686	unspecified product		
CNAG_12687		CNAG_12687	unspecified product		
CNAG_12688		CNAG_12688	unspecified product		
CNAG_12689		CNAG_12689	unspecified product		
CNAG_12690		CNAG_12690	unspecified product		
CNAG_12691		CNAG_12691	unspecified product		
CNAG_12692	CNAG_12692	unspecified product			
CNAG_12693	CNAG_12693	unspecified product			
CNAG_12694	CNAG_12694	unspecified product			
CNAG_12695	CNAG_12695	unspecified product			
CNAG_12696	CNAG_12696	unspecified product			
CNAG_12697	CNAG_12697	unspecified product			
CNAG_12698	CNAG_12698	unspecified product			
CNAG_12699	CNAG_12699	unspecified product			
CNAG_12700	CNAG_12700	unspecified product			
CNAG_12701	CNAG_12701	unspecified product			
CNAG_12702	CNAG_12702	unspecified product			
CNAG_12703	CNAG_12703	unspecified product			
CNAG_12704	CNAG_12704	unspecified product			
CNAG_12705	CNAG_12705	unspecified product			
CNAG_12706	CNAG_12706	unspecified product			
CNAG_12707	CNAG_12707	unspecified product			
CNAG_12708	CNAG_12708	unspecified product			
CNAG_12709	CNAG_12709	unspecified product			
CNAG_12710	CNAG_12710	unspecified product			
CNAG_12711	CNAG_12711	unspecified product			
CNAG_12712	CNAG_12712	unspecified product			
CNAG_01469	11	CNAG_01469	CSP-oligylglycerol-ester O-phosphatidyltransferase		
CNAG_01470		CNAG_01470	NADH dehydrogenase (ubiquinone) flavoprotein 2		
CNAG_01471		CNAG_01471	hypothetical protein		
CNAG_01472		CNAG_01472	endoplasmic reticulum protein		
CNAG_01473		CNAG_01473	hypothetical protein		
CNAG_01474		CNAG_01474	hypothetical protein, variant		
CNAG_01475		CNAG_01475	hypothetical protein		
CNAG_01476		CNAG_01476	sphingolipid C6-methyltransferase		
CNAG_01477		CNAG_01477	hypothetical protein		
CNAG_01478		CNAG_01478	serine palmitoyltransferase		
CNAG_01479	CNAG_01479	monooxygenase			
CNAG_01480	CNAG_01480	hypothetical protein			
CNAG_01481	CNAG_01481	large subunit ribosomal protein L13			
CNAG_01482	CNAG_01482	hypothetical protein			
CNAG_01483	CNAG_01483	soluble carrier family 25 (mitochondrial phosphate transporter), member 3/2/2/4/4			
CNAG_01484	CNAG_01484	E3 ubiquitin ligase-like protein			
CNAG_01485	CNAG_01485	D-lactate dehydrogenase (cytochrome)			
CNAG_01486	CNAG_01486	large subunit ribosomal protein L15A			
CNAG_01487	CNAG_01487	hypothetical protein			
CNAG_01488	CNAG_01488	maltose 2-epimerase			
CNAG_01489	CNAG_01489	hypothetical protein			
CNAG_01490	CNAG_01490	hypothetical protein, variant			
CNAG_01491	CNAG_01491	hypothetical protein			
CNAG_01492	CNAG_01492	unspecified product			
CNAG_01493	CNAG_01493	unspecified product			
CNAG_01494	CNAG_01494	hypothetical protein, variant			
CNAG_01495	CNAG_01495	hypothetical protein			
CNAG_01496	CNAG_01496	hypothetical protein, variant			
CNAG_01497	CNAG_01497	hypothetical protein			
CNAG_01498	CNAG_01498	myo-inositol 2-O-methyltransferase			
CNAG_01499	CNAG_01499	protein phosphatase 5			
CNAG_01500	CNAG_01500	integral membrane protein			
CNAG_01501	CNAG_01501	unspecified product			
CNAG_01502	CNAG_01502	unspecified product			
CNAG_01503	CNAG_01503	unspecified product			
CNAG_01504	CNAG_01504	unspecified product			
CNAG_01505	CNAG_01505	unspecified product			
CNAG_01506	CNAG_01506	unspecified product			
CNAG_01507	CNAG_01507	protein C6/121			
CNAG_01508	CNAG_01508	hypothetical protein			
CNAG_01509	CNAG_01509	unspecified product			
CNAG_01510	CNAG_01510	unspecified product			
CNAG_01511	CNAG_01511	unspecified product			
CNAG_01512	CNAG_01512	unspecified product			
CNAG_01513	CNAG_01513	hypothetical protein, variant			
CNAG_01514	CNAG_01514	hypothetical protein			
CNAG_01515	CNAG_01515	unspecified product			
CNAG_01516	CNAG_01516	phosphoglycerate mutase			
CNAG_01517	CNAG_01517	phosphoglycerate mutase, variant			
CNAG_01518	CNAG_01518	endonuclease/nucleoside diphosphate kinase			
CNAG_01519	CNAG_01519	histone arginine methyltransferase CARM1			
CNAG_01520	CNAG_01520	unspecified product			
CNAG_01521	CNAG_01521	metallo-beta-lactamase			
CNAG_01522	CNAG_01522	unspecified product			
CNAG_01523	CNAG_01523	hypothetical protein			
CNAG_01524	CNAG_01524	unspecified product			
CNAG_01525	CNAG_01525	unspecified product			
CNAG_01526	CNAG_01526	unspecified product			
CNAG_01527	CNAG_01527	unspecified product			
CNAG_01528	CNAG_01528	unspecified product			
CNAG_01529	CNAG_01529	unspecified product			
CNAG_01530	CNAG_01530	V-type H <sup>+</sup> transporting ATPase subunit C			
CNAG_01531	CNAG_01531	unspecified product			
CNAG_01532	CNAG_01532	mitochondrial metalloprotease OMA1			

Table 3.3: Genes Under the 37°C Growth QTL

Chromosome 5 QTL Genes				
Gene ID	Gene Name	Nonsynonymous	Nonsense	Description
CNAG_12462				unspecified product
CNAG_01132				nucleolar protein 6
CNAG_01131				hypothetical protein
CNAG_12463				unspecified product
CNAG_01130		1		hypothetical protein
CNAG_01129	<i>ERG7</i>			lanosterol synthase
CNAG_01128				Hydroxyacylglutathione hydrolase
CNAG_01127		2		hypothetical protein
CNAG_01126	<i>(SEC7)</i>	1		guanine nucleotide exchange protein for ADP-robosylation factor
CNAG_12464				unspecified product
CNAG_12465				unspecified product
CNAG_01125				hypothetical protein
CNAG_01124				hypothetical protein
CNAG_01123				DRAP deaminase
CNAG_01122				hypothetical protein
CNAG_01121				10 bp deletion in the 3' UTR hypothetical protein
CNAG_01120				pyruvate dehydrogenase complex dihydrolipoamide acetyltransferase
CNAG_12466				unspecified product
CNAG_01119				POT family proton-dependent oligopeptide transporter
CNAG_12467				unspecified product
CNAG_12468				unspecified product
CNAG_01118				AAT family amino acid transporter
CNAG_12469				unspecified product
CNAG_01117	<i>EF3</i>			elongation factor 3
CNAG_01116				beta-ketoacyl reductase; fatty acid synthesis activity (NADPH activity)
CNAG_01115				hypothetical protein
CNAG_01114				hypothetical protein
CNAG_01113				hypothetical protein
CNAG_01112				xenobiotic reductase
CNAG_01111			8 bp deletion	translation initiation factor 3 subunit K
CNAG_01110				co-chaperone
CNAG_01109				hypothetical protein
CNAG_12470				unspecified product
CNAG_12471				unspecified product
CNAG_01108	<i>DAL2</i>			Allantoicase
CNAG_01107		1		phosphatidylinositol glycan, class A
CNAG_01106	<i>VPH1</i>			9 bp deletion in intron 7 V-type H <sup>+</sup> -transporting ATPase subunit I
CNAG_01105		1		hypothetical protein

() = *Saccharomyces cerevisiae* homologous gene name

Table 3.4: Genes Under the Chromosome 5 QTL



65

**Figure 3.6: QTL mapping Gompertz growth parameters reveals further pleiotropy and condition specific QTL.** Manhattan plots representing the association between lag, maximum growth rate ( $\mu$ ), and maximum OD between the indicated condition and genotype. The x-axis represents the chromosomal haploblocks and the y-axis represents the strength of association.

### 3.3.5 The Chromosome 5 Growth QTL is Pleiotropic in YNB Media

To increase the control I have over assay conditions, I used a second media for testing growth. I chose YNB because it is a defined media. The ability to control nutrient state affords less noise in the data and reduces the potential for batch effects based on media components. Interestingly, the media change resulted in a dramatic shift in the QTL identified (Fig. 3.7).

Growth at 30°C presented with a single QTL on chromosome 5. This is the same QTL as the general lag QTL found in YPD. Notably, the chromosome 3 and 6 QTL are missing when YNB is used. At 39°C, I find QTL on chromosomes 5 and 6. This makes the chromosome 6 QTL high temperature specific and the chromosome 5 QTL a general growth QTL in YNB. Considering both YNB and YPD are complete media, it is surprising that there is a dramatic shift in the loci identified. This change in QTL presentations hints at the environmental component of QTL mapping and growth in general. In this case, the chromosome 3 QTL is specific to the YPD nutrient environment; whereas, the chromosome 5 and 6 QTL shift in how they are represented based on media. Further work is necessary to understand what is causing these QTL changes; however, it is clear that, even in permissive conditions, the genetic architecture of growth is greatly influenced by the environmental nutrient makeup.

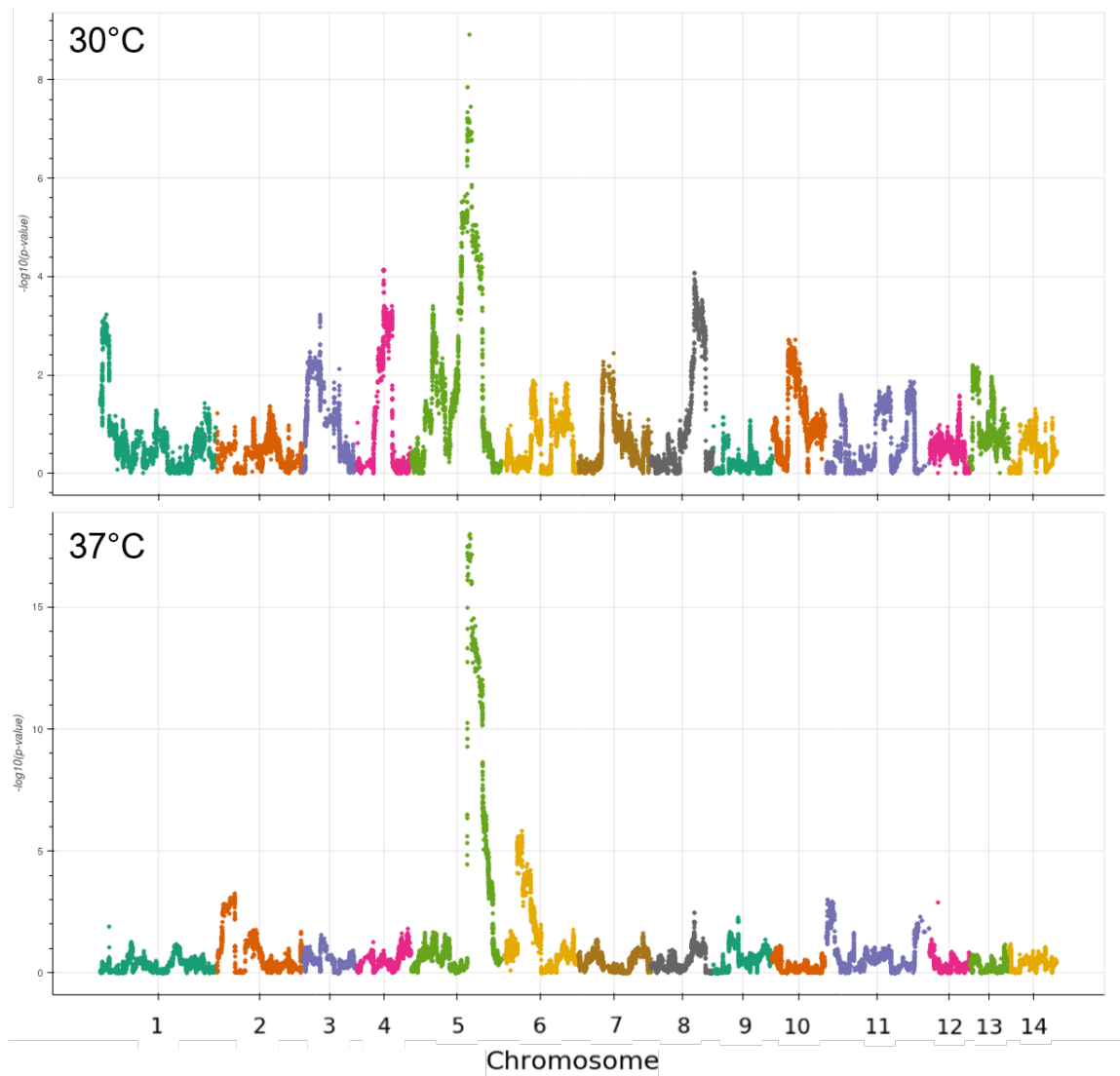


**Figure 3.7: Chromosome 5 becomes a general growth QTL in YNB.** Manhattan plots representing the association between growth in YNB at 30°C and 37°C and genotype. The x-axis represents the chromosomal haploblocks and the y-axis represents the strength of association.

### 3.4 Discussion

This study provides insight into the pleiotropy governing growth in stressful environments. By QTL mapping *C. neoformans* growth at 30°C, 37°C, and in pH 4 media, I discovered two general growth QTL, two thermal tolerance QTL, and one low pH tolerance QTL. I also demonstrate the power of fitting growth data to classical models by QTL mapping lag time and maximum growth rate, parameters derived by fitting growth data to the Gompertz growth model. Using these parameters, I discovered a maximum growth rate QTL for low pH tolerance on chromosome 10 and that a chromosome 5 QTL, originally only appearing for thermal tolerance, appears for lag in every growth environment, making it a “general lag QTL”.

My findings for high temperature specific QTL display the polygenic nature of thermal tolerance. The proteins with significant predicted changes are either hypothetical or not understood to be involved in pathways influencing high temperature tolerance. *CNAG\_01507*, which encodes Cig121p, has a predicted early stop gain in the Ftc555-1 background that significantly truncates the gene. Somewhat paradoxically, Cig121p influences low temperature growth in *S. cerevisiae* and *Candida parapsilosis* (Tóth *et al.*, 2018; Li and Deed, 2021). Previous QTL studies of thermal tolerance implicate variation in highly pleiotropic pathways. In *S. cerevisiae* genes involved in mitochondrial function are commonly found to control variation in high temperature growth (Riles and Fay, 2019; Wang *et al.*, 2019). While there are multiple genes under the chromosome 11 peak that are involved in mitochondrial function, the only gene that localizes to the mitochondria with an altered amino acid sequence is *CNAG\_07591*. This gene does not have a defined role in microbial thermal tolerance; however, it has been found to be involved in thermal adaptation in corals (Bland *et al.*, 2008; Lancaster *et al.*, 2016). A previous thermal tolerance QTL study

from the Magwene lab, in *C. deneoformans*, found a gene involved in cAMP–PKA signalling (Roth *et al.*, 2021). This QTL was pleiotropic for capsule size, melanization, and peroxide stress resistance. The pleiotropy seen in the genes found for thermal tolerance does fit with my findings for thermal tolerance QTL as general growth QTL have the highest effect sizes at 37°C.

The addition of the Gompertz growth parameter QTL mapping offered insight into the role QTL play in growth. Similar to the function valued QTL mapping from a prior study in the Magwene lab, the added information that comes from mapping based on classical growth models is also effective in dissecting the architecture of growth traits (Roth *et al.*, 2021). In the case of the QTL on chromosome 5, the common effect across growth conditions is consistent with the identification of *CNAG\_01111* as a candidate QTG. While not characterized in *Cryptococcus*, in the rice fungus *Magnaporthe oryzae Oryzae*, mutations in *Eif3k* have been found to impact growth initiation (Lin *et al.*, 2021). This finding corroborates the discovery made using the Gompertz fit, that the chromosome 5 locus is involved in lag. Since QTL regions in F<sub>1</sub> crosses tend to cover many genes, additional information, such as what phase of growth a QTL contributes most to, helps narrow down candidate genes and variants of interest.

The acid resistance QTL tell a similar story to the thermal tolerance QTL. For the QTL on chromosomes 1 and 10, there are not any candidate genes that have disrupted coding or cis-regulatory regions that are known to influence low pH tolerance or have pleiotropic signalling roles. The chromosome 1 QTL does appear to be pleiotropic for melanization, as the same QTL is found to be epistatic for melanization in chapter two. Melanin is known to impact pH tolerance; so, it is possible that the QTG under this peak influences the melanin synthesis pathway resulting in altered pH tolerance (Wang *et al.*, 1995). A prior study in *S. cerevisiae* implicated genes involved in cAMP

and HOG signalling as well as multiple genes involved in DNA integrity when QTL mapping acetic acid resistance (Stojiljkovic *et al.*, 2020). My findings also indicate that acid tolerance is a polygenic trait, as I find four QTL contribute to growth in this environment. While the role of the individual QTL need to be dissected in future work, there is a great potential to find new genes that influence important pleiotropic stress response pathways.

Looking broadly at strains in *C. neoformans*, I found that tolerance to acidic conditions is consistent across most strains. I do note that the strains Bt22, Bt1, and Bt65 shared a different growth curve shape than the other strains. This group took longer to start growing, however, they reached a higher maximal OD by the end of the experiment. This could represent a growth tactic that is advantageous in certain environments.

I was surprised to discover the change in QTL based on media change. Both media have abundant nutrients available providing a permissive environment for growth. The genotype by environment interaction changes general growth and temperature specific QTL, displaying a larger shift in QTL presentation than is seen between growth conditions using one media. This implicates nutrient environment as a larger factor in growth than high temperature or low pH stress. This raises the question of how nutrient environment is influencing the genotype–phenotype interactions I discover.

My findings in chapter three indicate genes underlying growth are highly pleiotropic. From permissive to stressful conditions, growth is influenced by a similar suite of genes with a smaller number of condition specific variants contributing to growth. In keeping with a generalist lifestyle, growth in one condition is highly predictive of growth in another. There are subtle differences to be dissected between these pleiotropic QTL, however. The QTL on chromosomes 3, 5, and 6 all have their

largest affect sizes in high temperature conditions. This is indicative of the degree of stress that high temperatures applies. That being said, the largest factor in predicting QTL seems to be nutrient conditions. Changing media from YPD to YNB drastically changed the QTL found at both 30°C and 37°C. This change in QTL landscape both serves to emphasize the impact that the chromosome 5 QTL has on general growth, and the importance of nutrient space on stress resistance.

## 3.5 Materials and methods

### Media

All strains were maintained in the same fashion as chapter two. Overnight cultures for growth assays were made in liquid YPD at 30°C on a rotor drum.

### Quantitative Growth Assays

All growth assays were carried out using TECAN absorbance microplate readers (Product number 30190079) in 96-well format using round bottom plates containing 150  $\mu$ L of YPD, 150  $\mu$ L YPD at pH 4, or 150  $\mu$ L YNB buffered with MOPS. The outer wells for the plates were not used for growth to avoid media evaporation affects, and plates were randomized with 3 replicates of each segregant per plate to account for spacial effects. Three randomizations were used for the mapping population and two were used for the study of multiple strains.

Plates were pinned from -80°C freezer stocks onto YPD omnitrays and allowed to grow at 30°C for two days before being pinned into 96-well plates with 150  $\mu$ L of YPD. 96-well plates were growth for two days at 30°C before being pinned to a second 96-well plate for the growth assay. Plates used for pH 4 growth were washed twice with pH 4 media prior to pinning to the 96-well plate used for the assay. Plates were grown in at either 30°C or 37°C for 72 hours shaking and having OD<sub>595</sub> measurements taken every 15 minutes. To prevent fogging of lids, they were washed in 0.05% Triton X-100 in 20% EtOH and were allowed to dry before the assay began.

### Growth Curve Baselineing and AUC Calculation

Growth curve baselineing and AUC calculations were performed using the same methods as Roth *et al.* (2021). In short, growth curves were baselineed by taking the average

of the blank wells around the outside of the plate and subtracting that value from the curves. The first two time points of each curve was removed. The next average of the following five timepoints were averaged and subtracted from the dataset as a baselining measure. Mean curves were then calculated for each segregants

AUC was calculated on a per segregant basis by taking the sum of OD<sub>595</sub> values across the 72 hour period and dividing it by time between measurements (15 minutes). This was performed for every condition.

### **Sequencing, Aligning, and Variant Calling**

Sequencing, Aligning, and Variant Calling are all detailed in chapter two.

### **Statistical methods**

Statistical methods for QTL mapping are described in chapter two modified here as follows. An ANOVA was applied on a per haploblock basis to establish p-values. Gompertz growth parameters were established using

$$g_t = g_0 \exp(-\exp(\mu(\exp(1)/g_0))(l - t) + 1)$$

where  $g_t$  represents the OD<sub>595</sub> at time  $t$ ,  $g_0$  represents the initial OD<sub>595</sub>,  $l$  lag time, and  $t$  represents time. This data was fit in python using the `curve_fit` function in the `scipy` package (Virtanen *et al.*, 2020). This function use non-linear least squares to optimally compute function parameters and fit data.

# *De Novo* Mutations Result in Growth Trade-off Between Heat and Fludioxonil Evolved in *Cryptococcus neoformans*

## 4.1 Author Contributions

The work presented in this chapter represents an ongoing project initially funded by the TriCEM graduate RFP.

Research reported in this chapter was also supported by the National Institute of Allergy and Infectious Diseases of the National Institutes of Health under award number R01AI133654. The content is solely the responsibility of the authors and does not necessarily represent the official views of the National Institutes of Health.

## 4.2 Introduction

Work understanding the impact of environmental stressors on the evolution of virulence traits of pathogenic fungi is becoming increasingly important. As global temperatures rise, the potential for evolved temperature tolerance, a key virulence trait, increases, and the number of fungi-friendly environmental niches multiply (Nnadi and Carter, 2021; Garcia-Solache and Casadevall, 2010). It is hypothesized that an outbreak of hypervirulent *Cryptococcus gattii* in the Pacific Northwest of North America originated as a consequence of changing climate driving adaptation to temperatures up to or exceeding the 37°C required for growth in humans. (Datta *et al.*, 2009; Nnadi and Carter, 2021). This outbreak is characterized by strains with increased thermal tolerance, illustrating the importance of understanding the routes fungi take to evolve increased heat resistance (Fernandes *et al.*, 2016).

Concurrently, global antimycotic resistance is on the rise (Fisher *et al.*, 2018).

Increases in the occurrence of antifungal drug resistance have been linked to the use of agriculture antifungal use (Takahashi *et al.*, 2020; Fisher *et al.*, 2022). In Europe and Asia, the use of azoles in agriculture correlates with a rise in azole resistance in *Aspergillus* both clinically and environmentally (Riat *et al.*, 2018; Jørgensen and Heick, 2021; Burks *et al.*, 2021). Increases in agricultural antifungal use is a growing concern for clinicians as there are few available treatments for fungal infections (Burks *et al.*, 2021). Much of the current understanding of environmentally acquired drug resistance in pathogenic fungi comes from *Aspergillus* studies (Takahashi *et al.*, 2020; Fisher *et al.*, 2022). This leaves a large gap in the understanding of how agricultural antifungals are affecting other environmental fungal pathogens. For example, in *C. neoformans* there is growing concern that agricultural azole use is reducing the efficacy of clinical azole treatment (Takahashi *et al.*, 2020).

Environmentally derived antifungal resistance research is primarily concerned with agricultural azole use. While it is important to understand the basis of azole resistance, there are a few key mutations that quickly arise to confer resistance to azoles for most pathogenic fungi (Sionov *et al.*, 2013; Berkow and Lockhart, 2017; Burks *et al.*, 2021). Duplications of ergosterol synthesis genes and mutations that increase multidrug transporter activity are the primary mutations that facilitate azole resistance (Sionov *et al.*, 2013; Chowdhary and Meis, 2018; Fan *et al.*, 2021). Alternative agricultural antifungals present more varied resistance mechanisms resulting from multiple modes of action. These antifungals require polygenic resistance mechanisms that have an increased number of off target effects in comparison with azoles (Kilani and Fillinger, 2016; Brauer *et al.*, 2019). These resistance mechanisms are more difficult to evolve; however, the resulting evolved resistance can affect pleiotropic stress response pathways, facilitating multidrug resistance (Kretschmer *et al.*, 2009; Leroch *et al.*, 2013).

Phenylpyrroles, such as fludioxonil, are a common class of antifungal used for grain storage and crop preservation (Kilani and Fillinger, 2016). They target signal transduction in multiple important stress response pathways including the high osmolarity glycerol (HOG) pathway; however, the full mode of action is still not fully understood (Kojima *et al.*, 2006). Phenylpyrrole treatment is known to result in hyperactivation of the HOG pathway leading to accumulation of glycerol resulting in cellular swelling. Resistance to fludioxonil is uncommon for agricultural fungal pests. It is hypothesized that the rarity of resistance is the result of the pleiotropic effects of phenylpyrroles (Kilani and Fillinger, 2016). In *C. neoformans*, resistance to fludioxonil has been linked to genes in the HOG pathway that reduce HOG signalling (Kojima *et al.*, 2006; sun Bahn *et al.*, 2007). This results in a myriad of pleiotropic effects, many of which are deleterious outside of fludioxonil treatment (Simoneau and vasilescu *Æ* Nelly Bataille, 2005; and Joseph Heitman Yong-Sun Bahn, 2005; Roth *et al.*, 2021). HOG signalling affects many stress response pathways, including ergosterol synthesis, potentially impacting resistance to fluconazole and amphotericin B, the primary antifungals used to treat *C. neoformans*.

In this chapter, I utilize experimental evolution to understand the evolutionary routes *C. neoformans* takes to overcome increased temperature and the agricultural antifungal, fludioxonil. After evolving strains for 18 passages, I find a trade-off between resistance to elevated temperature and resistance to fludioxonil. I also find multiple large scale deletions associated with resistance to both heat and fludioxonil. A fludioxonil resistant strain also carries a duplication of multiple genes on chromosome 3 that contains *ERG10* and *PDK1*, genes important for resistance to amphotericin B and fluconazole. Numerous candidate genes are also associated with resistance to both temperature and fludioxonil. These candidate genes involved both canonical resistance mechanisms, such as HOG pathway deletions, and novel mecha-

nisms involving undescribed multidrug transporters and genes involved in metabolism. This study illustrates the polygenic routes *C. neoformans* takes to resist temperature and fluoioxonil stress while displaying the complex trade-offs that come with that resistance.

## 4.3 Results

### 4.3.1 Establishing Evolution Parameters

The previous work detailed in chapters two and three utilized the natural variation of *C. neoformans* to understand the relationship between stress phenotypes and genotype. In this chapter, I explore how stress influences the evolution of isogenic populations through the lens of *de novo* mutations accrued over time. The stressors I chose to concentrate on were 39°C growth and fluoioxonil treatment for their pleiotropic nature and the relevance to both the environment and the clinic. I decided to use the commonly used *C. neoformans* strain KN99 as it has been used in studies involving fluoioxonil and high temperature growth previously and there is a deletion collection available in that background for testing individual mutations downstream (de Gontijo *et al.*, 2014; Paes *et al.*, 2018).

Initial studies to establish the evolutionary conditions were carried out in 20 mL of YPD media shaking at 170 RPM. These growth conditions were chosen to maximize the cell number and increase the cell density, as preliminary studies displayed increased cell densities in higher volume containers. Having populations with increased cell number and density increased the potential for evolved resistance to occur quickly as it offered more chances for *de novo* mutation to occur. I assayed the growth of KN99 at 30°C, 39°C, and with two different concentrations of fluoioxonil, 10 and

50  $\mu\text{g}/\text{mL}$ , taking measurements every 1.5 hours over a 72 hour period. I observed substantially lower growth rate and increased lag time following the low dose fludioxonil treatment. Paradoxically, higher doses had reduced impact on *Cryptococcus* than low doses, though all doses still reduced growth relative to untreated controls (Fig. 4.1). By 60 hours, every growth condition was either in, or nearing, stationary phase. Based on the time it took for growth to reach stationary phase, I decided that I would passage strains during the experiment every 48 hours. This would avoid evolution to saturated conditions. As an aside, strains grown in fludioxonil tended to flocculate at later time points leaving a biofilm near the meniscus of the flasks.

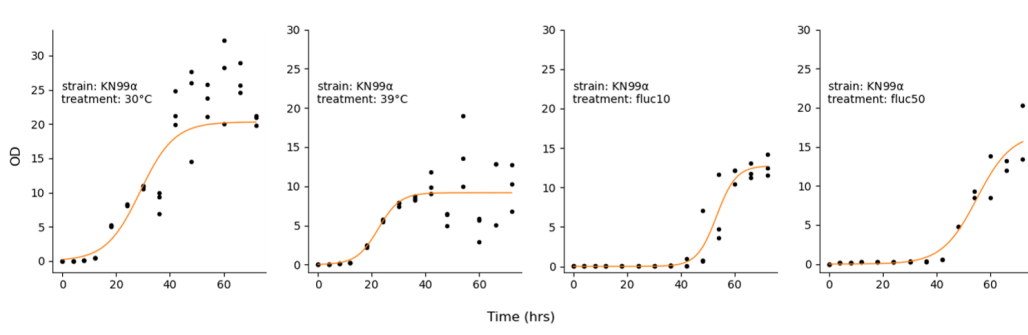


**Figure 4.1: 39°C and 10  $\mu\text{g}/\text{mL}$  growth conditions considerably restrict growth of KN99 cells.** Growth of KN99 at 30°C, 39°C, 10  $\mu\text{g}/\text{mL}$ , and 50  $\mu\text{g}/\text{mL}$  of fludioxonil sampled ever 1.5 hours across 72 hours. The y-axis represents ODs calculated from culture diluted 1:100 or 1:1000. Each dot represents a measurement, and the orange curve is a Gompertz growth curve fit to the data.

### 4.3.2 An Inverse Relationship Between Evolved Fludioxonil and Temperature Tolerance

Figure 4.2 depicts the experimental evolution workflow. Three parallel lineages, each derived from KN99, were grown at 30°C, 39°C, and 10  $\mu\text{g}/\text{mL}$  of fludioxonil for 18 passages. Populations were grown for 48 hours before sub-sampling into fresh media at an  $\text{OD}_{600}$  of 0.01. Every six days a sample of each population was frozen in glycerol for future analysis, and as potential backups in case of contamination.

Within a few passages, the population density at the time of passaging fludioxonil increased indicating that resistance was quickly acquired. After 18 passages, evolved lines had reached stable final OD readings after the 48 hour passage time, and spot assays ceased to indicate any changes in resistance.

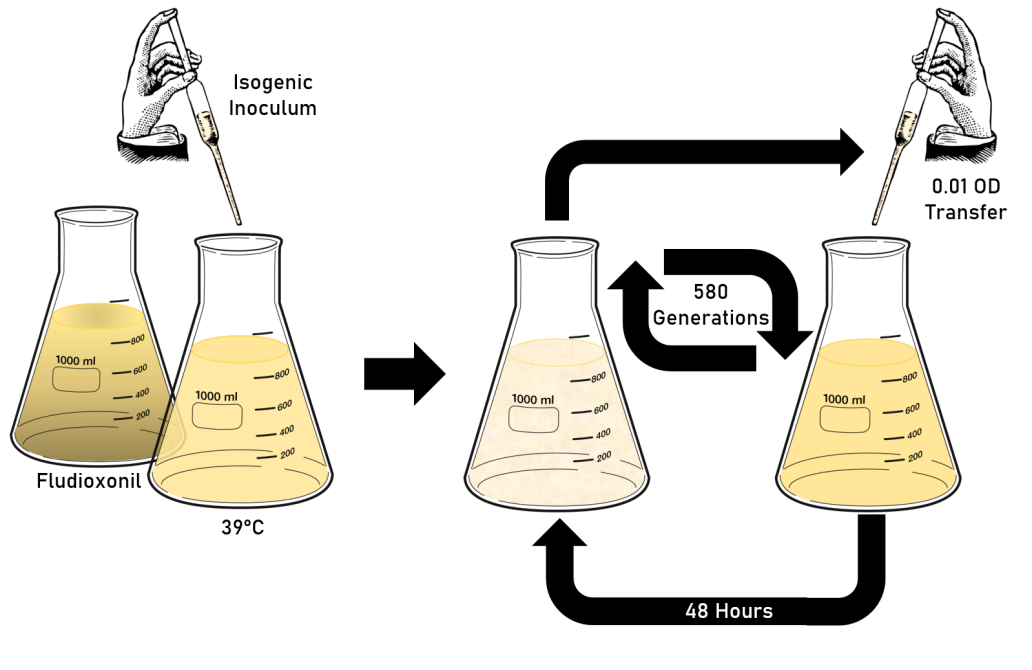


**Figure 4.2:** Isogenic cultures of KN99 were evolved at 30°C, 39°C, and with 10  $\mu\text{g}/\text{mL}$  fludioxonil in 20 mL of YPD. Cells were subsampled back to OD 0.01 in fresh media every 48 hours for 580 generations.

To test the phenotypic adaptations accrued through evolution, the evolved lines were assayed for growth at 30°C, 39°C, and in 10  $\mu\text{g}/\text{mL}$  fludioxonil using the same 96-well plate reader format as in chapter three. Growth reported is the AUC for each evolved line. All evolved lines maintained relatively similar growth at 30°C. Rather surprisingly, lines evolved at 39°C did not experience an increase in thermal tolerance over the naive strain suggesting there was no response to thermal selection (Fig. 4.3). The 30°C and in fludioxonil evolved lines grew poorly at 39°C while displaying higher growth in fludioxonil (Fig. 4.3). The growth of the 39°C evolved populations display much higher variance than the unevolved strain indicating the heat evolved lines have

mutational differences to the naive strain.

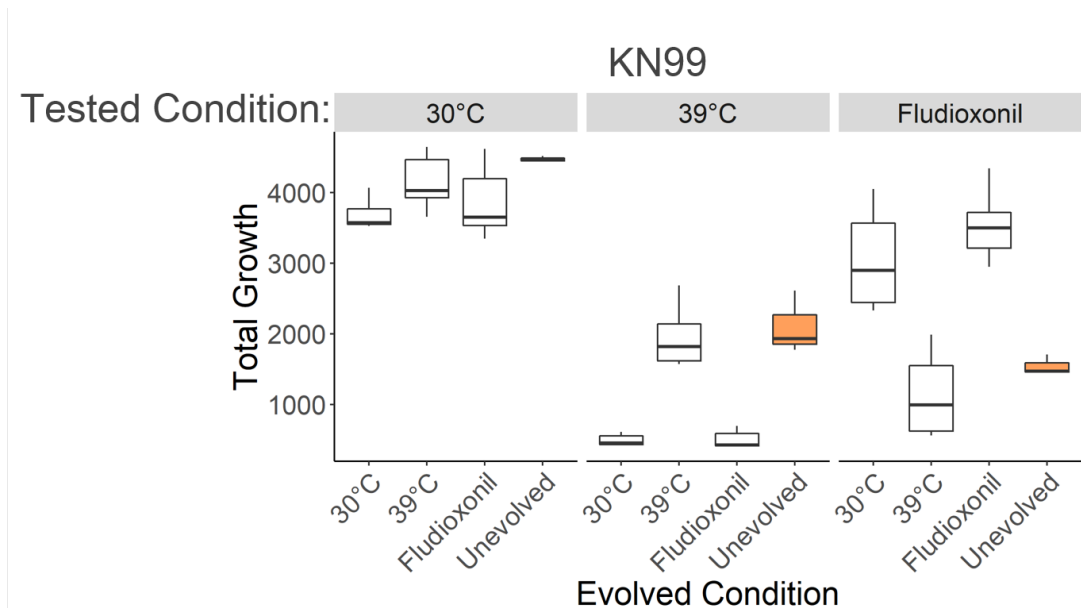


**Figure 4.3: There is an inverse relationship between evolution at 39°C and with fludioxonil.** Growth data calculated using the AUC of growth curves from a plate reader based assay. Strains were grown in the conditions indicated in the grey bars at the top for 72 hours in YPD. The x-axis displays the evolved line that was tested. The orange box plot represents the unevolved KN99 strain that every line started as pre-evolution.

### 4.3.3 Lines Evolved at 39°C Lose Thermal Tolerance During Extended Fludioxonil Challenge

One of the tests used to determine the phenotypic adaptations in the final evolved lines was a spot assay. Evolved lines were, added in serial dilution, onto solid media plates with or without 50  $\mu\text{g}/\text{mL}$  of fludioxonil and were grown at 30°C. I found that the 39°C evolved lines would not grow on plates containing fludioxonil within shorter testing periods; however, after a period of 1-2 weeks small, misshapen colonies would sporadically begin to grow. Collecting these colonies and testing their growth at 39°C and in 10  $\mu\text{g}/\text{mL}$  fludioxonil, revealed a greatly increased variance in both conditions, trending towards reduced thermal tolerance and increased fludioxonil tol-

erance (Fig. 4.4). Based on this change between thermal and drug tolerance, I labelled these new strains "revertants." Revertant strains further demonstrated the interesting trade-off that occurs between thermal tolerance and fludioxonil tolerance.

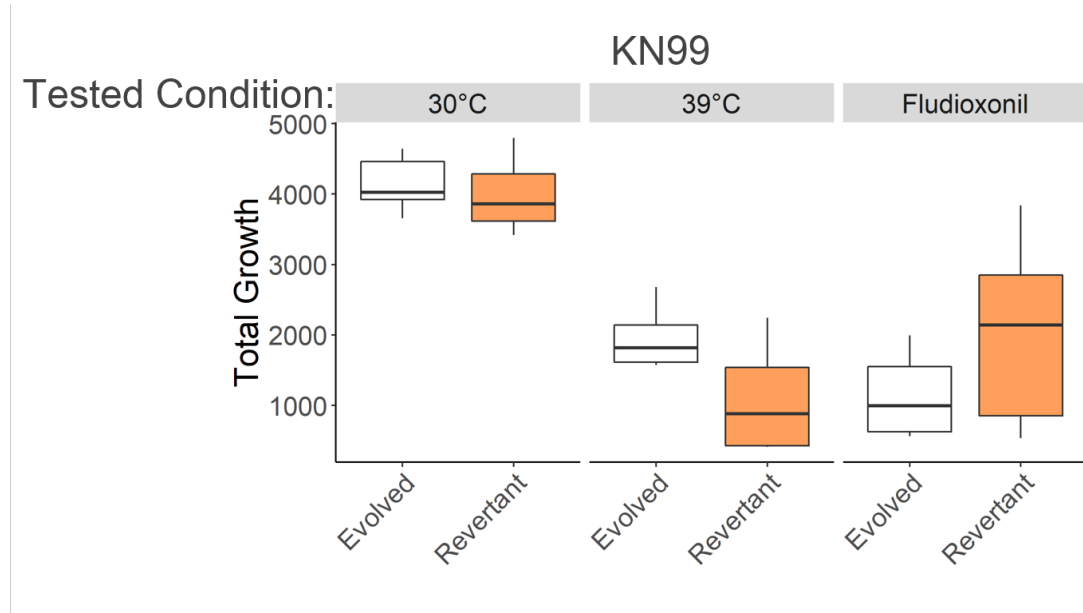


**Figure 4.4: Revertants lose temperature tolerance and gain some fludioxonil resistance.** Revertant strains derived from the 39°C line grown on solid fludioxonil media for 1-2 weeks were tested using the plate reaser based growth method. Grey bars indicate the condition strains were phenotyped in for 72 hours. The y-axis represents the AUC of the growth curves. The x-axis indicates the line tested with "Evolved" representing strains evolved at 39°C and "Revertant" as strains that regained the ability to grow on solid fludioxonil.

#### 4.3.4 Variants Associated with Evolved Thermal and Fludioxonil Tolerance

DNA from evolved lines was collected from three independently evolving populations for each selective regime. Three heat evolved lines (PMY3326 - PMY33328), three fludioxonil treated lines (PMY3336 - PMY3338), and three 30°C lines (PMY3316 - PMY3318) were sequenced. Sampling from a mixed population carries the risk of missing evolved mutations that exist at a lower frequency within a sample. To assess the degree of missed mutations, one of three evolved lines, representing each selective regime, was extracted in triplicate (PMY3318 - 3320 for 30°C, PMY3328 - PMY3330 for 39°C, and PMY3338 - PMY3340 for fludioxonil) (Table S4). Three revertants, derived from independent 39°C evolved populations, were also selected for sequencing (PMY3306 - PMY3308). They were sampled similarly to the evolved lines with one population being extracted three times (PMY3308 - PMY3310) (Table S4). Sequencing was performed using 150 bp paired-end reads on the Illumina NextSeq 6000 platform, and reads were aligned to the KN99 reference genome using the Snippy mapping pipeline (Seemann, 2015).

Initial variant filtering, based on depth and quality, resulted in 445 variants per evolved group. Variants shared across all sequenced samples were filtered out, as they likely represent mapping errors or sites that differ between the starting strains and the reference. After filtering, called variants were verified manually using IGV. Each evolved group had a similar number of unique variants. I found 84 heat evolved variants, 92 fludioxonil variants, 87 control variants, and 80 revertant variants (Fig. S5).

A number of mutations stand out based on the functional annotations of the genes they effect or because they represent multiple independent mutations in the same genomic region. These are detailed below by strain designation to specify which evolved line contains the variant. A list of strain names in relation to their evolved

condition is available S4. The HOG pathway signalling kinases *SSK1* and *SSK2* both have SNPS in revertant and fludioxonil treated lines (PMY3336 and PMY3308, respectively) indicating acquired resistance through reduced HOG pathway signalling (Table S5). One revertant line (PMY3309) has a 3 bp deletion in the gene *RCK2* (Table S5). *RCK2* is a kinase downstream of the HOG pathway involved in oxidative stress resistance, in *S. cerevisiae* (Bilsland *et al.*, 2004). In multiple heat evolved lines (PMY3328, PMY3329, and PMY3330) a 9 bp deletion disrupts the transcription factor *FZC4* (Table S5). *FZC4* is involved in multiple virulence related phenotypes including antifungal resistance (Jung *et al.*, 2015).

#### **4.3.5 Multi-gene Deletions in High Temperature and Fludioxonil Evolved Strains Impact Virulence and Drug Tolerance Associated Genes**

Filtering for regions with sequencing depth <10 reads, I discovered one multigene deletion in the 39°C evolved background and three multigene deletions in the revertant background (Table S5) (Fig. 4.8,4.7,4.6). The 39°C deletion occurs in one evolved strain (PMY3329). It covers 11.5 kb (from 918,500 - 930,000 on chromosome 14) and is comprised of 4 genes (Fig. 4.8). Among the genes deleted are, *ITR3B* and *CNAG\_05665* (Table S5). *ITR3B* is involved in inositol uptake from the environment, and *CNAG\_05665* a homolog of *S. cerevisiae ALR1* which is involved in Mg<sup>2+</sup> transport (Xue *et al.*, 2010; Suo *et al.*, 2018). Both metabolic pathways these genes are involved in have been implicated in their importance in virulence, specifically capsule production (Xue *et al.*, 2010; Suo *et al.*, 2018). Perplexingly, neither gene has a published role in thermal tolerance. Given the lack of increased thermal tolerance in the heat evolved lines, this mutation may have little to do with thermal tolerance. It may, however, influence fludioxonil resistance through a yet uncharacterized function.

Three deletions are found in revertant strains on chromosomes 11 and 12

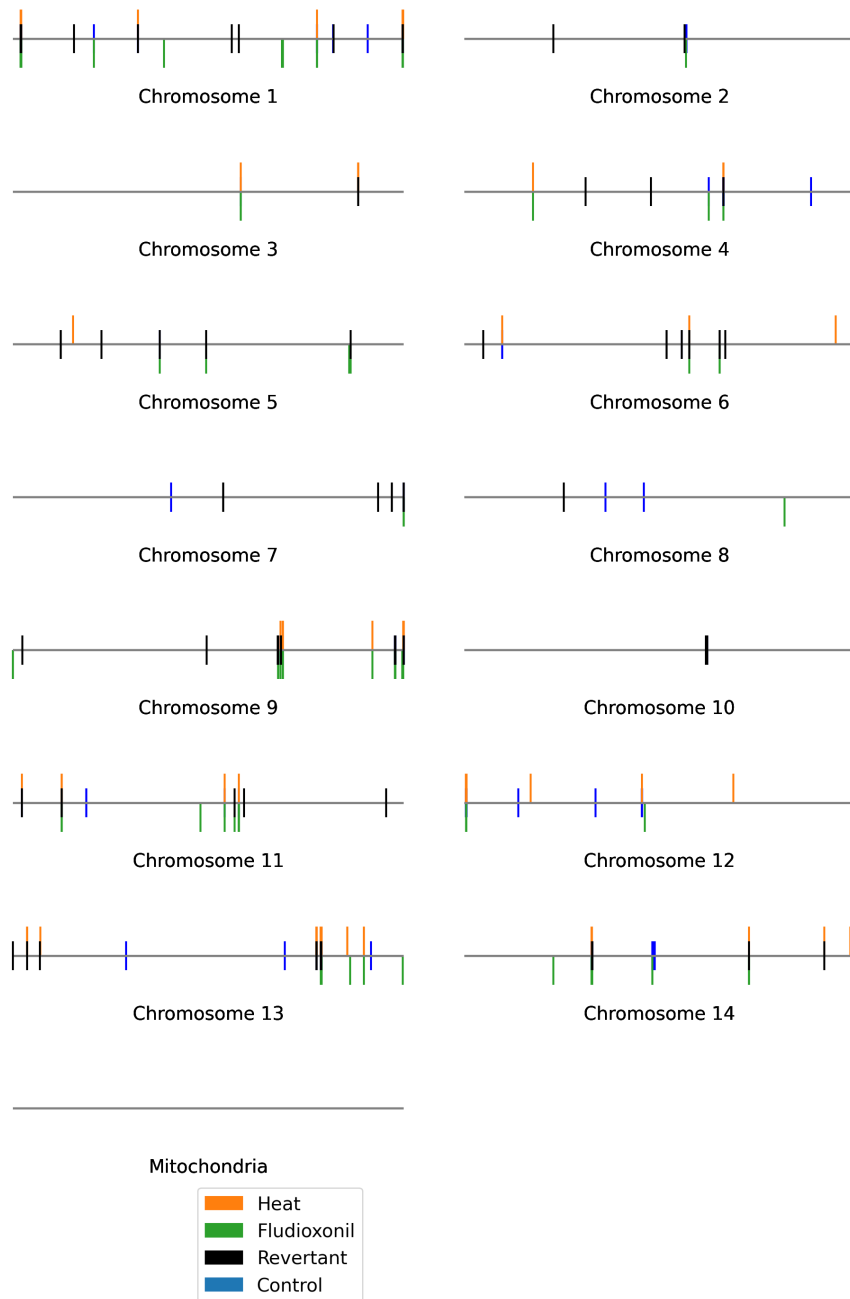


**Figure 4.5: A similar number of variants are present for each evolved line** A representation of variants across the genome. Horizontal grey lines represent individual chromosomes. Vertical bars represent the location of an identified variant. Variants associated with 39°C growth are in orange, fludioxonil variants are in green, control variants are in blue, and revertant variants are in black. Variant orientation (above, through, or below the chromosome line) are for readability when variants overlap.

Evolved Variant Gene List									
Evolved Condition	Genomic Change	Chromosome	Gene ID	Gene Name	Transcript	Description			
39°C	Deletion	14	CNAG_05665	( <i>ALR1</i> )	CNAG_05665-t26_1	hypothetical protein			
			CNAG_05666		CNAG_05666-t26_1				
			CNAG_05667	( <i>ITR3B</i> )	CNAG_05667-t26_1	myo-inositol transporter, putative			
Revertant		12	CNAG_05986		CNAG_05986-t26_1	hypothetical protein			
			CNAG_05987		CNAG_05987-t26_1				
			CNAG_05988		CNAG_05988-t26_1				
			CNAG_05989		CNAG_05989-t26_1				
			CNAG_05990		CNAG_05990-t26_1				
			CNAG_05991		CNAG_05991-t26_1	glycosyl hydrolase family 88			
			CNAG_05991		CNAG_05991-t26_2	glycosyl hydrolase family 88, variant			
			CNAG_05992		CNAG_05992-t26_1	hypothetical protein			
			CNAG_05993	( <i>SEO1</i> )	CNAG_05993-t26_1	transmembrane transporter Liz1p			
			CNAG_05993		CNAG_05993-t26_2	transmembrane transporter Liz1p, variant			
			CNAG_05994		CNAG_05994-t26_1	multidrug transporter			
			CNAG_05995		CNAG_05995-t26_1	hypothetical protein			
			CNAG_06938		CNAG_06938-t26_1				
			CNAG_06939		CNAG_06939-t26_1				
			CNAG_07026		CNAG_07026-t26_1				
			CNAG_07894		CNAG_07894-t26_1				
			Variant		11	CNAG_07619		CNAG_07619-t26_1	ATP-binding cassette, subfamily G (WHITE), member 2, PDR
						CNAG_02010		CNAG_02010-t26_1	tartrate transporter
						CNAG_02010		CNAG_02010-t26_2	tartrate transporter, variant
CNAG_02011		CNAG_02011-t26_1				PQQ enzyme repeat protein			
CNAG_02012		CNAG_02012-t26_1				TPR repeat-containing protein			
CNAG_02012		CNAG_02012-t26_2							
CNAG_02013		CNAG_02013-t26_1				hypothetical protein			
CNAG_02013		CNAG_02013-t26_2				hypothetical protein, variant			
CNAG_02016		CNAG_02016-t26_1				hypothetical protein			
CNAG_07619	( <i>PDR11</i> )	CNAG_07619-t26_2				ATP-binding cassette, subfamily G (WHITE), member 2, PDR, variant			
Revertant, Fludioxonil		13	1	CNAG_00130	( <i>RCK2</i> )	CNAG_00130-t26_1	CAMK/CAMK1/CAMK1-RCK protein kinase		
			2	CNAG_03815		CNAG_03815-t26_1	hypothetical protein		
			4	CNAG_05063	( <i>SSK2</i> )	CNAG_05063-t26_1	ste/ste11/ssk protein kinase		
			5	CNAG_01396		CNAG_01396-t26_1	protein SUS1		
				CNAG_07406		CNAG_07406-t26_1	pheromone alpha		
			9	CNAG_04109		CNAG_04109-t26_1	hypothetical protein		
			CNAG_07784		CNAG_07784-t26_1				
39°C	39°C, Revertant	13	CNAG_06271		CNAG_06271-t26_1				
CNAG_07922			( <i>FZC4</i> )	CNAG_07922-t26_1	transcription factor				
39°C, Revertant, Fludioxonil		14	CNAG_05436		CNAG_05436-t26_1	hypothetical protein			

( ) = *Saccharomyces cerevisiae* homologous gene name

**Table 4.1:** Genes either implicated as variants or that are deleted in each evolved line. Gene names homologous to *S. cerevisiae* are surrounded by parentheses.

(Fig. 4.7,4.6). The chromosome 12 deletion occurs in one strain (PMY3307) and covers 4.5 kb (from 423500-472000 on chromosome 12) including 14 genes. Among the genes deleted, *CNAG\_05993* and *CNAG\_05994* are both implicated in drug related membrane transport, possibly providing resistance to fludioxonil (Table S5). The deletion on chromosome 11 evolved independently in two evolved lines (PMY3307 and PMY3309) (Fig. 4.7). The deletions differ in size between the two lines that acquired them. One strain (PMY3307) has a 20 kb deletion consisting of 6 genes (from 1522000 - 1542000 on chromosome 11), and the other strain (PMY3309) has a 12 kb deletion (from 1530000 - 15420000 on chromosome 11) that disrupts 3 genes (Table S5)(Fig. 4.7). Within the deletion regions of both lines is the multidrug transporter *CNAG\_07619* a homolog of *PDR11* in *Cryptococcus gattii* that impacts resistance to fluconazole (Yang *et al.*, 2016). Given the appearance of this deletion in two evolved lines, loss of this multidrug transporter is likely to increase resistance to fludioxonil.

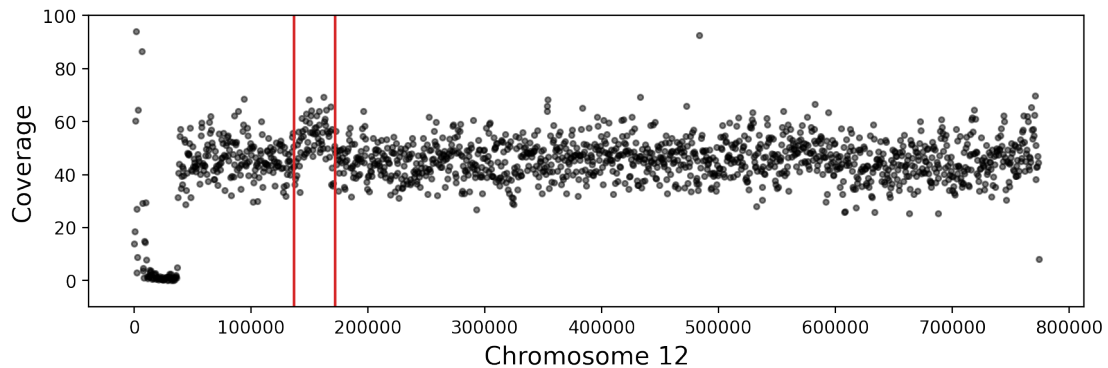


**Figure 4.6: One revertant line carries a deletion near a telomere of chromosome 12** A depiction of coverage across chromosome 12 for PMY3307. The red lines indicate the location of the centromere.

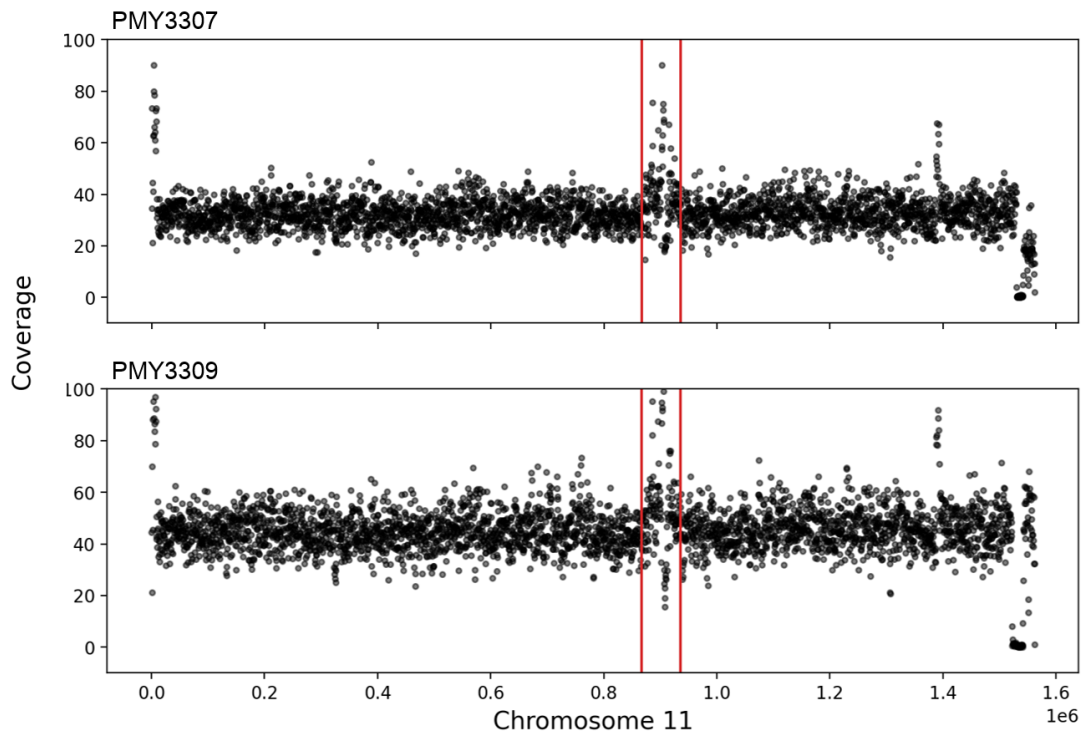


**Figure 4.7: Two revertant lines carry a deletion near a telomere of chromosome 11** A depiction of coverage across chromosome 11 for evolved lines PMY3307 and PMY3309. The red lines indicate the location of the centromere.

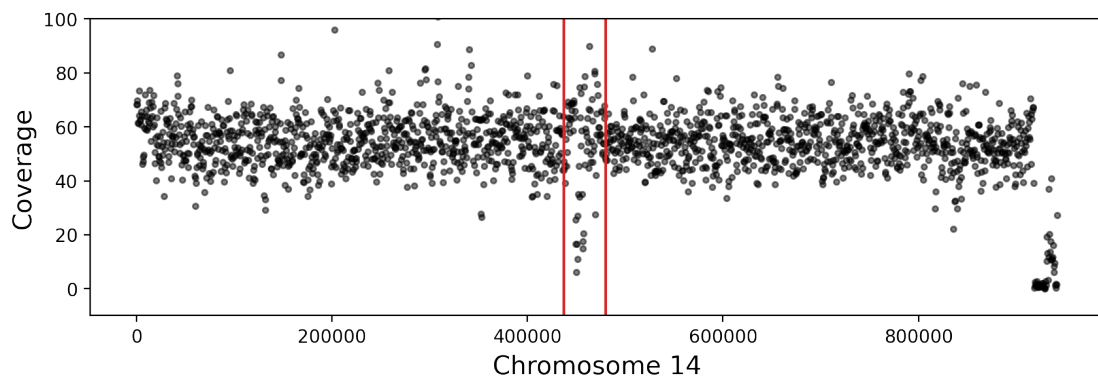


**Figure 4.8: One heat evolved line carries a deletion near a telomere of chromosome 14** A depiction of coverage across chromosome 14 for PMY3329. The red lines indicate the location of the centromere.

### 4.3.6 A Multi-gene Duplication in A Revertant Strain Impacts Multiple Pleiotropic Stress Response Pathways

Gene duplications often confer drug resistance by providing stoichiometric relief via production of more targeted molecules or increases in efflux pumps (Kwon-Chung and Chang, 2012). I investigated duplications by filtering for regions with double the chromosomal average read depth finding a 49 kb (from 423,500 - 472,500 on chromosome 3) duplication on chromosome 3 (Fig. 4.9). This duplication, discovered in one revertant strain (PMY3310), contained 18 genes (Table 4.2). Of the genes duplicated are *PDK1* and *ERG10*, both of which are involved in azole resistance (Lee *et al.*, 2012a; Yang *et al.*, 2017). There are also three nuclear encoded genes involved in mitochondrial maintenance duplicated in this region (*CNAG\_02914*, *CNAG\_02917*, *CNAG\_02923*), possibly indicating a role for mitochondrial maintenance in fludioxonil resistance (Table 4.2). Ultimately, this duplication offers the potential for the discovery of novel fludioxonil resistance methods with potential pleiotropic effects.

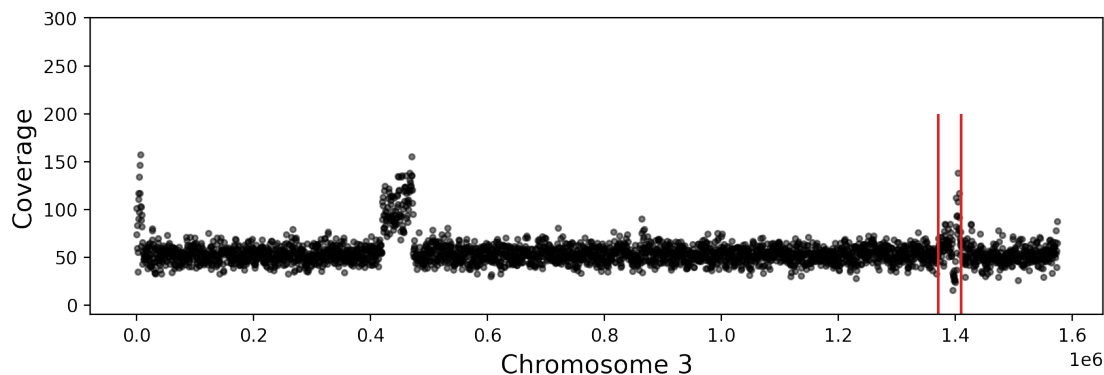


**Figure 4.9: A multi-gene duplication associated with revertants is present on chromosome 3.** A representation of read depth across chromosome 3 for revertant strains. The y-axis represents the read depth and the x-axis represents the location on chromosome 3. The centromere is marked by horizontal red bars. Telomeres ends also present with elevated read depth; however, this is a result of poor read mapping, not duplication.

Revertant Duplication						
Evolved Condition	Genomic Change	Chromosome	Gene ID	Gene Name	Transcript	Description
Revertant	Duplication	3	CNAG_02912		CNAG_02912-t26_1	hypothetical protein
			CNAG_02915	<i>PDK1</i>	CNAG_02915-t26_1	AGC/PDK1 protein kinase
			CNAG_02917	<i>(GGC1)</i>	CNAG_02917-t26_1	hypothetical protein
			CNAG_02919		CNAG_02919-t26_1	
			CNAG_02926		CNAG_02926-t26_1	
			CNAG_02929	<i>(TAF1)</i>	CNAG_02929-t26_1	transcription initiation factor TFIID subunit 1
			CNAG_02923		CNAG_02923-t26_1	large subunit ribosomal protein L14
			CNAG_02928	<i>(RPL5)</i>	CNAG_02928-t26_1	large subunit ribosomal protein L5e
			CNAG_02911	<i>(SRF1)</i>	CNAG_02911-t26_1	hypothetical protein
			CNAG_02913		CNAG_02913-t26_1	
			CNAG_02914	<i>(IMG2)</i>	CNAG_02914-t26_1	
			CNAG_02918	<i>ERG10</i>	CNAG_02918-t26_1	Acetyl-CoA C-acetyltransferase
			CNAG_02921		CNAG_02921-t26_1	hypothetical protein
			CNAG_02922		CNAG_02922-t26_1	
			CNAG_02924		CNAG_02924-t26_1	histone H1/5
			CNAG_02925	<i>(OAR1)</i>	CNAG_02925-t26_1	D-arabinitol 2-dehydrogenase
			CNAG_02927	<i>(MPD1)</i>	CNAG_02927-t26_1	protein disulfide-isomerase
			CNAG_02930	<i>LIV10</i>	CNAG_02930-t26_1	virulence related protein of unknown function

( ) = *Saccharomyces cerevisiae* homologous gene name

**Table 4.2:** A list of the genes duplicated on chromosome 3 for PMY3310.

## 4.4 Discussion

Understanding the routes that fungal pathogens take to resist environmental and clinical stressors can lead to understanding of both their evolutionary past and the complications of the future. For *Cryptococcus*, understanding the *de novo* mechanisms it employs to survive in increased temperature environments and in the presence of antifungals provides a view of the complicated trade-offs that arise from evolving in harsh environments. Using evolution in fludioxonil and 39°C, I discovered a trade-off between drug resistance and thermal tolerance in *C. neoformans*. Fludioxonil tolerance is rare in the fungal species that the drug was designed to treat; however, fludioxonil tolerance in the laboratory is not uncommon (Kilani and Fillingner, 2016). *C. neoformans* fludioxonil resistance is known to occur through alteration of the HOG pathway (Kojima *et al.*, 2006; sun Bahn *et al.*, 2007). The trade-off between fludioxonil tolerance and high temperature tolerance discovered here could be related to the HOG pathway mutations in (*SSK1*, *SSK2*, and *Rck2*) that are found in the revertant and drug evolved strains as *HOG1* knockouts have been found to lose extreme (above 37°C) temperature tolerance (and Joseph Heitman Yong-Sun Bahn, 2005). This

trade-off presents a positive view for the use of fludioxonil, and other phenylpyrroles, as global temperatures rise, resistance may be balanced by temperature adaptation.

The similarity in growth at 39°C between the unevolved strain and the 39°C evolved lines was a surprise. Seemingly, the evolution at 39°C did not result in an increase in thermal tolerance. I did note an increase in the final OD of the flasks when passaging during the evolution period; however, that is not reflected in this test. It is possible that subtle increases in temperature tolerance are missed when assaying these strains in a 96-well format as opposed to the larger volume used during evolution. Regardless, it appears that thermal tolerance is a trait not easily evolved given the constraints I applied.

Finding a similar number of *de novo* mutations between evolved environments implies that the different stressors did not impact mutation rate; however, verification of mutations has proven to be complicated by the fact that many variants are in repetitive region of the genome, often near the begin of introns. Repetitive regions present a complication because reads may not align correctly when there are long strings of single nucleotides. Repetitive regions are also common sights of mutation, resulting from errors during replication, further adding to the complication (and Eric Alani Xin Ma, 2012). Additional validation of variant calls via Sanger sequencing will be necessary to verify whether variants discovered in repeat rich regions are artifacts or variants of interest. The result of this abundance of repeat rich variants is apparent in the number of variants discovered for fludioxonil evolved strains. Despite finding a similar number of variants between all evolved conditions, I have only identified one variant for the fludioxonil evolved lines. The other variants identified either fall in these repeat rich regions or they are the result of poorly mapping reads. While I am confident in the variant discovered, further variant validation will be required to discover additional mutations of interest.

Many of the genes that either have SNPs or full deletions from the revertant and fludioxonil evolved lines are involved in antifungal drug resistance. *SSK1*, *SSK2*, and *FZC4* mutations have all been linked to alterations in amphotericin B resistance. Loss of *FZC4* dramatically increases resistance to amphotericin B, while loss of *SSK1* and *SSK2* leads to sensitivity; however, gain of function mutations in *SSK2* that lead to increased Hog1 phosphorylation increasing amphotericin B resistance in previous studies (Jung *et al.*, 2015; Roth *et al.*, 2021). For loss of function mutations in *SSK1* and *SSK2*, there is an inverse relationship in the resulting fludioxonil resistance and amphotericin B resistance (sun Bahn *et al.*, 2007; Roth *et al.*, 2021). Fludioxonil resistance often arises as a result of a reduction in HOG pathway signalling while the opposite is true for amphotericin B (and Joseph Heitman Yong-Sun Bahn, 2005; sun Bahn *et al.*, 2007; Shivarathri *et al.*, 2020; Roth *et al.*, 2021). For *FZC4* on the other hand, loss of function has been linked to amphotericin B resistance with no alteration in fludioxonil resistance (Jung *et al.*, 2015). The pathway *FZC4* is involved in is currently unknown. Phenotypically, loss of *FZC4* seems to display the inverse of the HOG signalling genes, namely, decreased peroxide resistance and increased resistance to amphotericin B (Jung *et al.*, 2015). This provides a picture of the potential pleiotropic effects that evolution in the presence of fludioxonil can produce. Mutations within the HOG pathway will have the affect of decreasing amphotericin B resistance while other mutations can lead to the opposite effect.

The multi-gene deletions found in relation to fludioxonil resistance in the revertant background also tell a story of pleiotropic effects to antifungal resistance. The deletions on chromosomes 11 and 12 remove multidrug transporters that have not been functionally characterized in *C. neoformans*. Multidrug transporters have been implicated as targets for azole and fludioxonil resistance in multiple species (Kilani and Fillinger, 2016; Fan *et al.*, 2021). Multidrug resistance due to multidrug trans-

porter mutation has also been found to increase resistance to fludioxonil (Kilani and Fillinger, 2016). The genes identified here, *CNAG\_05993* and *CNAG\_07619*, both have homologs in *S. cerevisiae* (*PDR11* and *SEO1*) (Papay *et al.*, 2020; Nelissen *et al.*, 1997). *PDR11* is an ATP-binding cassette (ABC) transporter. Of the 54 ABC transporters predicted to exist in *C. neoformans* very few have been described. Those that have been studied (*ADR1*, *PDR5*, *MDR1*, and *PDR6*) play important roles in fluconazole resistance (Posteraro *et al.*, 2003; Sionov *et al.*, 2009; Winski *et al.*, 2022). Loss of these genes leads to sensitivity to fluconazole. In *C. gattii* loss of *PDR11* has been found to reduce resistance to fluconazole (Yang *et al.*, 2016). A possible mechanism for the PDR11 in antifungal resistance is in non-yeast sterol import. In *S. cerevisiae* *PDR11* is involved in the uptake of non-yeast sterols when sterol synthesis is arrested (Papay *et al.*, 2020). This deletion occurring twice in the revertant lines speaks to an important function in fludioxonil resistance. These deletions also carry the potential to broadly affect antifungal resistance. The multidrug transporter on chromosome 12, *SEO1*, was previously identified in a GWAS for *A. fumigatus* azole resistance (Fan *et al.*, 2021). The finding of *SEO1* in association with fludioxinol resistance provides the potential for pleiotropic effects for azole resistance.

One caveat with the mutation in *SEO1* results from the fludioxonil media used in the evolution experiment. *SEO1* loss of function has been shown to increase resistance to sulfoxides in *S. cerevisiae* (Isnard *et al.*, 1996). Fludioxonil media contains 1% DMSO to aid in solubility. While I did not find a growth defect in media with 1% DMSO in preliminary tests, it is possible that this mutation is related to growth with DMSO and not fludioxonil. Further characterization of this mutation is necessary to determine its effect on fludioxonil resistance.

The duplication on chromosome 3 also carries the potential to pleiotropically impact antifungal resistance with the increased copy number of *PDK1*. *PDK1* is an

important gene for resistance to rapamycin and fluconazole (Lee *et al.*, 2012b). It phosphorylates the last step in the protein kinase-C (PKC) signalling pathway and contributes to downstream TOR signalling. Both pathways are involved in antifungal resistance, with TOR also contributing to a myriad of stress responses and PKC regulating cell wall integrity. Deletion of *PDK1* results in reduced growth, fluconazole and rapamycin sensitivity, and reduced virulence (Lee *et al.*, 2012b). A duplication in *PDK1* could result in increased phosphorylation of Mpk1, a master cell wall integrity regulator, required for resistance to most antifungals and general stressors (Jung *et al.*, 2015). Increased phosphorylation could result in increased resistance to fludioxonil as well as other stressors, including temperature and other antifungals. Further characterization of the effects of an extra copy of *PDK1* will be necessary to understand how it effects the pleiotropic PKC and TOR pathways.

The duplication of genes (*CNAG\_02914*, *CNAG\_02917*, *CNAG\_02923*) that traffic to the mitochondria also carry interesting potential stress resistance capabilities. Mitochondrial membrane potentials are reduced in human cells treated by fludioxonil (Lee *et al.*, 2019a). Similarly, reduction in the potential for heme containing enzymes, made in the mitochondria, have been shown in animal cells treated with fludioxonil (Karadag and Ozhan, 2015). *CNAG\_02914* and *CNAG\_02923* are both homologs of *S. cerevisiae* mitochondrial, ribosomal subunits, and *CNAG\_02917* is a homolog of an *S. cerevisiae* mitochondrial iron influx transporter (Gan *et al.*, 2002; Lesuisse *et al.*, 2004; Graack and Wittmann-Liebold, 1998). Given the mitochondrial destabilization that could be caused by fludioxonil, increased copy number of ribosomal subunits and iron uptake could provide resistance to fludioxonil.

The deletion on chromosome 14 in the 39°C evolved line, PMY3329, presents an intriguing look at the effects of elevated temperature evolution. The gene *ITR3B* is a non essential part of the inositol metabolic pathway involved in inositol uptake (Xue

*et al.*, 2010). Inositol is an important carbon source during infection as it is abundant in the central nervous system (Xue *et al.*, 2010). *ITR3B* should have a minor impact in inositol uptake; however, study of this gene is lacking. Interestingly, *ITR3B* is under selection in the VNBI lineage of *C. neoformans* indicating that it is playing an important role in the environment (Desjardins *et al.*, 2017). *ALR1* has not been characterized in *C. neoformans*; however, its role in *S. cerevisiae* indicates that it plays an important role in vacuolar regulation of  $Mg^{2+}$  levels (Suo *et al.*, 2018).  $Mg^{2+}$  is an important regulator of *C. neoformans* virulence. Capsule and melanin are both regulated, in part, by  $Mg^{2+}$  levels (Rathore *et al.*, 2016; Suo *et al.*, 2018). Disruption of  $Mg^{2+}$  signalling results in increased capsule formation and decreased melanization. Deletion of the putative *ALR1* could have an impact on the virulence of the 39°C evolved cells. While the heat evolved strains did not increase in thermal tolerance, the metabolic effects of evolution to a hotter environment may impact their virulence phenotypes.

The findings here reflect the complex nature of thermal and antifungal tolerance. There is not only a trade-off between thermal tolerance and fludioxonil resistance, but I also see potential trade-offs in the pleiotropic effects on other antifungals that result from the *de novo* mutations acquired. Mutations in the, as of yet, uncharacterized multidrug transporters present new mechanisms for acquired fludioxonil resistance, and the duplication on chromosome 3 provides multiple mechanisms that can contribute to fludioxonil resistance. Further validation of mutational effects is required for understanding of the basis of the temperature trade-off, and functional validation is necessary to identify if the mutations found affect resistance to antifungals other than fludioxonil. However, the variants found offer interesting insights into the pathways that govern resistance to both thermal tolerance and fludioxonil resistance.

## 4.5 Materials and methods

### Strains and Media

Strains were maintained and initially grown using the same protocol as chapter two. Fludioxonil media consisted of 10 or 50  $\mu\text{g}/\text{mL}$  in liquid and solid YPD with 1% DMSO added.

### Evolution Assay

KN99 was initially struck out onto solid YPD and grown at 30°C for 48 hours. Colonies were picked and grown in liquid YPD at 30°C for 48 hours in a rotor drum. Liquid cultures were then suspended in 20 mL of media at an OD 0.01 in flasks. Three flasks for each evolved condition (30°C, 39°C, and 10  $\mu\text{g}/\text{mL}$ ) were grown simultaneously, for a total of 15 evolved lines. Flask cultures were grown at 30°C and 39°C shaking at 170 RPM. Every 48 hours flasks were subsampled into fresh media at an OD of 0.01. Every third passage, cultures were frozen in glycerol at -80°C and spot assays were performed to determine resistance acquisition. Populations were grown for 48 hours before subsampling into fresh media at an OD of 0.01. Every six days, a sample of each population was frozen in glycerol for future analysis, and as potential backups in case of contamination. Evolution was halted after 1 passages, approximately 508 generations, because increases in resistance had halted.

### Isolation of Revertants

Revertants were isolated by streaking 39°C evolved lines onto solid YPD with 50  $\mu\text{g}/\text{mL}$  fludioxonil. Plates were grown at 30°C for 1-2 weeks. Colonies that grew after that period were then grown at 30°C YPD for 48 hours before being frozen at -80°C in glycerol.

## Heat and Antifungal Resistance Assays

All growth assays were carried out using TECAN absorbance microplate readers (Product number 30190079) in 96-well format using round bottom plates containing 150  $\mu\text{L}$  of YPD or 150  $\mu\text{L}$  YPD with 10  $\mu\text{g}/\text{mL}$  added. The outer wells of the plates were not used for growth to avoid media evaporation affects, and plates were randomized with 3 replicates of each evolved line per plate to account for spacial effects. Two randomized plates were used for the assay. 16 picked revertants were also arrayed onto the plates without technical replicates.

Plates were pinned from  $-80^{\circ}\text{C}$  freezer stocks onto YPD omnitrays and allowed to grow at  $30^{\circ}\text{C}$  for two days before being pinned into 96-well plates with 150  $\mu\text{L}$  of YPD. 96-well plates were growth for two days at  $30^{\circ}\text{C}$  before being pinned to a second 96-well plate for the growth assay. Plates used for fludioxonil growth growth were washed twice with fludioxonil containing media prior to pinning to the 96-well plate used for the assay. Plates were grown at either  $30^{\circ}\text{C}$  or  $39^{\circ}\text{C}$  for 72 hours shaking and having  $\text{OD}_{595}$  measurements taken every 15 minutes. To prevent fogging of lids, they were washed in 0.05% Triton X-100 in 20% EtOH and were allowed to dry before the assay began.

Initial assays for establishing temperature and concentration of fludioxonil were performed as follows. KN99 was initially struck out onto solid YPD and grown at  $30^{\circ}\text{C}$  for 48 hours. Colonies were picked and grown in liquid YPD at  $30^{\circ}\text{C}$  for 48 hours in a rotor drum. Liquid cultures were then suspended in 20 mL of media at an OD 0.01 in flasks. Three flasks for each tested condition ( $30^{\circ}\text{C}$ ,  $39^{\circ}\text{C}$ , 10  $\mu\text{g}/\text{mL}$ , and 50  $\mu\text{g}/\text{mL}$ ) were grown simultaneously shaking at 170 RPM. Every 1.5 hours 900 mL of media were withdrawn from the flasks for measuring  $\text{OD}_{595}$ . Measurements were taken for 72 hours.

## **DNA Isolation and Library Preparation**

DNA was isolated and library preps were performed in the same fashion as in chapter two with the following addition: DNA was extracted for each evolved line. The third evolved line was extracted in triplicate. In the strain list S4 the first three samples for each evolved line are independently evolved and the last two are replicates of the third evolved line.

## **Sequencing, Alignment, and Variant Calling**

DNA was sequenced on NovaSeq 6000 S-Prime with 150 basepair paired end reads with an average coverage, calculated using 500 bp windows in mosdepth, of 61X. KN99 sequences were aligned to the KN99 reference using Snippy. Variants were called using GATK. Variants with less than 10 reads and a quality score lower than 30 were filtered out. Additionally, variants that appeared in every sample were filtered, because they represent SNPs present in the starting strain that differ from the reference strain. Deletions were discovered by filtering for coverage less than 10. Duplications were discovered by calculating the per chromosome average coverage and then filtering for areas where the coverage was double the average. Variants, Deletions, and Duplications were manually verified using IGV. Variants not discussed were discarded based on the mapping of reads (poorly mapping variants in IGV were discarded) and the resemblance between the control strains and the evolved strains (if the same variant was apparent in both in IGV they were not considered).

# Conclusions

## 5.1 Conclusions

*Cryptococcus* research is headed in exciting directions. With increased genetic data available and efforts to collect and share diverse strain collections, there are abundant resources further developing *Cryptococcus* as a model for fungal pathogenesis and for exploring the evolutionary origins of virulence. In this thesis, I utilize these resources to explore the accidental pathogen hypothesis and the consequences of a continually warming planet on *C. neoformans*.

In chapter two, I study the relationship between amoebae and virulence using *C. neoformans* and *C. deneoformans*. Using an assay developed to study the consumption of *Cryptococcus* cells by amoeba, I find a homologous QTL between *C. neoformans* and *C. deneoformans* that explains a substantial degree of variation for amoeba resistance. I also find that this QTL is pleiotropic for melanization in *C. neoformans*. A deletion that, includes a truncation in the 5' UTR of *BZP4*, is responsible for this trait. This deletion results in reduced transcription which, in turn, leads to reduced amoeba resistance and melanization. This finding follows the discovery by the Cuomo lab that *BZP4* loss of function is associated with reduced melanization in clinical isolates (Desjardins *et al.*, 2017). This division between amoeba resistance and virulence is further explored in chapter two through the comparison of amoeba resistance and virulence in macrophages and mice. I find that the truncation in *BZP4* does not influence macrophage or mouse interactions. Using a diverse set of *C. neoformans* strains, I also find no broad correlation between amoeba resistance and virulence in mice. This finding complements a recent experimental evolution result from the Casadevall lab. They find that evolution with amoebae actually decreased

the ability for *C. neoformans* to persist during animal infection (Fu *et al.*, 2021). This prompts more questions into the role of amoeba in accidental pathogenesis and opens the field up to alternative hypotheses for the evolution of virulence that rely less on interactions with amoebae.

Looking further at transcriptional profiles, I find that the transcription of the canonical downstream target of *BZP4*, *LAC1*, remains unchanged in amoeba conditions, regardless of *BZP4* allele. This indicates that amoeba do not trigger melanization, and melanization does not influence interactions with amoeba despite the shared QTL. While surprising, this finding indicates that there is an alternative role for *BZP4* that is unrelated to its melanin signalling function. Follow up experiments utilizing ChIP-seq in tandem with the transcriptional data described in chapter two would help answer the question of what other genes *BZP4* is responsible for activating. Work elucidating the pathway of *BZP4* would also provide insight into why it is seemingly selected against in clinical strains (Desjardins *et al.*, 2017; Yu *et al.*, 2020).

The cross between XL280 and 431 revealed a homologous QTL to our finding in the *C. neoformans* cross. When I look at the genes under the *C. deneoformans* QTL, I find a potential 3 kb deletion 3' of *BZP4*, based on a drop off in read depth. The deletion hits the first 5 base pairs of the 431 *BZP4* 3' UTR. At first, this is a puzzling result because the more resistant strain, 431, harbors the deletion. This is in contrast to the less resistant strain, Bt22, harboring the deletion 5' of *BZP4* in the *C. neoformans* cross. The potential result of this deletion is also the opposite of our finding in *C. neoformans* as 431 is more resistant to amoeba. I hypothesize this increase in resistance could result from the deletion of a sequence motif that reduces the expression of *BZP4*. A 5-mer consisting of GGGGT is deleted in the 431 background. Studies in *S. cerevisiae* indicate that poly(G) repeats in the 3' UTR can result in reduced expression (Savinov *et al.*, 2021). It is also postulated that

these regions are selected against because of their suppressive effects. So, a deletion of this, potentially suppressive, motif could result in increased expression of *BZP4*. However, I will not discount the potential for the deletion to also interrupt a non-coding regulatory motif outside of the UTR.

Chapter three extends my study of accidental pathogenesis to other important virulence factors that also play a role in environmental survival, thermal and low pH tolerance. Using a plate reader based phenotyping approach to assay growth at 30°C, 37°C, and pH 4, I discovered two general growth QTL, three thermal tolerance QTL, and two acid tolerance QTL. I further characterized the pleiotropic effects of these loci by fitting the growth data to a Gompertz growth model and QTL mapping based on the parameters max growth rate and lag. This analysis revealed that one of the thermal tolerance QTL was a general lag QTL. The number of pleiotropic QTL across conditions both signal the importance of general fitness for growth in stressful environments and delineate important, phenotype specific, loci. The importance of general fitness on the growth of strains in stressful environments speaks to the plastic nature of generalist organisms. The ability to grow in a multitude of environments necessitates the use of interconnected pleiotropic stress resistance mechanisms (Remold, 2012). While stress response pathways such as the HOG, PKA, RAM, and cAMP pathways are understood to have pleiotropic stress response roles, my data indicates that there are uncharacterized genes that naturally vary that also contribute to both general and stressful growth (and Joseph Heitman Yong-Sun Bahn, 2005; Saputo *et al.*, 2012; Maliehe *et al.*, 2020).

The use of QTL mapping based on Gompertz growth model parameters was a valuable addition to this analysis that aided in both increasing my knowledge of pleiotropic QTL. Similarly, a prior paper from the Magwene lab utilized function valued QTL mapping to precisely pinpoint when QTL have their highest associations

during growth (Roth *et al.*, 2021). Both methods provide further information into the function of the implicated QTL. In the case of the Gompertz growth fitting, further pleiotropy was uncovered for the chromosome 5 QTL. Methods such as these will be important as more quantitative studies of *Cryptococcus* are conducted. As is shown in this study, a study with only 3 phenotypes can implicate hundreds of genes. Understanding the phase of growth a QTL contributes to can help lead to QTG by speaking to its function. My confidence in further exploring the role of *CNAG\_01111* as a general lag QTL is bolstered by the understanding that it is involved in growth initiation in other fungal species. Without the knowledge of the lag parameter QTL mapping, it would be more difficult to distinguish this gene from the rest simply based on mutational differences between the parental strains.

A recurrent theme of this thesis is polygeny and pleiotropy. Combining results from chapters two and three, I find pleiotropy between a chromosome one QTL for melanin and pH tolerance. Furthermore, preliminary studies in the lab indicates that this QTL is also responsible for controlling FK506 tolerance. Follow up work from chapter three will involve investigating pleiotropic connections between phenotypes such as this. While there is evidence that melanin aids in regulating pH during infection, the genes under the peak on chromosome one are not understood to be involved in the canonical mechanisms for melanin signalling. This work presents the opportunity to discover new genes involved with pleiotropic roles in fungal virulence.

One interesting finding from chapters two and three involves the most studied strain in *C. neoformans* research, H99. I find H99 to be an outlier in amoeba resistance, growth at 30°C, and growth at pH 4. This suggests that more information is needed on what makes H99 different from the various other strains studied. Considering many of the findings in the *C. neoformans* literature are based on the H99 strain, it will be important to further dissect the ways in which H99 differs from the rest of

the species and to determine the genetic underpinnings of those differences. There has been some discussion of variation within the H99 strain. One study mapped a number of H99 variants, determining that the original H99 strain from 1980 has most likely been lost (Perfect *et al.*, 1980; Arras *et al.*, 2017). They further display that the most prevalently used laboratory variant displays increased melanization, hypervirulence, and increased azole resistance as a consequence of a mutation in *SGF29*. The confusing results that come from the within strain variation of H99 and the anomalous nature of H99 phenotypes, further displays the importance of utilizing diverse strains. By mapping genotype to phenotype in broad strain sets, the field can avoid potentially anomalous findings and get a better grasp on the genes that control virulence related stress responses.

In chapter four, I take a different approach to understand the evolution of *Cryptococcus*. This chapter explores the potential future trajectories of *Cryptococcus* evolution given the continuing rise in global temperature and agricultural antifungal use. I did this by experimentally evolving the *C. neoformans* strain, KN99, at 39°C and in fludioxonil for 18 passages. I discovered that there is a trade-off in the evolved fitness between 39°C growth and fludioxonil growth. Strains that evolved at 39°C have reduced fitness when grown with fludioxonil, and strains evolved with fludioxonil lose thermal tolerance. Strains that evolved at 39°C can re-gain the ability to grow on fludioxonil containing media if left on solid fludioxonil plates for an extended period of time. These "revertant" strains were an accidental discovery that resulted in more prospective fludioxonil tolerance mutations than the original lines evolved in fludioxonil.

Further characterization of the individual genetic variants will be necessary to unravel the trade-off between fludioxonil and high temperature growth. None of the variants found have obvious connections to the trade-off between thermal tolerance

and fludioxonil tolerance based on their known function. The testing of individual knockouts and over-expression of duplicated genes in the KN99 background will help elucidate the genetic underpinnings of this interesting trade-off and inform their role in resistance to their respective evolved environments.

Many of the candidate genetic variants associated with fludioxonil tolerance also play a role in the tolerance to other antifungals. Deletions in *SSK1* and *SSK2* both impact HOG pathway signalling, and as a consequence, amphotericin B resistance. The deletion of numerous multidrug transporters has the potential to impact fluconazole resistance, as multidrug transport has been found to be important in azole resistance (Kilani and Fillinger, 2016; Fan *et al.*, 2021). The *FZC4* variant offers the potential to affect amphotericin B resistance through a currently unknown mechanism (Jung *et al.*, 2015). Further phenotyping the resistance of the evolved lines to other antifungals will inform the pleiotropic impacts that these variants have on antifungal resistance. I predict there will be trade-offs in the resistance afforded by the individual variants, as there are contrasting roles between the loss of function of genes such as *SSK2* and *FZC4* for amphotericin B resistance.

The work presented here is an important step in testing the hypotheses surrounding the origin of *Cryptococcus* pathogenesis. I add nuance to the hypothesized connection between amoebae and macrophages, reveal the pleiotropy that dictates growth across stressful environments, and discover trade-offs that occur during evolution in different high temperature and antifungal treated environments. This is accomplished through the generation of novel assays and datasets that will be resources in future work. I also demonstrate the power of utilizing natural variation in the discovery of novel genes and gene functions.

Future studies that utilize the work presented here have the potential to discover a novel function for the gene *BZP4*, novel genes involved in the pleiotropic control of

low pH tolerance and melanin, and the basis of a trade-off between fludioxonil and thermal tolerance. These findings will contribute to the understanding of current and future selection of *Cryptococcus* phenotypes in the environment and guide the development of the Accidental Pathogen Hypothesis.

# Appendix

## Chapter 2 supplementary material

**Table S1: Genetic variants under the Chromosome 8 QTL Homology to *S. cerevisiae* indicated with a “()” . Nonsynonymous changes indicate the reference amino acid on the left and the new amino acid on the right.**

Gene Designation	Gene Name	snps	insertions	deletions	synonymous changes	nonsynonymous changes	nonsense changes
CNAG_03342	Trm82	6	1	0	3	A - S I - V	1 bp insertion
CNAG_03343		2	0	0	1	R - K	-
CNAG_03344		1	0	0	0	R - K	-
CNAG_03345	Ssd1	2	0	0	2	-	-
CNAG_03345	Ssd1	2	0	0	2	-	-
CNAG_03346	Bzp4	0	0	0	-	-	-
CNAG_03347	(HSP78)	1	0	0	0	N - D	-
CNAG_03348		2	0	0	2	-	-
CNAG_03349	(CDC40)	2	0	0	1	S - T	-
CNAG_03352		0	0	0	0	-	-
CNAG_03353		4	0	0	2	F - L S - A	-
CNAG_03354		0	0	0	-	-	-
CNAG_03355	TCO4	1	0	0	1	-	-
CNAG_03356		1	1	0	1	F	3 bp insertion
CNAG_03357		0	0	0	-	-	-
CNAG_03358	(PGK1)	0	0	0	-	-	-
CNAG_03359	(COX9)	0	0	0	-	-	-
CNAG_03360		2	1	0	2	S - T	60 bp insertion
CNAG_03361		8	0	0	3	F - L V - L S - P I - T P - Q	-
CNAG_03362		5	0	0	1	K - E T - I I - T R - H	-
CNAG_03363		1	0	0	0	P - R	-
CNAG_03364		3	0	0	2	I - V	-
CNAG_03365		4	0	0	2	T - S Y - H	-
CNAG_03365		4	0	0	2	T - S Y - H	-
CNAG_03366	Znf2	6	0	0	3	F - S A - V N - S	-
CNAG_03366	Znf2	6	0	0	3	F - S A - V N - S	-
CNAG_07723		0	0	0	-	-	-
CNAG_07724	Cuf1	8	0	0	5	Q - H P - L I - V	-

**Table S2:** Genes Under the Chromosome 7 QTL

Gene Designation	Gene Name	SNPs	Insertions	Deletions	Synonymous Changes	Nonsynonymous Changes	Nonsense Changes
CNG02310	(HSP78)	7	0	0	5	I - T D - E	- -
CNG02330	BZP4					-	-
CNG02335						-	-
CNG02350	SSD1	7	0	0	6	S - P	-
CNG02355		9	0	0	5	K - E G - D V - L F - L -	- - - - -
CNG02360		2	0	0	2	-	-
CNG02370	TRM82	8	1	0	5	P - A L - F I - V K	- - - 3 bp insertion

CNG02380	(MCM2)	11	0	0	11	-	-
CNG02390		3	0	0	2	K - E	-
CNG02400		10	0	0	8	G - R	-
						early stop gain (431)	-
CNG02410		4	0	0	2	Q - E	-
						H - Y	-
CNG02420		1	0	0	1	I - M	-
CNG02430	FZC50	7	0	0	4	V - A	-
						P - S	-
						H - R	-
CNG02440	(PRS4)	3	1	0	0	early stop gain (431)	2bp insertion
CNG02460	(TVS1)	10	0	0	7	G - E	-
						D - N	-
						L - F	-
CNG02470	(RFC3)					-	-
CNG02480	(PSD1)	3	0	0	3	-	-
CNG02490	(RMI1)	13	0	0	7	A - T	-
						I - V	-

						L - S	-
						L - P	-
						G - R	-
						D - G	-
	CNG02500	15	0	0	10	I - T	-
						K - R	-
						G - A	-
						G - V	-
						Y - S	-
	CNG02510	9	0	0	6	S - F	-
						S - P	-
						N - D	-
	CNG02515	10	0	0	5	S - G	-
						G - D	-
						S - F	-
						P - S	-
						E - G	-
	CNG02520	13	0	0	12	R - K	-
	CHS2						

CNG02530	BCH1	14	0	0	14	-	-
CNG02540	(VPS52)	7	0	0	5	V - I	-
						A - V	-
CNG02550		2	0	1	1	A - T	-
						AE	6 bp insertion
CNG02560		2	0	0	2	-	-
CNG02570	(VPS9)	19	0	0	13	A - T	-
						INT - MIN	-
						K - E	-
						D - N	-
						A - T	-
CNG02580		3	0	0	3	-	-
CNG02590	(BOI1)	14	0	0	9	K - R	-
						A - T	-
						A - V	-
						V - A	-
						P - S	-
CNG02600		11	2	0	9	P	3 bp insertion

CNG02610	(APM1)	6	0	0	6	W - C	-
						S - P	-
						G	3 bp insertion
						-	-

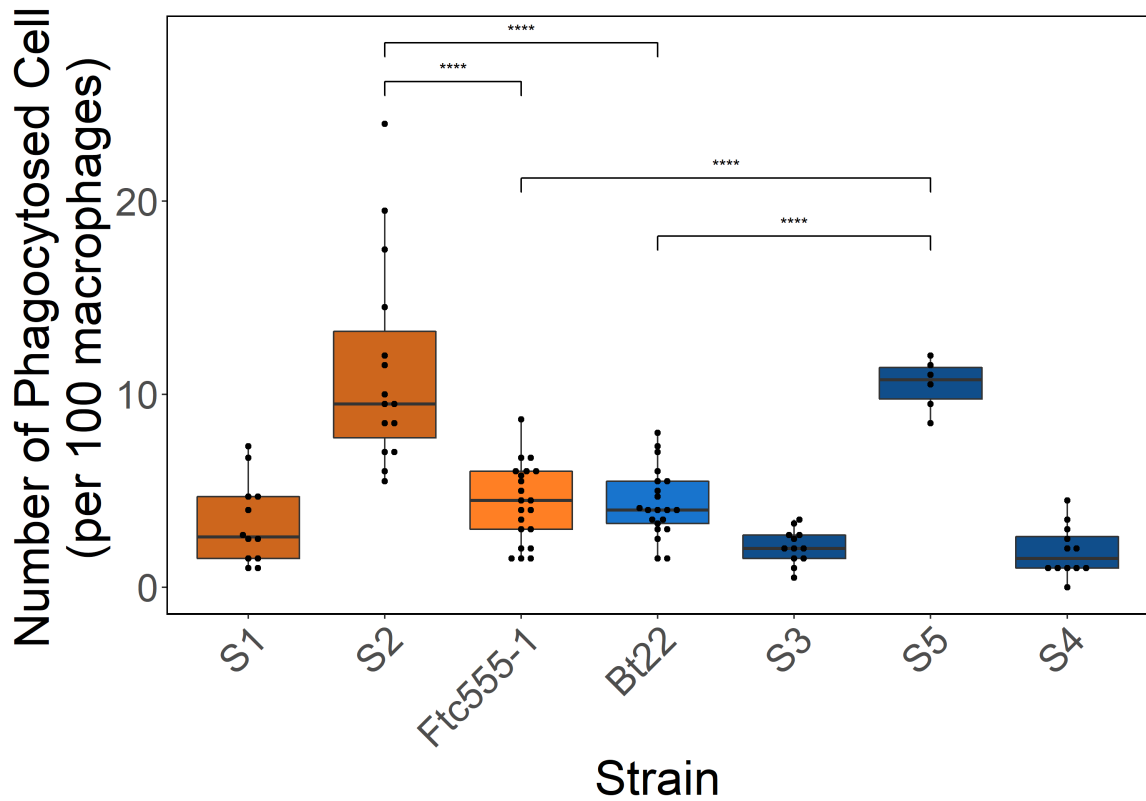


**Figure S1: Phagocytic index does not correlate with parental genotype at the chromosome 8 QTL.** Boxplots representing the phagocytic index of parental strains and segregants. Strains are oriented in rank order of amoeba resistance. Boxplots are colored by the chromosome 8 allele. Orange boxes have the Ftc555-1 allele and blue have the Bt22 allele, darker colors indicate segregants. Significance determined by Anova  $F = 22.18$ ;  $p < 0.0001$ .

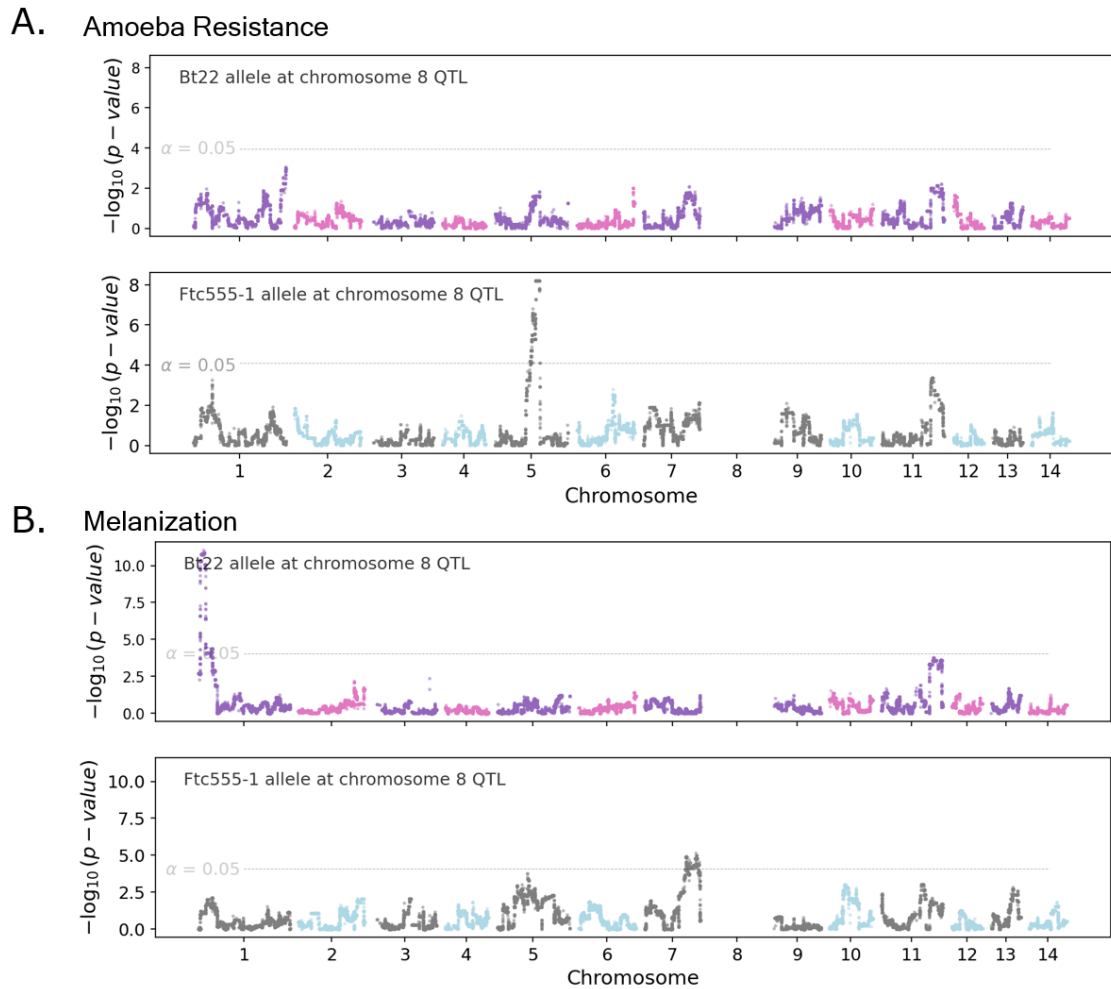


**Figure S2: Epistasis contributes to variation in both amoeba resistance and melanization.** **A.** Manhattan plots for segregants divided by allele on under the chromosome 8 QTL. The y-axis represents the strength of the association between genotype and amoeba resistance. **B.** Manhattan plots for segregants divided by allele on under the chromosome 8 QTL. The y-axis represents the strength of the association between genotype and melanization.



**Figure S3: All strains considerably melanize after 3 days** Strains pinned onto L-DOPA plates. Images taken on days 2 and 3. Images of colonies are uniformly brightened by 30% to better visually contrast the level of melanization.

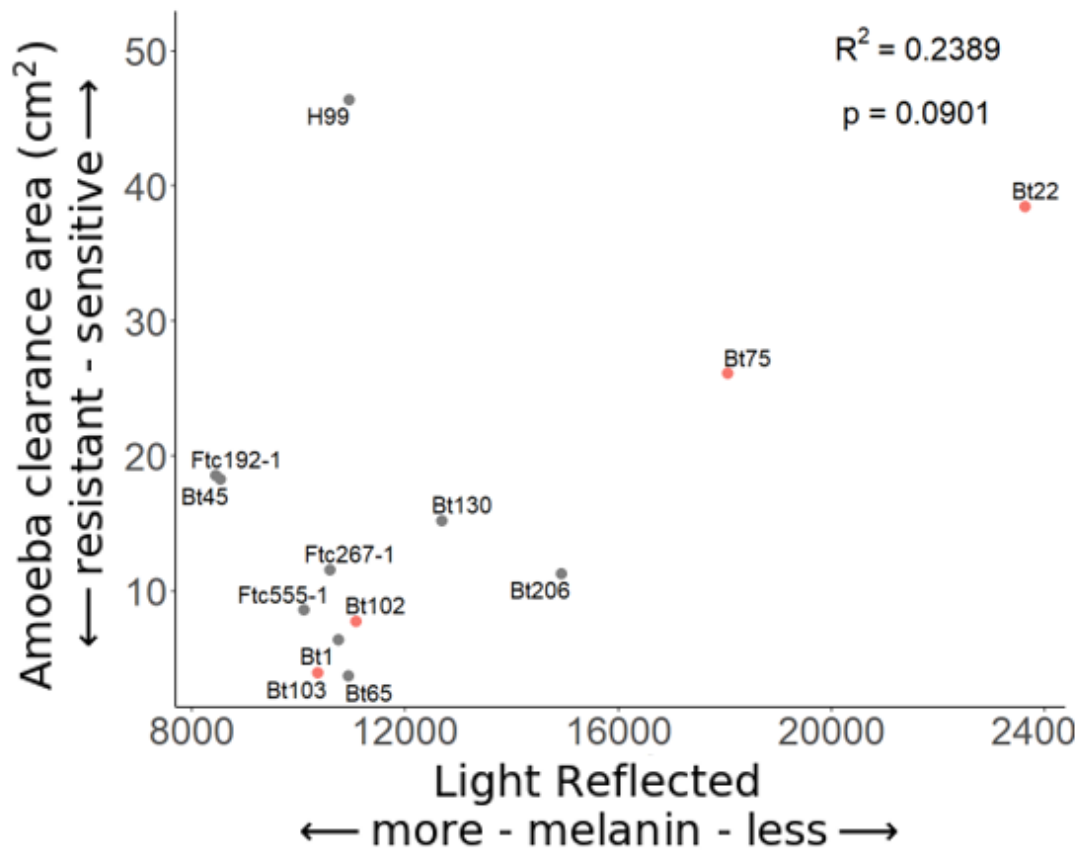


**Figure S4: Amoeba resistance and melanin does not correlate when H99 is in the strains tested.** Correlation between amoeba resistance and melanization with the strain H99 removed. Significance was determined using linear regression. Strains highlighted in orange are predicted to have impaired *BZP4* function.

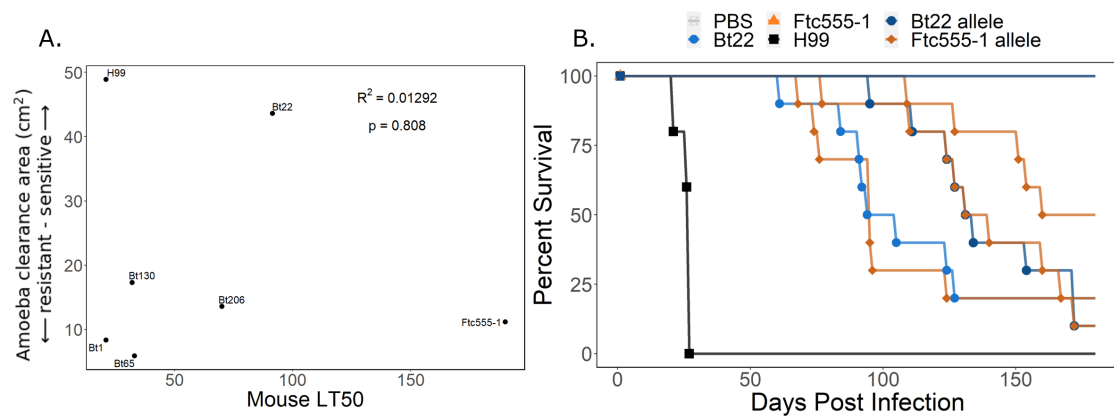


**Figure S5: Amoeba resistance does not correlate with virulence in mice. A.** Correlation between amoeba resistance and LT50. Significance determined by linear regression. Segregants that were avirulent were assigned a value of 190 days for LD50. **B.** Mouse survival curves for the parental strains and a group of segregants. H99 is in black, PBS is in grey, Ftc555-1 is in orange, and Bt22 is in blue. Segregant curves are colored by parental allele under the chromosome 8 QTL, dark blue represents the Bt22 allele and darker orange represents the Ftc555-1 allele.



**Table S3: General Growth QTL Genes**

Chromosome	Gene Name	Transcript	Description
CNAG_02685	3		CNAG_02685-t26_1
CNAG_02686	3		CNAG_02686-t26_1
CNAG_02687	3		CNAG_02687-t26_1
CNAG_02688	3		CNAG_02688-t26_1
CNAG_02689	3		CNAG_02689-t26_1
CNAG_02690	3		CNAG_02690-t26_1
CNAG_02691	3		CNAG_02691-t26_1
CNAG_02692	3		CNAG_02692-t26_1
CNAG_02694	3		CNAG_02694-t26_1
CNAG_02695	3		CNAG_02695-t26_1
CNAG_02696	3		CNAG_02696-t26_1
CNAG_02697	3		CNAG_02697-t26_1
CNAG_02698	3		CNAG_02698-t26_1
CNAG_02699	3		CNAG_02699-t26_1
CNAG_02700	3	ZFC8	CNAG_02700-t26_1
CNAG_02700	3	ZFC8	CNAG_02700-t26_2
CNAG_02701	3		CNAG_02701-t26_1
CNAG_02702	3	CLC-A	CNAG_02702-t26_1
CNAG_02703	3		CNAG_02703-t26_1
CNAG_02704	3		CNAG_02704-t26_1
CNAG_02705	3		CNAG_02705-t26_1
CNAG_02706	3		CNAG_02706-t26_1
CNAG_02707	3		CNAG_02707-t26_1

CNAG_02708	3		CNAG_02708-t26_1
CNAG_02709	3		CNAG_02709-t26_1
CNAG_02710	3		CNAG_02710-t26_1
CNAG_02711	3		CNAG_02711-t26_1
CNAG_02712	3	BUD32	CNAG_02712-t26_1
CNAG_02713	3		CNAG_02713-t26_1
CNAG_02714	3		CNAG_02714-t26_1
CNAG_02716	3		CNAG_02716-t26_1
CNAG_02717	3		CNAG_02717-t26_1
CNAG_02718	3		CNAG_02718-t26_1
CNAG_02719	3		CNAG_02719-t26_1
CNAG_02720	3		CNAG_02720-t26_1
CNAG_02721	3		CNAG_02721-t26_1
CNAG_02722	3		CNAG_02722-t26_1
CNAG_02723	3	FZC23	CNAG_02723-t26_1
CNAG_02724	3		CNAG_02724-t26_1
CNAG_02725	3		CNAG_02725-t26_1
CNAG_02726	3		CNAG_02726-t26_1
CNAG_02728	3		CNAG_02728-t26_1
CNAG_02729	3		CNAG_02729-t26_1
CNAG_02730	3		CNAG_02730-t26_1
CNAG_02733	3		CNAG_02733-t26_1
CNAG_02734	3		CNAG_02734-t26_1
CNAG_02735	3		CNAG_02735-t26_1
CNAG_02736	3		CNAG_02736-t26_1
CNAG_02737	3		CNAG_02737-t26_1

CNAG_02738	3		CNAG_02738-t26_1
CNAG_02739	3		CNAG_02739-t26_1
CNAG_02740	3	RPP1	CNAG_02740-t26_1
CNAG_02741	3		CNAG_02741-t26_1
CNAG_02742	3	DCR1	CNAG_02742-t26_1
CNAG_02744	3		CNAG_02744-t26_1
CNAG_02745	3	DCR2	CNAG_02745-t26_1
CNAG_02747	3		CNAG_02747-t26_1
CNAG_02748	3		CNAG_02748-t26_1
CNAG_02749	3		CNAG_02749-t26_1
CNAG_02750	3		CNAG_02750-t26_1
CNAG_02751	3		CNAG_02751-t26_1
CNAG_02752	3		CNAG_02752-t26_1
CNAG_02753	3	LIV13	CNAG_02753-t26_1
CNAG_02754	3		CNAG_02754-t26_1
CNAG_02755	3		CNAG_02755-t26_1
CNAG_02756	3	CDC43	CNAG_02756-t26_1
CNAG_02757	3		CNAG_02757-t26_1
CNAG_02758	3		CNAG_02758-t26_1
CNAG_02759	3		CNAG_02759-t26_1
CNAG_02760	3		CNAG_02760-t26_1
CNAG_02761	3		CNAG_02761-t26_1
CNAG_02762	3		CNAG_02762-t26_1
CNAG_02765	3		CNAG_02765-t26_1
CNAG_02766	3		CNAG_02766-t26_1
CNAG_02767	3		CNAG_02767-t26_1

CNAG_02768	3		CNAG_02768-t26_1
CNAG_02769	3		CNAG_02769-t26_1
CNAG_02770	3		CNAG_02770-t26_1
CNAG_02771	3		CNAG_02771-t26_1
CNAG_02772	3	PMU101	CNAG_02772-t26_1
CNAG_02773	3	RRP6	CNAG_02773-t26_1
CNAG_02774	3	MAL13	CNAG_02774-t26_1
CNAG_02775	3	BIM1	CNAG_02775-t26_1
CNAG_02776	3		CNAG_02776-t26_1
CNAG_02777	3	PHO84	CNAG_02777-t26_1
CNAG_02779	3	BNA6	CNAG_02779-t26_1
CNAG_02780	3	BNA5	CNAG_02780-t26_1
CNAG_02781	3		CNAG_02781-t26_1
CNAG_02782	3		CNAG_02782-t26_1
CNAG_02783	3		CNAG_02783-t26_1
CNAG_02784	3		CNAG_02784-t26_1
CNAG_02785	3		CNAG_02785-t26_1
CNAG_02786	3	FOL1	CNAG_02786-t26_1
CNAG_02787	3		CNAG_02787-t26_1
CNAG_02788	3		CNAG_02788-t26_1
CNAG_02789	3		CNAG_02789-t26_1
CNAG_02790	3		CNAG_02790-t26_1
CNAG_02791	3		CNAG_02791-t26_1
CNAG_02792	3		CNAG_02792-t26_1
CNAG_02793	3		CNAG_02793-t26_1
CNAG_02794	3		CNAG_02794-t26_1

CNAG_02795	3	CNAG_02795-t26_1
CNAG_02796	3	CNAG_02796-t26_1
CNAG_07523	3	CNAG_07523-t26_1
CNAG_07524	3	CNAG_07524-t26_1
CNAG_07525	3	CNAG_07525-t26_1
CNAG_07526	3	CNAG_07526-t26_1
CNAG_07969	3	CNAG_07969-t26_1
CNAG_10029	3	CNAG_10029-t26_1
CNAG_12268	3	CNAG_12268-t26_1
CNAG_12269	3	CNAG_12269-t26_1
CNAG_12270	3	CNAG_12270-t26_1
CNAG_12271	3	CNAG_12271-t26_1
CNAG_12272	3	CNAG_12272-t26_1
CNAG_12273	3	CNAG_12273-t26_1
CNAG_12274	3	CNAG_12274-t26_1
CNAG_12275	3	CNAG_12275-t26_1
CNAG_12276	3	CNAG_12276-t26_1
CNAG_12277	3	CNAG_12277-t26_1
CNAG_12278	3	CNAG_12278-t26_1
CNAG_12279	3	CNAG_12279-t26_1
CNAG_12280	3	CNAG_12280-t26_1
CNAG_12281	3	CNAG_12281-t26_1
CNAG_12282	3	CNAG_12282-t26_1
CNAG_12283	3	CNAG_12283-t26_1
CNAG_12284	3	CNAG_12284-t26_1
CNAG_12285	3	CNAG_12285-t26_1

CNAG_12286	3		CNAG_12286-t26_1
CNAG_12287	3		CNAG_12287-t26_1
CNAG_12288	3		CNAG_12288-t26_1
CNAG_02685	3		CNAG_02685-t26_1
CNAG_02686	3		CNAG_02686-t26_1
CNAG_02687	3		CNAG_02687-t26_1
CNAG_02688	3		CNAG_02688-t26_1
CNAG_02689	3		CNAG_02689-t26_1
CNAG_02690	3		CNAG_02690-t26_1
CNAG_02691	3		CNAG_02691-t26_1
CNAG_02692	3		CNAG_02692-t26_1
CNAG_02694	3		CNAG_02694-t26_1
CNAG_02695	3		CNAG_02695-t26_1
CNAG_02696	3		CNAG_02696-t26_1
CNAG_02697	3		CNAG_02697-t26_1
CNAG_02698	3		CNAG_02698-t26_1
CNAG_02699	3		CNAG_02699-t26_1
CNAG_02700	3	ZFC8	CNAG_02700-t26_1
CNAG_02700	3	ZFC8	CNAG_02700-t26_2
CNAG_02701	3		CNAG_02701-t26_1
CNAG_02702	3	CLC-A	CNAG_02702-t26_1
CNAG_02703	3		CNAG_02703-t26_1
CNAG_02704	3		CNAG_02704-t26_1
CNAG_02705	3		CNAG_02705-t26_1
CNAG_02706	3		CNAG_02706-t26_1
CNAG_02707	3		CNAG_02707-t26_1

CNAG_02708	3		CNAG_02708-t26_1
CNAG_02709	3		CNAG_02709-t26_1
CNAG_02710	3		CNAG_02710-t26_1
CNAG_02711	3		CNAG_02711-t26_1
CNAG_02712	3	BUD32	CNAG_02712-t26_1
CNAG_02713	3		CNAG_02713-t26_1
CNAG_02714	3		CNAG_02714-t26_1
CNAG_02716	3		CNAG_02716-t26_1
CNAG_02717	3		CNAG_02717-t26_1
CNAG_02718	3		CNAG_02718-t26_1
CNAG_02719	3		CNAG_02719-t26_1
CNAG_02720	3		CNAG_02720-t26_1
CNAG_02721	3		CNAG_02721-t26_1
CNAG_02722	3		CNAG_02722-t26_1
CNAG_02723	3	FZC23	CNAG_02723-t26_1
CNAG_02724	3		CNAG_02724-t26_1
CNAG_02725	3		CNAG_02725-t26_1
CNAG_02726	3		CNAG_02726-t26_1
CNAG_02728	3		CNAG_02728-t26_1
CNAG_02729	3		CNAG_02729-t26_1
CNAG_02730	3		CNAG_02730-t26_1
CNAG_02733	3		CNAG_02733-t26_1
CNAG_02734	3		CNAG_02734-t26_1
CNAG_02735	3		CNAG_02735-t26_1
CNAG_02736	3		CNAG_02736-t26_1
CNAG_02737	3		CNAG_02737-t26_1

CNAG_02738	3		CNAG_02738-t26_1
CNAG_02739	3		CNAG_02739-t26_1
CNAG_02740	3	RPP1	CNAG_02740-t26_1
CNAG_02741	3		CNAG_02741-t26_1
CNAG_02742	3	DCR1	CNAG_02742-t26_1
CNAG_02744	3		CNAG_02744-t26_1
CNAG_02745	3	DCR2	CNAG_02745-t26_1
CNAG_02747	3		CNAG_02747-t26_1
CNAG_02748	3		CNAG_02748-t26_1
CNAG_02749	3		CNAG_02749-t26_1
CNAG_02750	3		CNAG_02750-t26_1
CNAG_02751	3		CNAG_02751-t26_1
CNAG_02752	3		CNAG_02752-t26_1
CNAG_02753	3	LIV13	CNAG_02753-t26_1
CNAG_02754	3		CNAG_02754-t26_1
CNAG_02755	3		CNAG_02755-t26_1
CNAG_02756	3	CDC43	CNAG_02756-t26_1
CNAG_02757	3		CNAG_02757-t26_1
CNAG_02758	3		CNAG_02758-t26_1
CNAG_02759	3		CNAG_02759-t26_1
CNAG_02760	3		CNAG_02760-t26_1
CNAG_02761	3		CNAG_02761-t26_1
CNAG_02762	3		CNAG_02762-t26_1
CNAG_02765	3		CNAG_02765-t26_1
CNAG_02766	3		CNAG_02766-t26_1
CNAG_02767	3		CNAG_02767-t26_1

CNAG_02768	3		CNAG_02768-t26_1
CNAG_02769	3		CNAG_02769-t26_1
CNAG_02770	3		CNAG_02770-t26_1
CNAG_02771	3		CNAG_02771-t26_1
CNAG_02772	3	PMU101	CNAG_02772-t26_1
CNAG_02773	3	RRP6	CNAG_02773-t26_1
CNAG_02774	3	MAL13	CNAG_02774-t26_1
CNAG_02775	3	BIM1	CNAG_02775-t26_1
CNAG_02776	3		CNAG_02776-t26_1
CNAG_02777	3	PHO84	CNAG_02777-t26_1
CNAG_02779	3	BNA6	CNAG_02779-t26_1
CNAG_02780	3	BNA5	CNAG_02780-t26_1
CNAG_02781	3		CNAG_02781-t26_1
CNAG_02782	3		CNAG_02782-t26_1
CNAG_02783	3		CNAG_02783-t26_1
CNAG_02784	3		CNAG_02784-t26_1
CNAG_02785	3		CNAG_02785-t26_1
CNAG_02786	3	FOL1	CNAG_02786-t26_1
CNAG_02787	3		CNAG_02787-t26_1
CNAG_02788	3		CNAG_02788-t26_1
CNAG_02789	3		CNAG_02789-t26_1
CNAG_02790	3		CNAG_02790-t26_1
CNAG_02791	3		CNAG_02791-t26_1
CNAG_02792	3		CNAG_02792-t26_1
CNAG_02793	3		CNAG_02793-t26_1
CNAG_02794	3		CNAG_02794-t26_1

CNAG_02795	3	CNAG_02795-t26_1
CNAG_02796	3	CNAG_02796-t26_1
CNAG_07523	3	CNAG_07523-t26_1
CNAG_07524	3	CNAG_07524-t26_1
CNAG_07525	3	CNAG_07525-t26_1
CNAG_07526	3	CNAG_07526-t26_1
CNAG_07969	3	CNAG_07969-t26_1
CNAG_10029	3	CNAG_10029-t26_1
CNAG_12268	3	CNAG_12268-t26_1
CNAG_12269	3	CNAG_12269-t26_1
CNAG_12270	3	CNAG_12270-t26_1
CNAG_12271	3	CNAG_12271-t26_1
CNAG_12272	3	CNAG_12272-t26_1
CNAG_12273	3	CNAG_12273-t26_1
CNAG_12274	3	CNAG_12274-t26_1
CNAG_12275	3	CNAG_12275-t26_1
CNAG_12276	3	CNAG_12276-t26_1
CNAG_12277	3	CNAG_12277-t26_1
CNAG_12278	3	CNAG_12278-t26_1
CNAG_12279	3	CNAG_12279-t26_1
CNAG_12280	3	CNAG_12280-t26_1
CNAG_12281	3	CNAG_12281-t26_1
CNAG_12282	3	CNAG_12282-t26_1
CNAG_12283	3	CNAG_12283-t26_1
CNAG_12284	3	CNAG_12284-t26_1
CNAG_12285	3	CNAG_12285-t26_1

CNAG_12286	3	CNAG_12286-t26_1
CNAG_12287	3	CNAG_12287-t26_1
CNAG_12288	3	CNAG_12288-t26_1
CNAG_07607	11	CNAG_07607-t26_1
CNAG_07608	11	CNAG_07608-t26_1
CNAG_07609	11	CNAG_07609-t26_1
CNAG_07610	11	CNAG_07610-t26_1
CNAG_07611	11	CNAG_07611-t26_1
CNAG_07612	11	CNAG_07612-t26_1
CNAG_08003	11	CNAG_08003-t26_1
CNAG_08009	11	CNAG_08009-t26_1
CNAG_12951	11	CNAG_12951-t26_1
CNAG_12952	11	CNAG_12952-t26_1
CNAG_12953	11	CNAG_12953-t26_1
CNAG_12954	11	CNAG_12954-t26_1
CNAG_12955	11	CNAG_12955-t26_1
CNAG_12956	11	CNAG_12956-t26_1
CNAG_12957	11	CNAG_12957-t26_1
CNAG_12958	11	CNAG_12958-t26_1
CNAG_13013	11	CNAG_13013-t26_1
CNAG_13014	11	CNAG_13014-t26_1
CNAG_13015	11	CNAG_13015-t26_1
CNAG_01787	11	CNAG_01787-t26_1
CNAG_01788	11	CNAG_01788-t26_1
CNAG_01789	11	CNAG_01789-t26_1
CNAG_01790	11	CNAG_01790-t26_1

CNAG_01791	11		CNAG_01791-t26_1
CNAG_01792	11		CNAG_01792-t26_1
CNAG_01793	11		CNAG_01793-t26_1
CNAG_01794	11		CNAG_01794-t26_1
CNAG_01795	11		CNAG_01795-t26_1
CNAG_01796	11		CNAG_01796-t26_1
CNAG_01797	11		CNAG_01797-t26_1
CNAG_01798	11		CNAG_01798-t26_1
CNAG_01799	11		CNAG_01799-t26_1
CNAG_01800	11		CNAG_01800-t26_1
CNAG_01801	11		CNAG_01801-t26_1
CNAG_01802	11		CNAG_01802-t26_1
CNAG_01803	11		CNAG_01803-t26_1
CNAG_01806	11		CNAG_01806-t26_1
CNAG_01807	11	UPF1	CNAG_01807-t26_1
CNAG_01809	11		CNAG_01809-t26_1
CNAG_01810	11		CNAG_01810-t26_1
CNAG_01811	11		CNAG_01811-t26_1
CNAG_01812	11		CNAG_01812-t26_1
CNAG_01813	11		CNAG_01813-t26_1
CNAG_01814	11		CNAG_01814-t26_1
CNAG_01815	11		CNAG_01815-t26_1
CNAG_01816	11		CNAG_01816-t26_1
CNAG_01817	11		CNAG_01817-t26_1
CNAG_01818	11		CNAG_01818-t26_1
CNAG_01819	11		CNAG_01819-t26_1

CNAG_01820	11	PYK1	CNAG_01820-t26_1
CNAG_01821	11		CNAG_01821-t26_1
CNAG_01822	11		CNAG_01822-t26_1
CNAG_01823	11	INM1	CNAG_01823-t26_2
CNAG_01824	11		CNAG_01824-t26_1
CNAG_01825	11		CNAG_01825-t26_1
CNAG_01826	11		CNAG_01826-t26_1
CNAG_01827	11		CNAG_01827-t26_4
CNAG_01828	11		CNAG_01828-t26_1
CNAG_01832	11		CNAG_01832-t26_1
CNAG_01833	11		CNAG_01833-t26_1
CNAG_01834	11		CNAG_01834-t26_1
CNAG_01835	11		CNAG_01835-t26_1
CNAG_01836	11		CNAG_01836-t26_1
CNAG_01837	11		CNAG_01837-t26_1
CNAG_01839	11	ESS1	CNAG_01839-t26_1
CNAG_01840	11	TUB1	CNAG_01840-t26_1
CNAG_01841	11	GLN3	CNAG_01841-t26_1
CNAG_01842	11		CNAG_01842-t26_1
CNAG_01844	11		CNAG_01844-t26_1
CNAG_01845	11	PKC1	CNAG_01845-t26_1
CNAG_01846	11		CNAG_01846-t26_1
CNAG_01847	11		CNAG_01847-t26_1
CNAG_01848	11		CNAG_01848-t26_1
CNAG_01849	11		CNAG_01849-t26_1
CNAG_01850	11	TCO1	CNAG_01850-t26_1

CNAG_01851	11		CNAG_01851-t26_1
CNAG_01852	11		CNAG_01852-t26_1
CNAG_01853	11		CNAG_01853-t26_1
CNAG_01854	11		CNAG_01854-t26_1
CNAG_01855	11		CNAG_01855-t26_1
CNAG_01856	11		CNAG_01856-t26_1
CNAG_01857	11		CNAG_01857-t26_1
CNAG_01858	11	HOB2	CNAG_01858-t26_1
CNAG_01859	11		CNAG_01859-t26_1
CNAG_01860	11		CNAG_01860-t26_1
CNAG_01861	11		CNAG_01861-t26_1
CNAG_01862	11		CNAG_01862-t26_1
CNAG_01863	11	SNF2	CNAG_01863-t26_1
CNAG_01864	11	NDX5	CNAG_01864-t26_1
CNAG_01865	11		CNAG_01865-t26_1
CNAG_01866	11		CNAG_01866-t26_1
CNAG_01867	11		CNAG_01867-t26_1
CNAG_01868	11		CNAG_01868-t26_1
CNAG_01869	11		CNAG_01869-t26_1
CNAG_01870	11		CNAG_01870-t26_1
CNAG_01871	11		CNAG_01871-t26_1
CNAG_01873	11		CNAG_01873-t26_1
CNAG_01874	11		CNAG_01874-t26_1
CNAG_01875	11		CNAG_01875-t26_1
CNAG_01876	11		CNAG_01876-t26_1
CNAG_01877	11	GUA1	CNAG_01877-t26_1

CNAG_01878	11		CNAG_01878-t26_1
CNAG_01879	11		CNAG_01879-t26_1
CNAG_01880	11		CNAG_01880-t26_1
CNAG_01881	11		CNAG_01881-t26_1
CNAG_01883	11	GAT8	CNAG_01883-t26_1
CNAG_01884	11		CNAG_01884-t26_1
CNAG_01885	11	CID14	CNAG_01885-t26_1
CNAG_01886	11		CNAG_01886-t26_1
CNAG_01889	11		CNAG_01889-t26_1
CNAG_01890	11	MET6	CNAG_01890-t26_1
CNAG_01891	11		CNAG_01891-t26_1
CNAG_01892	11		CNAG_01892-t26_1
CNAG_01893	11		CNAG_01893-t26_1
CNAG_01894	11		CNAG_01894-t26_1
CNAG_01130	5		CNAG_01130-t26_2
CNAG_01131	5		CNAG_01131-t26_1
CNAG_01132	5		CNAG_01132-t26_1
CNAG_01133	5		CNAG_01133-t26_1
CNAG_01134	5		CNAG_01134-t26_1
CNAG_12462	5		CNAG_12462-t26_1
CNAG_12463	5		CNAG_12463-t26_1
CNAG_02439	6		CNAG_02439-t26_1
CNAG_02440	6		CNAG_02440-t26_1
CNAG_02441	6		CNAG_02441-t26_1
CNAG_02442	6		CNAG_02442-t26_1
CNAG_02443	6		CNAG_02443-t26_1

CNAG_02444	6		CNAG_02444-t26_1
CNAG_02445	6		CNAG_02445-t26_1
CNAG_02446	6		CNAG_02446-t26_1
CNAG_02447	6		CNAG_02447-t26_1
CNAG_02448	6		CNAG_02448-t26_1
CNAG_02449	6		CNAG_02449-t26_1
CNAG_02452	6		CNAG_02452-t26_1
CNAG_02453	6	PTP5	CNAG_02453-t26_1
CNAG_02454	6		CNAG_02454-t26_1
CNAG_02455	6		CNAG_02455-t26_1
CNAG_02457	6		CNAG_02457-t26_1
CNAG_02458	6		CNAG_02458-t26_1
CNAG_07628	6		CNAG_07628-t26_1
CNAG_07629	6	EPP1	CNAG_07629-t26_1
CNAG_07630	6		CNAG_07630-t26_1
CNAG_10065	6		CNAG_10065-t26_1

## Chapter 4 supplementary material

Table S4: Strain Names for Evolved Lines

Evolved Line	Replicate	Strain Name
30		PMY3316
30		PMY3317
30	1	PMY3318
30	2	PMY3319
30	3	PMY3320
39		PMY3326
39		PMY3327
39	1	PMY3328
39	2	PMY3329
39	3	PMY3330
Fludioxonil		PMY3336
Fludioxonil		PMY3337
Fludioxonil	1	PMY3338
Fludioxonil	2	PMY3339
Fludioxonil	3	PMY3340
Revertant		PMY3306
Revertant		PMY3307
Revertant	1	PMY3308
Revertant	2	PMY3309
Revertant	3	PMY3310

**Table S5:** Variant Information for Evolved Lines

Strain	Group	Chromosome	Coordinate	Gene	Notes
PMY3336	Drug	CP022321.1	47553		Reads Poorly aligned
PMY3338	Drug	CP022321.1	47553		Reads Poorly aligned
PMY3339	Drug	CP022321.1	47553		Reads Poorly aligned
PMY3340	Drug	CP022321.1	47553		Reads Poorly aligned
PMY3336	Drug	CP022321.1	47575		Reads Poorly aligned
PMY3338	Drug	CP022321.1	47575		Reads Poorly aligned
PMY3339	Drug	CP022321.1	47575		Reads Poorly aligned
PMY3340	Drug	CP022321.1	47575		Reads Poorly aligned
PMY3336	Drug	CP022321.1	47599		Reads Poorly aligned
PMY3339	Drug	CP022321.1	47634		Reads Poorly aligned
PMY3339	Drug	CP022321.1	47684		Reads Poorly aligned
PMY3339	Drug	CP022321.1	47686		Reads Poorly aligned
PMY3337	Drug	CP022321.1	47811		Reads Poorly aligned
PMY3338	Drug	CP022321.1	47811		Reads Poorly aligned
PMY3340	Drug	CP022321.1	47811		Reads Poorly aligned

PMY3337	Drug	CP022321.1	47821	Reads Poorly aligned
PMY3338	Drug	CP022321.1	47821	Reads Poorly aligned
PMY3340	Drug	CP022321.1	47821	Reads Poorly aligned
PMY3337	Drug	CP022321.1	47827	Reads Poorly aligned
PMY3338	Drug	CP022321.1	47827	Reads Poorly aligned
PMY3340	Drug	CP022321.1	47827	Reads Poorly aligned
PMY3337	Drug	CP022321.1	47839	Reads Poorly aligned
PMY3338	Drug	CP022321.1	47839	Reads Poorly aligned
PMY3340	Drug	CP022321.1	47839	Reads Poorly aligned
PMY3337	Drug	CP022321.1	47844	Reads Poorly aligned
PMY3338	Drug	CP022321.1	47844	Reads Poorly aligned
PMY3340	Drug	CP022321.1	47844	Reads Poorly aligned
PMY3337	Drug	CP022321.1	47849	Reads Poorly aligned
PMY3338	Drug	CP022321.1	47849	Reads Poorly aligned
PMY3340	Drug	CP022321.1	47849	Reads Poorly aligned
PMY3340	Drug	CP022321.1	47877	Reads Poorly aligned
PMY3340	Drug	CP022321.1	47889	Reads Poorly aligned
PMY3339	Drug	CP022321.1	474303	Repeat Region; Appears in control

PMY3338	Drug	CP022321.1	884330		Repeat Region; Appears in control
PMY3338	Drug	CP022321.1	1577680		Repeat Region; Appears in control
PMY3339	Drug	CP022321.1	1581503		Repeat Region; Appears in control
PMY3340	Drug	CP022321.1	1581503		Repeat Region; Appears in control
PMY3337	Drug	CP022321.1	1783770		Repeat Region; Appears in control
PMY3339	Drug	CP022321.1	1783770		Repeat Region; Appears in control
PMY3340	Drug	CP022321.1	1783770		Repeat Region; Appears in control
PMY3336	Drug	CP022321.1	2286962		Telomeric
PMY3337	Drug	CP022321.1	2286962		Telomeric
PMY3338	Drug	CP022321.1	2286962		Telomeric
PMY3339	Drug	CP022321.1	2286962		Telomeric
PMY3339	Drug	CP022321.1	2287023		Telomeric
PMY3338	Drug	CP022321.1	2287032		Telomeric
PMY3339	Drug	CP022321.1	2287032		Telomeric
PMY3336	Drug	CP022322.1	919710	CKF44_03818	Deletion
PMY3339	Drug	CP022323.1	918327		Repeat Region; Appears in control
PMY3340	Drug	CP022323.1	918327		Repeat Region; Appears in control
PMY3338	Drug	CP022324.1	190912		Repeat Region; Appears in control

PMY3338	Drug	CP022324.1	678589	Repeat Region; Appears in control
PMY3339	Drug	CP022324.1	719381	Reads Poorly aligned
PMY3339	Drug	CP022324.1	719382	Reads Poorly aligned
PMY3336	Drug	CP022325.1	681504	Reads Poorly aligned
PMY3336	Drug	CP022325.1	896231	Reads Poorly aligned
PMY3340	Drug	CP022325.1	1561083	Reads Poorly aligned
PMY3336	Drug	CP022325.1	1567278	Reads Poorly aligned
PMY3336	Drug	CP022326.1	819066	Reads Poorly aligned
PMY3338	Drug	CP022326.1	929254	Repeat Region; Appears in control
PMY3339	Drug	CP022326.1	929254	Repeat Region; Appears in control
PMY3336	Drug	CP022327.1	1398732	Telomeric
PMY3337	Drug	CP022327.1	1398732	Telomeric
PMY3340	Drug	CP022327.1	1398732	Telomeric
PMY3339	Drug	CP022328.1	1147232	Reads Poorly aligned
PMY3338	Drug	CP022329.1	56	Telomeric
PMY3338	Drug	CP022329.1	62	Telomeric
PMY3336	Drug	CP022329.1	804812	Reads Poorly aligned
PMY3338	Drug	CP022329.1	804812	Reads Poorly aligned

PMY3336	Drug	CP022329.1	805050	Reads Poorly aligned
PMY3340	Drug	CP022329.1	805050	Reads Poorly aligned
PMY3337	Drug	CP022329.1	812793	Reads Poorly aligned
PMY3338	Drug	CP022329.1	820206	Reads Poorly aligned
PMY3340	Drug	CP022329.1	820513	Reads Poorly aligned
PMY3340	Drug	CP022329.1	820516	Reads Poorly aligned
PMY3337	Drug	CP022329.1	1091273	Repeat Region; Appears in control
PMY3340	Drug	CP022329.1	1160225	Reads Poorly aligned
PMY3340	Drug	CP022329.1	1160228	Reads Poorly aligned
PMY3337	Drug	CP022329.1	1160267	Reads Poorly aligned
PMY3340	Drug	CP022329.1	1160267	Reads Poorly aligned
PMY3337	Drug	CP022329.1	1160271	Reads Poorly aligned
PMY3340	Drug	CP022329.1	1160271	Reads Poorly aligned
PMY3337	Drug	CP022329.1	1160278	Reads Poorly aligned
PMY3340	Drug	CP022329.1	1160278	Reads Poorly aligned
PMY3337	Drug	CP022329.1	1160306	Reads Poorly aligned
PMY3340	Drug	CP022329.1	1160306	Reads Poorly aligned
PMY3336	Drug	CP022329.1	1181942	Telomeric

PMY3337	Drug	CP022329.1	1185920	Telomeric
PMY3340	Drug	CP022329.1	1185920	Telomeric
PMY3336	Drug	CP022331.1	194596	Reads Poorly aligned
PMY3337	Drug	CP022331.1	194596	Reads Poorly aligned
PMY3338	Drug	CP022331.1	194596	Reads Poorly aligned
PMY3336	Drug	CP022331.1	749051	Repeat Region; Appears in control
PMY3340	Drug	CP022331.1	845317	Repeat Region; Appears in control
PMY3339	Drug	CP022331.1	885667	Telomeric
PMY3337	Drug	CP022331.1	902396	Reads Poorly aligned
PMY3338	Drug	CP022331.1	902396	Reads Poorly aligned
PMY3339	Drug	CP022331.1	902396	Reads Poorly aligned
PMY3338	Drug	CP022331.1	902487	Reads Poorly aligned
PMY3339	Drug	CP022331.1	902487	Reads Poorly aligned
PMY3339	Drug	CP022332.1	3809	Telomeric
PMY3339	Drug	CP022332.1	3812	Telomeric
PMY3339	Drug	CP022332.1	3813	Telomeric
PMY3339	Drug	CP022332.1	3817	Telomeric
PMY3339	Drug	CP022332.1	3820	Telomeric

PMY3339	Drug	CP022332.1	357497	Repeat Region; Appears in control
PMY3337	Drug	CP022332.1	774033	Telomeric
PMY3338	Drug	CP022332.1	774033	Telomeric
PMY3340	Drug	CP022332.1	774033	Telomeric
PMY3338	Drug	CP022333.1	595980	Reads Poorly aligned
PMY3338	Drug	CP022333.1	596016	Reads Poorly aligned
PMY3340	Drug	CP022333.1	596016	Reads Poorly aligned
PMY3338	Drug	CP022333.1	596019	Reads Poorly aligned
PMY3340	Drug	CP022333.1	596019	Reads Poorly aligned
PMY3338	Drug	CP022333.1	596047	Reads Poorly aligned
PMY3340	Drug	CP022333.1	596047	Reads Poorly aligned
PMY3338	Drug	CP022333.1	596064	Reads Poorly aligned
PMY3340	Drug	CP022333.1	596064	Reads Poorly aligned
PMY3336	Drug	CP022333.1	596158	Reads Poorly aligned
PMY3338	Drug	CP022333.1	596158	Reads Poorly aligned
PMY3340	Drug	CP022333.1	596158	Reads Poorly aligned
PMY3336	Drug	CP022333.1	596160	Reads Poorly aligned
PMY3338	Drug	CP022333.1	596160	Reads Poorly aligned

PMY3340	Drug	CP022333.1	596160	Reads Poorly aligned
PMY3336	Drug	CP022333.1	596166	Reads Poorly aligned
PMY3338	Drug	CP022333.1	596166	Reads Poorly aligned
PMY3340	Drug	CP022333.1	596166	Reads Poorly aligned
PMY3336	Drug	CP022333.1	596193	Reads Poorly aligned
PMY3338	Drug	CP022333.1	596193	Reads Poorly aligned
PMY3340	Drug	CP022333.1	596193	Reads Poorly aligned
PMY3340	Drug	CP022333.1	596261	Reads Poorly aligned
PMY3336	Drug	CP022333.1	596802	Reads Poorly aligned
PMY3338	Drug	CP022333.1	652595	Reads Poorly aligned
PMY3337	Drug	CP022333.1	679354	Reads Poorly aligned
PMY3338	Drug	CP022333.1	753750	Telomeric
PMY3340	Drug	CP022334.1	214341	Repeat Region; Appears in control
PMY3337	Drug	CP022334.1	307866	Reads Poorly aligned
PMY3337	Drug	CP022334.1	307871	Reads Poorly aligned
PMY3337	Drug	CP022334.1	307875	Reads Poorly aligned
PMY3337	Drug	CP022334.1	307892	Reads Poorly aligned
PMY3340	Drug	CP022334.1	307892	Reads Poorly aligned

PMY3337	Drug	CP022334.1	307895	Reads Poorly aligned
PMY3336	Drug	CP022334.1	307944	Reads Poorly aligned
PMY3337	Drug	CP022334.1	307944	Reads Poorly aligned
PMY3337	Drug	CP022334.1	308021	Reads Poorly aligned
PMY3338	Drug	CP022334.1	308117	Reads Poorly aligned
PMY3340	Drug	CP022334.1	308117	Reads Poorly aligned
PMY3338	Drug	CP022334.1	453357	Reads Poorly aligned
PMY3338	Drug	CP022334.1	453358	Reads Poorly aligned
PMY3336	Drug	CP022334.1	686462	Reads Poorly aligned
PMY3338	Drug	CP022334.1	686462	Reads Poorly aligned
PMY3339	Drug	CP022334.1	686462	Reads Poorly aligned
PMY3327	Heat	CP022321.1	2286962	Telomeric
PMY3330	Heat	CP022321.1	2286962	Reads Poorly aligned
PMY3326	Heat	CP022321.1	2287024	Telomeric
PMY3328	Heat	CP022321.1	2287024	Reads Poorly aligned
PMY3329	Heat	CP022321.1	2287024	Reads Poorly aligned
PMY3326	Heat	CP022321.1	2287027	Telomeric
PMY3328	Heat	CP022321.1	2287117	Reads Poorly aligned

PMY3328	Heat	CP022321.1	2287128	Reads Poorly aligned
PMY3326	Heat	CP022323.1	1391280	Substitution; intergenic
PMY3327	Heat	CP022323.1	1391280	Substitution; intergenic
PMY3326	Heat	CP022323.1	1391290	Substitution; intergenic
PMY3327	Heat	CP022323.1	1391290	Substitution; intergenic
PMY3327	Heat	CP022324.1	190912	Repeat Region; Appears in control
PMY3328	Heat	CP022324.1	719308	Substitution; intergenic
PMY3326	Heat	CP022325.1	279976	Repeat Region; Appears in control
PMY3329	Heat	CP022326.1	819066	Substitution; intergenic
PMY3327	Heat	CP022326.1	1351736	no reads
PMY3326	Heat	CP022329.1	812853	Substitution; intergenic
PMY3326	Heat	CP022329.1	812855	Substitution; intergenic
PMY3327	Heat	CP022329.1	820206	Reads Poorly aligned
PMY3328	Heat	CP022329.1	820206	Reads Poorly aligned
PMY3329	Heat	CP022329.1	820206	Reads Poorly aligned
PMY3328	Heat	CP022329.1	1186235	Reads Poorly aligned
PMY3326	Heat	CP022331.1	194596	Reads Poorly aligned
PMY3327	Heat	CP022331.1	194596	Reads Poorly aligned

PMY3328	Heat	CP022331.1	194596		Reads Poorly aligned
PMY3326	Heat	CP022332.1	131021		Repeat Region; Appears in control
PMY3326	Heat	CP022332.1	532814		Repeat Region; Appears in control
PMY3328	Heat	CP022333.1	27078	CKF44_07922	insertion
PMY3329	Heat	CP022333.1	27078	CKF44_07922	insertion
PMY3330	Heat	CP022333.1	27078	CKF44_07922	insertion
PMY3329	Heat	CP022333.1	52595	CKF44_06271	insertion
PMY3326	Heat	CP022333.1	586924		Substitution; intergenic
PMY3327	Heat	CP022333.1	586924		Substitution; intergenic
PMY3330	Heat	CP022333.1	586924		Substitution; intergenic
PMY3326	Heat	CP022333.1	586975		Substitution; intergenic
PMY3327	Heat	CP022333.1	586975		Substitution; intergenic
PMY3330	Heat	CP022333.1	586975		Substitution; intergenic
PMY3327	Heat	CP022333.1	595914		Reads Poorly aligned
PMY3328	Heat	CP022333.1	595914		Reads Poorly aligned
PMY3327	Heat	CP022333.1	595926		Reads Poorly aligned
PMY3328	Heat	CP022333.1	595926		Reads Poorly aligned
PMY3326	Heat	CP022333.1	596016		Substitution; intergenic

PMY3327	Heat	CP022333.1	596016		Reads Poorly aligned
PMY3328	Heat	CP022333.1	596016		Reads Poorly aligned
PMY3329	Heat	CP022333.1	596016		Reads Poorly aligned
PMY3326	Heat	CP022333.1	596019		Substitution; intergenic
PMY3327	Heat	CP022333.1	596019		Reads Poorly aligned
PMY3328	Heat	CP022333.1	596019		Reads Poorly aligned
PMY3329	Heat	CP022333.1	596019		Reads Poorly aligned
PMY3326	Heat	CP022333.1	596047		Substitution; intergenic
PMY3327	Heat	CP022333.1	596047		Reads Poorly aligned
PMY3328	Heat	CP022333.1	596047		Reads Poorly aligned
PMY3326	Heat	CP022333.1	596064		Substitution; intergenic
PMY3328	Heat	CP022333.1	596064		Reads Poorly aligned
PMY3326	Heat	CP022333.1	596277		Substitution; intergenic
PMY3326	Heat	CP022333.1	596283		Substitution; intergenic
PMY3326	Heat	CP022333.1	596310		Substitution; intergenic
PMY3326	Heat	CP022333.1	596312		Substitution; intergenic
PMY3330	Heat	CP022333.1	647277	CKF44_06487	Deletion
PMY3330	Heat	CP022333.1	647278	CKF44_06487	Deletion

PMY3328	Heat	CP022333.1	679354		Repeat Region; Appears in control
PMY3329	Heat	CP022333.1	679354		Repeat Region; Appears in control
PMY3326	Heat	CP022334.1	307963	CKF44_05436	Substitution; intergenic
PMY3326	Heat	CP022334.1	307964	CKF44_05436	Substitution; intergenic
PMY3326	Heat	CP022334.1	307992	CKF44_05436	Substitution; intergenic
PMY3329	Heat	CP022334.1	307992	CKF44_05436	Substitution
PMY3327	Heat	CP022334.1	868510		Repeat Region; Appears in control
PMY3329	Heat	CP022334.1	931144		Reads Poorly aligned
PMY3329	Heat	CP022334.1	931195		Reads Poorly aligned
PMY3309	Rev	CP022321.1	357202	ckf44_00130	3bp Deletion
PMY3308	Rev	CP022321.1	1282647		Repeat Region; Appears in control
PMY3309	Rev	CP022321.1	1323198		Repeat Region; Appears in control
PMY3308	Rev	CP022321.1	1880653		Repeat Region; Appears in control
PMY3308	Rev	CP022321.1	2286962		Telomeric
PMY3309	Rev	CP022321.1	2287019		Telomeric
PMY3306	Rev	CP022321.1	2287024		Reads Poorly aligned
PMY3309	Rev	CP022321.1	2287024		Telomeric
PMY3309	Rev	CP022321.1	2287027		Telomeric

PMY3308	Rev	CP022322.1	370242		Repeat Region; Appears in control
PMY3306	Rev	CP022322.1	914777	CKF44_03815	Elevated Coverage
PMY3309	Rev	CP022323.1	1391280		Substitution; Intergenic
PMY3309	Rev	CP022323.1	1391290		Substitution; Intergenic
PMY3308	Rev	CP022324.1	337042	CKF44_05063	Substitution
PMY3309	Rev	CP022324.1	518922		Repeat Region; Appears in control
PMY3306	Rev	CP022325.1	222289	CKF44_07406	Substitution
PMY3306	Rev	CP022325.1	222294	CKF44_07406	Substitution
PMY3308	Rev	CP022325.1	411667	CKF44_01396	2bp Deletion
PMY3310	Rev	CP022325.1	896231		Repeat Region; Appears in control
PMY3309	Rev	CP022325.1	1567278		Substitution; Intergenic
PMY3309	Rev	CP022326.1	69431		Repeat Region; Appears in control
PMY3307	Rev	CP022326.1	737090		Repeat Region; Appears in control
PMY3310	Rev	CP022326.1	737090		Repeat Region; Appears in control
PMY3308	Rev	CP022326.1	791796		Substitution; Intergenic
PMY3310	Rev	CP022326.1	818697		Substitution; Intergenic
PMY3308	Rev	CP022326.1	819066		Substitution; Intergenic
PMY3308	Rev	CP022326.1	929254		Repeat Region; Appears in control

PMY3310	Rev	CP022326.1	929254		Repeat Region; Appears in control
PMY3308	Rev	CP022326.1	950114		Substitution; Intergenic
PMY3306	Rev	CP022327.1	752859		Repeat Region; Appears in control
PMY3307	Rev	CP022327.1	752859		Repeat Region; Appears in control
PMY3309	Rev	CP022327.1	1308145		Repeat Region; Appears in control
PMY3306	Rev	CP022327.1	1357323		Repeat Region; Appears in control
PMY3310	Rev	CP022327.1	1357323		Repeat Region; Appears in control
PMY3309	Rev	CP022328.1	356400		Substitution; Intergenic
PMY3308	Rev	CP022329.1	28327	CKF44_04109	insertion
PMY3309	Rev	CP022329.1	588276		insertion; Intergenic
PMY3310	Rev	CP022329.1	804247		Substitution; Intergenic
PMY3306	Rev	CP022329.1	804812		Repeat Region; Appears in control
PMY3307	Rev	CP022329.1	813451		Substitution; Intergenic
PMY3307	Rev	CP022329.1	1160206	CKF44_07784	Deletion?
PMY3307	Rev	CP022329.1	1160225	CKF44_07784	Substitution
PMY3309	Rev	CP022329.1	1160225	CKF44_07784	Substitution
PMY3307	Rev	CP022329.1	1160228	CKF44_07784	Substitution
PMY3309	Rev	CP022329.1	1160228	CKF44_07784	Substitution

PMY3308	Rev	CP022330.1	655257		Repeat Region; Appears in control
PMY3307	Rev	CP022331.1	194596		Reads Poorly aligned
PMY3309	Rev	CP022331.1	194597		Reads Poorly aligned
PMY3310	Rev	CP022331.1	194597		Reads Poorly aligned
PMY3306	Rev	CP022331.1	885667		Substitution; Intergenic
PMY3307	Rev	CP022331.1	924601		Substitution; intergenic
PMY3309	Rev	CP022331.1	1492635		Repeat Region; Appears in control
PMY3307	Rev	CP022333.1	211		Reads Poorly aligned
PMY3310	Rev	CP022333.1	27078	CKF44_07922	insertion
PMY3308	Rev	CP022333.1	52207	CKF44_06271	Substitution
PMY3308	Rev	CP022333.1	586924		Substitution; Intergenic
PMY3309	Rev	CP022333.1	586924		Substitution; Intergenic
PMY3309	Rev	CP022333.1	586975		Substitution; Intergenic
PMY3310	Rev	CP022333.1	586975		Substitution; Intergenic
PMY3307	Rev	CP022333.1	595926		Reads Poorly aligned
PMY3307	Rev	CP022333.1	596016		Reads Poorly aligned
PMY3307	Rev	CP022333.1	596019		Reads Poorly aligned
PMY3309	Rev	CP022333.1	596047		Reads Poorly aligned

PMY3307	Rev	CP022334.1	308154	CKF44_05436	Substitution
PMY3309	Rev	CP022334.1	308154	CKF44_05436	Substitution
PMY3310	Rev	CP022334.1	868510		Repeat Region; Appears in control

## Bibliography

- Adiba, S., C. Nizak, M. van Baalen, E. Denamur, and F. Depaulis, 2010 From grazing resistance to pathogenesis: The coincidental evolution of virulence factors. *PLoS ONE* **5**: 1–10.
- Akya, A., A. Pointon, and C. Thomas, 2009 Mechanism involved in phagocytosis and killing of *Listeria monocytogenes* by *Acanthamoeba polyphaga*. *Parasitology Research* **105**: 1375–1383, type of bacteria that halt reproduction.
- Albuquerque, P., A. M. Nicola, D. A. G. Magnabosco, L. da Silveira Derengowski, L. S. Crisóstomo, *et al.*, 2019 A hidden battle in the dirt: Soil amoebae interactions with paracoccidioides spp. *PLoS Neglected Tropical Diseases* **13**.
- and Eric Alani Xin Ma, K. T. N. S. Z. C. D. B., Maria V. Rogacheva, 2012 Mutation hotspots in yeast caused by long-range clustering of homopolymeric sequences **26**: 36 – 42.
- and Joseph Heitman Yong-Sun Bahn, G. M. C., Kaihei Kojima, 2005 Specialization of the hog pathway and its impact on differentiation and virulence of *Cryptococcus neoformans*. *Mol Biol Cell* **16**: 2285–2300.
- Arras, S. D., K. L. Ormerod, P. E. Erpf, M. I. Espinosa, A. C. Carpenter, *et al.*, 2017 Convergent microevolution of *Cryptococcus neoformans* hypervirulence in the laboratory and the clinic. *Scientific Reports* **7**: 1–14.
- Aubry, L., G. Klein, J. L. Martiel, and M. Satre, 1993 Kinetics of endosomal pH evolution in *Dictyostelium discoideum* amoebae. study by fluorescence spectroscopy. *Journal of Cell Science* **105**: 861–866.
- Bergman, A. and A. Casadevall, 2010 Mammalian endothermy optimally restricts fungi and metabolic costs. *mBio* **1**: 0–1.
- Berkow, E. L. and S. R. Lockhart, 2017 Fluconazole resistance in candida species: A current perspective. *Infection and Drug Resistance* **10**: 237–245.
- Best, A. and A. Kwaik, 2018 Evolution of the arsenal of legionella pneumophila effectors to modulate protist hosts **9**: 1–16.
- Bilsland, E., C. Molin, S. Swaminathan, A. Ramne, and P. Sunnerhagen, 2004 Rck1 and rck2 mapkap kinases and the hog pathway are required for oxidative stress resistance. *Molecular Microbiology* **53**: 1743–1756.
- Bland, N. D., J. W. Pinney, J. E. Thomas, A. J. Turner, and R. E. Isaac, 2008

- Bioinformatic analysis of the neprilysin (m13) family of peptidases reveals complex evolutionary and functional relationships. *BMC Evolutionary Biology* **8**: 1–10.
- Botts, M. R. and C. M. Hull, 2010 Dueling in the lung: How cryptococcus spores race the host for survival.
- Brauer, V. S., C. P. Rezende, A. M. Pessoni, R. G. D. Paula, K. S. Rangappa, *et al.*, 2019 Antifungal agents in agriculture: Friends and foes of public health. *Biomolecules* **9**: 1–21.
- Brown, G. D., D. W. Denning, N. A. Gow, S. M. Levitz, M. G. Netea, *et al.*, 2012a Hidden killers: Human fungal infections. *Science Translational Medicine* **4**.
- Brown, S. P., D. M. Cornforth, and N. Mideo, 2012b Evolution of virulence in opportunistic pathogens: Generalism, plasticity, and control. *Trends in Microbiology* **20**: 336–342.
- Burks, C., A. Darby, L. G. Londoño, M. Momany, and M. T. Brewer, 2021 Azole-resistant *aspergillus fumigatus* in the environment: Identifying key reservoirs and hotspots of antifungal resistance. *PLoS Pathogens* **17**: 1–15.
- Campbell, M. T., A. Grondin, H. Walia, and G. Morota, 2020 Leveraging genome-enabled growth models to study shoot growth responses to water deficit in rice. *Journal of Experimental Botany* **71**: 5669–5679.
- Casadevall, A., 2006 Cards of virulence and the global virulome for humans. *Microbe* **1**: 359–364.
- Casadevall, A., 2008 Evolution of intracellular pathogens. *Annual Review of Microbiology* **62**: 19–33.
- Casadevall, A., M. Fu, A. Guimaraes, and P. Albuquerque, 2019 The ‘amoeboid predator-fungal animal virulence’ hypothesis. *Journal of Fungi* **5**: 10.
- Casadevall, A. and L. A. Pirofski, 2007 Accidental virulence, cryptic pathogenesis, martians, lost hosts, and the pathogenicity of environmental microbes. *Eukaryotic Cell* **6**: 2169–2174, accidental virulence paper.
- Castellani, A., 1930 An amoeba found in culture of yeast: preliminary note. *Journal of Tropical Medicine London* **33**: 160.
- Chai, H. H., W. K. Ho, N. Graham, S. May, F. Massawe, *et al.*, 2017 A cross-species gene expression marker-based genetic map and qtl analysis in bambara groundnut. *Genes* **8**.

- Chen, M., Y. Xing, A. Lu, W. Fang, B. Sun, *et al.*, 2015a Internalized *Cryptococcus neoformans* activates the canonical caspase-1 and the noncanonical caspase-8 inflammasomes. *The Journal of Immunology* **195**: 4962–4972.
- Chen, Y., A. P. Litvintseva, A. E. Frazzitta, M. R. Haverkamp, L. Wang, *et al.*, 2015b Comparative analyses of clinical and environmental populations of *Cryptococcus neoformans* in botswana. *Molecular Ecology* **24**: 3559–3571.
- Chen, Y. L., J. H. Konieczka, D. J. Springer, S. E. Bowen, J. Zhang, *et al.*, 2012 Convergent evolution of calcineurin pathway roles in thermotolerance and virulence in *Candida glabrata*. *G3: Genes, Genomes, Genetics* **2**: 675–691.
- Chen, Y. L., V. N. Lehman, Y. Lewit, A. F. Averette, and J. Heitman, 2013 Calcineurin governs thermotolerance and virulence of *Cryptococcus gattii*. *G3: Genes, Genomes, Genetics* **3**: 527–539.
- Chowdhary, A. and J. F. Meis, 2018 Emergence of azole resistant aspergillus fumigatus and one health: time to implement environmental stewardship. *Environmental Microbiology* **20**: 1299–1301.
- Chrisman, C. J., M. Alvarez, and A. Casadevall, 2010 Phagocytosis of *Cryptococcus neoformans* by, and nonlytic exocytosis from, *Acanthamoeba castellanii*. *Applied and Environmental Microbiology* **76**: 6056–6062.
- Churchill, G. A. and R. W. Doerge, 1994 Empirical threshold values for quantitative trait mapping. *Genetics* **138**: 963–971.
- Cordero, A. C. R. J., 2017 Functions of fungal melanin beyond virulence **31**: 99–112.
- Cordero, R. J., V. Robert, G. Cardinali, E. S. Arinze, S. M. Thon, *et al.*, 2018 Impact of yeast pigmentation on heat capture and latitudinal distribution. *Current Biology* **28**: 2657–2664.e3.
- Cox, G. M., H. C. McDade, S. C. Chen, S. C. Tucker, M. Gottfredsson, *et al.*, 2001 Extracellular phospholipase activity is a virulence factor for *Cryptococcus neoformans*. *Molecular Microbiology* **39**: 166–175.
- Cox, G. M., J. Mukherjee, G. T. Cole, A. Casadevall, and J. R. Perfect, 2000 Urease as a virulence factor in experimental cryptococcosis. *Infection and Immunity* **68**: 443–448.
- Cuomo, C. A., J. Rhodes, and C. A. Desjardins, 2018 Advances in *Cryptococcus genomics*: Insights into the evolution of pathogenesis. *Memorias do Instituto Oswaldo Cruz* **113**: 1–7.

- da S. Derengowski, L., H. C. Paes, P. Albuquerque, A. H. F. Tavares, L. Fernandes, *et al.*, 2013 The transcriptional response of *Cryptococcus neoformans* to ingestion by *Acanthamoeba castellanii* and macrophages provides insights into the evolutionary adaptation to the mammalian host. *Eukaryotic Cell* **12**: 761–774.
- Datta, K., K. H. Bartlett, R. Baer, E. Byrnes, E. Galanis, *et al.*, 2009 Spread of *Cryptococcus gattii* into Pacific Northwest region of the United States. *Emerging Infectious Diseases* **15**: 1185–1191.
- Davies, B., L. S. Chatterjee, and S. W. Edwards, 1991 Superoxide generation during phagocytosis by *Acanthamoeba castellanii*: similarities to the respiratory burst of immune phagocytes pp. 705–710.
- de Gontijo, F. A., R. C. Pascon, L. Fernandes, J. Machado, J. A. Alspaugh, *et al.*, 2014 The role of the de novo pyrimidine biosynthetic pathway in *Cryptococcus neoformans* high temperature growth and virulence. *Fungal Genetics and Biology* **70**: 12–23.
- DeLeon-Rodriguez, C. M. and A. Casadevall, 2016 *Cryptococcus neoformans*: Tripping on acid in the phagolysosome. *Frontiers in Microbiology* **7**: 1–9.
- Desjardins, C. A., C. Giamberardino, S. Sykes, C.-H. Yu, J. Tenor, *et al.*, 2017 Population genomics and the evolution of virulence in the fungal pathogen *Cryptococcus neoformans*. Cold Springs Harbor Laboratory Press p. 118323, All lineages except for VNBS mata is rare.
- Desjardins CA Muñoz JF, F. R., S. S. Misas E Gallo JE, Sykes S, S. C. Teixeira Whiston EA, Bagagli E, C. O. McEwen JG MDM, Taylor JW, C. Cuomo, *et al.*, 2016 Virulence across the major lineages of. *mSphere* **1**: 1–18.
- Djordjevic, J. T., 2010 Role of phospholipases in fungal fitness, pathogenicity, and drug development - lessons from *Cryptococcus neoformans*. *Frontiers in Microbiology* **1**: 1–13.
- Doering, T. L., J. D. Nosanchuk, W. K. Roberts, and A. Casadevall, 1999 Melanin as a potential cryptococcal defence against microbicidal proteins. *Medical Mycology* **37**: 175–181.
- Dromer, F., S. Mathoulin-Pélissier, O. Launay, O. Lortholary, J. Achard, *et al.*, 2007 Determinants of disease presentation and outcome during cryptococcosis: The cryptoa/d study. *PLoS Medicine* **4**: 0297–0308.
- Escoll, P., M. Rolando, L. Gomez-Valero, and C. Buchrieser, 2013 *From Amoeba to Macrophages: Exploring the Molecular Mechanisms of Legionella pneumophila Infection in Both Hosts*.

- Fan, W., P. R. Kraus, M. J. Boily, and J. Heitman, 2005 *Cryptococcus neoformans* gene expression during murine macrophage infection. *Eukaryotic Cell* **4**: 1420–1433.
- Fan, Y., Y. Wang, G. A. Korfanty, M. Archer, and J. Xu, 2021 Genome-wide association analysis for triazole resistance in *aspergillus fumigatus*. *Pathogens* **10**.
- Farrer, R. A., C. A. Desjardins, S. Sakthikumar, S. Gujja, S. Saif, *et al.*, 2015 Genome evolution and innovation across the four major lineages of *Cryptococcus gattii*. *mBio* **6**: 1–12.
- Farrer, R. A., K. Voelz, D. A. Henk, S. A. Johnston, M. C. Fisher, *et al.*, 2016 Microevolutionary traits and comparative population genomics of the emerging pathogenic fungus *Cryptococcus gattii*. *Philosophical Transactions of the Royal Society B: Biological Sciences* **371**.
- Fernandes, K. E., C. Dwyer, L. T. Campbell, and D. A. Carter, 2016 Species in the *cryptococcus gattii* complex differ in capsule and cell size following growth under capsule-inducing conditions. *mSphere* **1**.
- Findley, K., M. Rodriguez-Carres, B. Metin, J. Kroiss, Álvaro Fonseca, *et al.*, 2009 Phylogeny and phenotypic characterization of pathogenic *cryptococcus* species and closely related saprobic taxa in the tremellales. *Eukaryotic Cell* **8**: 353–361.
- Fisher, M. C., A. Alastruey-Izquierdo, J. Berman, T. Bicanic, E. M. Bignell, *et al.*, 2022 Tackling the emerging threat of antifungal resistance to human health. *Nature Reviews Microbiology* **20**: 557–571.
- Fisher, M. C., N. J. Hawkins, D. Sanglard, and S. J. Gurr, 2018 Worldwide emergence of resistance to antifungal drugs challenges human health and food security. *Science* **742**: 739–742.
- Fu, M. S., C. Coelho, C. M. D. Leon-Rodriguez, D. C. Rossi, E. Camacho, *et al.*, 2018 *Cryptococcus neoformans* urease affects the outcome of intracellular pathogenesis by modulating phagolysosomal pH, volume 14.
- Fu, M. S., L. C. Liporagi-Lopes, S. R. dos Santos Júnior, J. L. Tenor, J. R. Perfect, *et al.*, 2021 Amoeba predation of *Cryptococcus neoformans* results in pleiotropic changes to traits associated with virulence. *mBio* **12**.
- Gan, X., M. Kitakawa, K. I. Yoshino, N. Oshiro, K. Yonezawa, *et al.*, 2002 Tag-mediated isolation of yeast mitochondrial ribosome and mass spectrometric identification of its new components. *European Journal of Biochemistry* **269**: 5203–5214.
- Garcia-Solache, M. A. and A. Casadevall, 2010 Global warming will bring new fungal diseases for mammals. *mBio* **1**.

- German, N., D. Doyscher, and C. Rensing, 2013 Bacterial killing in macrophages and amoeba: Do they all use a brass dagger? *Future Microbiology* **8**: 1257–1264.
- Graack, H. R. and B. Wittmann-Liebold, 1998 Mitochondrial ribosomal proteins (mrps) of yeast.
- Handelman, M. and N. Osherov, 2022 Experimental and in-host evolution of triazole resistance in human pathogenic fungi. *Frontiers in Fungal Biology* **3**: 1–21.
- Heinekamp, T., H. Schmidt, K. Lapp, V. Pätz, I. Shopova, *et al.*, 2015 Interference of *aspergillus fumigatus* with the immune response.
- Huang, C. J., M. Y. Lu, Y. W. Chang, and W. H. Li, 2018 Experimental evolution of yeast for high-temperature tolerance. *Molecular biology and evolution* **35**: 1823–1839.
- Huang, M. Y., M. B. Joshi, M. J. Boucher, S. Lee, L. C. Loza, *et al.*, 2022 Short homology-directed repair using optimized cas9 in the pathogen *Cryptococcus neoformans* enables rapid gene deletion and tagging. *Genetics* **220**.
- Isnard, A. D., D. Thomas, and Y. Surdin-Kerjan, 1996 The study of methionine uptake in *saccharomyces cerevisiae* reveals a new family of amino acid permeases. *Journal of Molecular Biology* **262**: 473–484.
- Jason E. Stajich Lotus A. Lofgren, R. A. C., Brandon S. Ross, 2022 *Combined Pan-, Population-, and Phylo-Genomic Analysis of Aspergillus fumigatus Reveals Population Structure and Lineage-Specific Diversity*.
- Johnston, S. A., K. Voelz, and R. C. May, 2016 *Cryptococcus neoformans* thermo-tolerance to avian body temperature is sufficient for extracellular growth but not intracellular survival in macrophages. *Scientific Reports* **6**: 1–9.
- Jung, K. W., D. H. Yang, S. Maeng, K. T. Lee, Y. S. So, *et al.*, 2015 Systematic functional profiling of transcription factor networks in *Cryptococcus neoformans*. *Nature Communications* **6**: 1–14.
- Jørgensen, L. N. and T. M. Heick, 2021 Azole use in agriculture, horticulture, and wood preservation – is it indispensable? *Frontiers in Cellular and Infection Microbiology* **11**: 1–16.
- Kappaun, K., A. R. Piovesan, C. R. Carlini, and R. Ligabue-Braun, 2018 Ureases: Historical aspects, catalytic, and non-catalytic properties – a review. *Journal of Advanced Research* **13**: 3–17.
- Karadag, H. and F. Ozhan, 2015 Effect of cyprodinil and fludioxonil pesticides on

- bovine liver catalase activity. *Biotechnology and Biotechnological Equipment* **29**: 40–44.
- Kilani, J. and S. Fillinger, 2016 Phenylpyrroles: 30 years, two molecules and (nearly) no resistance. *Frontiers in Microbiology* **7**: 1–10.
- Kojima, K., Y.-S. Bahn, and J. Heitman, 2006 Calcineurin, mpk1 and hog1 mapk pathways independently control fludioxonil antifungal sensitivity in *Cryptococcus neoformans*. *Microbiology* **152**: 591–604.
- Kretschmer, M., M. Leroch, A. Mosbach, A. S. Walker, S. Fillinger, *et al.*, 2009 Fungicide-driven evolution and molecular basis of multidrug resistance in field populations of the grey mould fungus *botrytis cinerea*. *PLoS Pathogens* **5**.
- Kwon-Chung, K. J. and Y. C. Chang, 2012 Aneuploidy and drug resistance in pathogenic fungi. *PLoS Pathogens* **8**: 8–11.
- Kwon-Chung, K. J. and J. A. Sugui, 2013 *Aspergillus fumigatus*-what makes the species a ubiquitous human fungal pathogen? *PLoS Pathogens* **9**: 1–4.
- Lancaster, L. T., R. Y. Dudaniec, P. Chauhan, M. Wellenreuther, E. I. Svensson, *et al.*, 2016 Gene expression under thermal stress varies across a geographical range expansion front. *Molecular Ecology* **25**: 1141–1156.
- Lanzas, C., K. Davies, S. Erwin, and D. Dawson, 2020 On modelling environmentally transmitted pathogens. *Interface Focus* **10**.
- Leach, M. D. and L. E. Cowen, 2013 Surviving the heat of the moment: A fungal pathogens perspective. *PLoS Pathogens* **9**: 1–4.
- Lee, D., E. H. Jang, M. Lee, S. W. Kim, Y. Lee, *et al.*, 2019a Unraveling melanin biosynthesis and signaling networks in *Cryptococcus neoformans*. *mBio* **10**.
- Lee, D., E. H. Jang, M. Lee, S. W. Kim, Y. Lee, *et al.*, 2019b Unraveling melanin biosynthesis and signaling networks in *Cryptococcus neoformans*. *mBio* **10**.
- Lee, H., A. K. Lamichhane, H. M. Garraffo, K. J. Kwon-Chung, and Y. C. Chang, 2012a Involvement of pdk1, pkc and tor signalling pathways in basal fluconazole tolerance in *Cryptococcus neoformans*. *Molecular Microbiology* **84**: 130–146.
- Lee, H., A. K. Lamichhane, H. M. Garraffo, K. J. Kwon-Chung, and Y. C. Chang, 2012b Involvement of pdk1, pkc and tor signalling pathways in basal fluconazole tolerance in *Cryptococcus neoformans*. *Molecular Microbiology* **84**: 130–146.
- Leon-Rodriguez, C. M. D., M. S. Fu, M. O. Çorbali, R. J. Cordero, and A. Casadevall,

- 2018 The capsule of *Cryptococcus neoformans* modulates phagosomal pH through its acidbase properties. *mSphere* **3**: 1–8.
- Leroch, M., C. Plesken, R. W. Weber, F. Kauff, G. Scalliet, *et al.*, 2013 Gray mold populations in German strawberry fields are resistant to multiple fungicides and dominated by a novel clade closely related to *Botrytis cinerea*. *Applied and Environmental Microbiology* **79**: 159–167.
- Lesuisse, E., E. R. Lyver, S. A. Knight, and A. Dancis, 2004 Role of *yhm1*, encoding a mitochondrial carrier protein, in iron distribution of yeast. *Biochemical Journal* **378**: 599–607.
- Levin, R., S. Grinstein, and J. Canton, 2016 The life cycle of phagosomes: formation, maturation, and resolution. *Immunological Reviews* **273**: 156–179.
- Li, R. and R. C. Deed, 2021 Reciprocal hemizyosity analysis reveals that the *Saccharomyces cerevisiae* *cg121* gene affects lag time duration in synthetic grape must. *G3: Genes, Genomes, Genetics* **11**.
- Lin, J., Y. Fan, and X. Lin, 2020 Transformation of *Cryptococcus neoformans* by electroporation using a transient CRISPR-Cas9 expression (trace) system. *Fungal Genetics and Biology* **138**: 103364.
- Lin, J., A. Idnurm, and X. Lin, 2015 Morphology and its underlying genetic regulation impact the interaction between *Cryptococcus neoformans* and its hosts. *Medical Mycology* **53**: 493–504.
- Lin, L., J. Cao, A. Du, Q. An, X. Chen, *et al.*, 2021 *eif3k* domain-containing protein regulates conidiogenesis, appressorium turgor, virulence, stress tolerance, and physiological and pathogenic development of *Magnaporthe oryzae*. *Frontiers in Plant Science* **12**: 1–20.
- Lin, X., J. C. Huang, T. G. Mitchell, and J. Heitman, 2006 Virulence attributes and hyphal growth of *C. neoformans* are quantitative traits and the *mat* allele enhances filamentation. *PLoS Genetics* **2**: 1801–1814.
- Litvintseva, A. P., R. E. Marra, K. Nielsen, J. Heitman, R. Vilgalys, *et al.*, 2003 Evidence of sexual recombination among *Cryptococcus neoformans* serotype a isolates in sub-Saharan Africa. *Eukaryotic Cell* **2**: 1162–1168.
- Litvintseva, A. P. and T. G. Mitchell, 2009 Most environmental isolates of *Cryptococcus neoformans* var. *grubii* (serotype a) are not lethal for mice. *Infection and Immunity* **77**: 3188–3195.
- Liu, S., S. Youngchim, D. Zamith-Miranda, and J. D. Nosanchuk, 2021 Fungal

- melanin and the mammalian immune system. *Journal of Fungi* **7**: 1–15.
- Luo, Y., A. Widmer, and S. Karrenberg, 2015 The roles of genetic drift and natural selection in quantitative trait divergence along an altitudinal gradient in *Arabidopsis thaliana*. *Heredity* **114**: 220–228.
- Macoris, S. A., M. F. Sugizaki, M. T. Peraçoli, S. M. Bosco, F. Hebelers-Barbosa, *et al.*, 2006 Virulence attenuation and phenotypic variation of *Paracoccidioides brasiliensis* isolates obtained from armadillos and patients. *Memorias do Instituto Oswaldo Cruz* **101**: 331–334.
- Maliehe, M., M. A. Ntoi, S. Lahiri, O. S. Folorunso, A. O. Ogundeji, *et al.*, 2020 Environmental factors that contribute to the maintenance of *Cryptococcus neoformans* pathogenesis. *Microorganisms* **8**.
- Martinez, L. R., J. Garcia-Rivera, and A. Casadevall, 2001 *Cryptococcus neoformans* var. *neoformans* (serotype d) strains are more susceptible to heat than *C. neoformans* var. *grubii* (serotype a) strains. *Journal of Clinical Microbiology* **39**: 3365–3367.
- May, R. C., N. R. Stone, D. L. Wiesner, T. Bicanic, and K. Nielsen, 2016 *Cryptococcus*: From environmental saprophyte to global pathogen. *Nature Reviews Microbiology* **14**: 106–117.
- Morrow, C. A., R. Lee, E. W. Chow, K. L. Ormerod, A. Goldinger, *et al.*, 2012 A unique chromosomal rearrangement in the *Cryptococcus neoformans* var. *grubii* type strain enhances key phenotypes associated with virulence. *mBio* **3**: 1–11.
- Nelissen, B., R. D. Wachter, and A. Goffeau, 1997 Classification of all putative permeases and other membrane plurispansers of the major facilitator superfamily encoded by the complete genome of *Saccharomyces cerevisiae*. *FEMS Microbiology Reviews* **21**: 113–134.
- Nielsen, K., G. M. Cox, P. Wang, D. L. Toffaletti, J. R. Perfect, *et al.*, 2003 Sexual cycle of *Cryptococcus neoformans* var. *grubii* and virulence of congenic a and isolates. *Infection and Immunity* **71**: 4831–4841.
- Nnadi, N. E. and D. A. Carter, 2021 Climate change and the emergence of fungal pathogens. *PLoS Pathogens* **17**: 1–6.
- Nosanchuk, J. D., P. Valadon, M. Feldmesser, and A. Casadevall, 1999 Melanization of *Cryptococcus neoformans* in murine infection. *Molecular and Cellular Biology* **19**: 745–750.
- Odom, A., S. Muir, E. Lim, D. L. Toffaletti, J. Perfect, *et al.*, 1997 Calcineurin is required for virulence of *Cryptococcus neoformans*. *EMBO Journal* **16**: 2576–2589.

- O'Meara, T. R. and J. A. Alspaugh, 2012 The *Cryptococcus neoformans* capsule: A sword and a shield. *Clinical Microbiology Reviews* **25**: 387–408.
- Paes, H. C., L. da Silveira Derengowski, L. D. F. Peconick, P. Albuquerque, G. J. Pappas, *et al.*, 2018 A wor1-like transcription factor is essential for virulence of *Cryptococcus neoformans*. *Frontiers in Cellular and Infection Microbiology* **8**: 1–17.
- Papay, M., C. Klein, I. Hapala, L. Petriskova, K. Kuchler, *et al.*, 2020 Mutations in the nucleotide-binding domain of putative sterol importers *aus1* and *pdr11* selectively affect utilization of exogenous sterol species in yeast. *Yeast* **37**: 5–14.
- Paulussen, C., J. E. Hallsworth, S. Álvarez Pérez, W. C. Nierman, P. G. Hamill, *et al.*, 2017 Ecology of aspergillosis: insights into the pathogenic potency of *Aspergillus fumigatus* and some other *Aspergillus* species. *Microbial Biotechnology* **10**: 296–322.
- Perfect, J. R., 2006 *Cryptococcus neoformans*: The yeast that likes it hot. *FEMS Yeast Research* **6**: 463–468.
- Perfect, J. R., S. D. Lang, and D. T. Durack, 1980 Chronic cryptococcal meningitis. a new experimental model in rabbits. *American Journal of Pathology* **101**: 177–193.
- Podisi, B. K., S. A. Knott, D. W. Burt, and P. M. Hocking, 2013 Comparative analysis of quantitative trait loci for body weight, growth rate and growth curve parameters from 3 to 72 weeks of age in female chickens of a broiler-layer cross. *BMC Genetics* **14**: 1–11.
- Posteraro, B., M. Sanguinetti, D. Sanglard, M. L. Sorda, S. Boccia, *et al.*, 2003 Identification and characterization of a *Cryptococcus neoformans* atp binding cassette (*abc*) transporter-encoding gene, *cnafr1*, involved in the resistance to fluconazole. *Molecular Microbiology* **47**: 357–371.
- Puértolas-Balint, F., J. W. Rossen, C. O. dos Santos, M. M. Chlebowicz, E. C. Raangs, *et al.*, 2019 Revealing the virulence potential of clinical and environmental *Aspergillus fumigatus* isolates using whole-genome sequencing. *Frontiers in Microbiology* **10**.
- Rajasingham, R., R. M. Smith, B. J. Park, J. N. Jarvis, N. P. Govender, *et al.*, 2017 Global burden of disease of hiv-associated cryptococcal meningitis: an updated analysis. *The Lancet Infectious Diseases* **17**: 873–881.
- Rathore, S. S., T. Raman, and J. Ramakrishnan, 2016 Magnesium ion acts as a signal for capsule induction in *Cryptococcus neoformans*. *Frontiers in Microbiology* **7**: 1–16.

- Rayamajhee, B., M. D. Willcox, F. L. Henriquez, C. Petsoglou, D. Subedi, *et al.*, 2022 Acanthamoeba, an environmental phagocyte enhancing survival and transmission of human pathogens. *Trends in Parasitology* **38**: 975–990.
- Remold, S., 2012 Understanding specialism when the jack of all trades can be the master of all pp. 4861–4869.
- Riat, A., J. Plojoux, K. Gindro, and J. Schrenzel, 2018 Azole resistance of environmental and clinical aspergillus. *Antimicrobial Agents and Chemotherapy* pp. 1–7.
- Riles, L. and J. C. Fay, 2019 Genetic basis of variation in heat and ethanol tolerance in *saccharomyces cerevisiae*. *G3: Genes, Genomes, Genetics* **9**: 179–188.
- Rizzo, J., P. C. Albuquerque, J. M. Wolf, R. Nascimento, M. D. Pereira, *et al.*, 2017 Analysis of multiple components involved in the interaction between *Cryptococcus neoformans* and *Acanthamoeba castellanii*. *Fungal Biology* **121**: 602–614.
- Robert, V., G. Cardinali, and A. Casadevall, 2015 Distribution and impact of yeast thermal tolerance permissive for mammalian infection. *BMC Biology* **13**: 1–14.
- Robert, V. A. and A. Casadevall, 2009 Vertebrate endothermy restricts most fungi as potential pathogens. *Journal of Infectious Diseases* **200**: 1623–1626.
- Rossi, S. A., N. Trevijano-Contador, L. Scorzoni, A. C. Mesa-Arango, H. C. D. Oliveira, *et al.*, 2016 Impact of resistance to fluconazole on virulence and morphological aspects of *Cryptococcus neoformans* and *Cryptococcus gattii* isolates. *Frontiers in Microbiology* **7**: 1–14.
- Roth, C., D. Murray, A. Scott, C. Fu, A. F. Averette, *et al.*, 2021 *Pleiotropy and epistasis within and between signaling pathways defines the genetic architecture of fungal virulence*, volume 17.
- Roth, C., S. Sun, R. B. Billmyre, J. Heitman, and P. M. Magwene, 2018 A high-resolution map of meiotic recombination in *Cryptococcus deneoformans* demonstrates decreased recombination in unisexual reproduction. *Genetics* **209**: 567–578.
- Ruiz, A., J. B. Neilson, and G. S. Bulmer, 1982 Control of *Cryptococcus neoformans* in nature by biotic factors. *Sabouraudia* pp. 21–29.
- Saputo, S., Y. Chabrier-Rosello, F. C. Luca, A. Kumar, and D. J. Krysan, 2012 The ram network in pathogenic fungi. *Eukaryotic Cell* **11**: 708–717.
- Savinov, A., B. M. Brandsen, B. E. Angell, J. T. Cuperus, and S. Fields, 2021 Effects of sequence motifs in the yeast 3' untranslated region determined from massively parallel assays of random sequences. *Genome Biology* **22**: 1–27.

- Seemann, T., 2015 Snippy: fast bacterial variant calling from ngs reads.
- Shivarathri, R., M. C. R. M. Ashutosh Singh Sabrina Jenull, Anton Stoiber, K. K. F. Nogueira, A. Chowdhary, and N. Chauhan, 2020 The two-component response regulator *ssk1* and the mitogen-activated protein kinase *hog1* control antifungal drug resistance and cell wall architecture of *candida auris*. *mSphere* **5**.
- Sia, R. A., K. B. Lengeler, and J. Heitman, 2000 Diploid strains of the pathogenic basidiomycete *Cryptococcus neoformans* are thermally dimorphic. *Fungal Genetics and Biology* **29**: 153–163.
- Siddiqui, N. A. K. R., 2012 Biology and pathogenesis of *acanthamoeba*. *Parasites Vectors* **5**: 269–294.
- Siddiqui, R., S. Lakhundi, and N. A. Khan, 2015 Interactions of *pseudomonas aeruginosa* and *corynebacterium* spp. with non-phagocytic brain microvascular endothelial cells and phagocytic *extitAcanthamoeba castellanii*. *Parasitology Research* **114**: 2349–2356.
- Simoneau, A. P. and I. vasilescu Æ Nelly Bataille, 2005 Characterization of mutations in the two-component histidine kinase gene *abn1k1* from *alternaria brassicicola* that confer high dicarboximide and phenylpyrrole resistance pp. 234–243.
- Sionov, E., Y. C. Chang, H. M. Garraffo, and K. J. Kwon-Chung, 2009 Heteroresistance to fluconazole in *Cryptococcus neoformans* is intrinsic and associated with virulence. *Antimicrobial Agents and Chemotherapy* **53**: 2804–2815.
- Sionov, E., Y. C. Chang, and K. J. Kwon-Chung, 2013 Azole heteroresistance in *Cryptococcus neoformans*: Emergence of resistant clones with chromosomal disomy in the mouse brain during fluconazole treatment. *Antimicrobial Agents and Chemotherapy* **57**: 5127–5130.
- Smith, M. D., Y. Gu, J. Querol-Audí, J. M. Vogan, A. Nitido, *et al.*, 2013 Human-like eukaryotic translation initiation factor 3 from *neurospora crassa*. *PLoS ONE* **8**.
- Soumana, I. H., B. Linz, and E. T. Harvill, 2017 Environmental origin of the genus *bordetella*. *Frontiers in Microbiology* **8**: 1–10.
- Spennemann, D. H., M. Pike, and M. J. Watson, 2017 Effects of acid pigeon excreta on building conservation. *International Journal of Building Pathology and Adaptation* **35**: 2–15.
- Sriswasdi, S., C. C. Yang, and W. Iwasaki, 2017 Generalist species drive microbial dispersion and evolution. *Nature Communications* **8**.

- Stajich, J. E., 2017 Fungal genomes and insights into the evolution of the kingdom. *Microbiol Spectr.* **5**.
- Steenbergen, J. N., J. D. Nosanchuk, S. D. Malliaris, and A. Casadevall, 2003 *Cryptococcus neoformans* virulence is enhanced after growth in the genetically malleable host dictyostelium discoideum. *Infection and Immunity* **71**: 4862–4872.
- Steenbergen, J. N., H. A. Shuman, and A. Casadevall, 2001 *Cryptococcus neoformans* interactions with amoebae suggest an explanation for its virulence and intracellular pathogenic strategy in macrophages. *Proceedings of the National Academy of Sciences* **98**: 15245–15250.
- Stempinski, P. R., J. M. Zielinski, N. H. Dbouk, E. S. Huey, E. C. McCormack, *et al.*, 2021 Genetic contribution to high temperature tolerance in *Cryptococcus neoformans*. *Genetics* **217**.
- Stojiljkovic, M., M. R. Foulquié-Moreno, and J. M. Thevelein, 2020 Polygenic analysis of very high acetic acid tolerance in the yeast *saccharomyces cerevisiae* reveals a complex genetic background and several new causative alleles. *Biotechnology for Biofuels* **13**: 1–27.
- Sun, S., S. J. Priest, and J. Heitman, 2019 *Cryptococcus neoformans* mating and genetic crosses. *Current Protocols in Microbiology* **53**: 1–16.
- Sun, S., C. Roth, A. F. Averette, P. M. Magwene, and J. Heitman, 2022 Epistatic genetic interactions govern morphogenesis during sexual reproduction and infection in a global human fungal pathogen. *Proceedings of the National Academy of Sciences of the United States of America* **119**: 1–12.
- sun Bahn, Y., S. Geunes-boyer, and J. Heitman, 2007 Ssk2 mitogen-activated protein kinase kinase kinase governs divergent patterns of the stress-activated hog1 signaling pathway in *Cryptococcus neoformans* † **6**: 2278–2289.
- Suo, C. H., L. J. Ma, H. L. Li, J. F. Sun, C. Li, *et al.*, 2018 Investigation of *Cryptococcus neoformans* magnesium transporters reveals important role of vacuolar magnesium transporter in regulating fungal virulence factors. *MicrobiologyOpen* **7**: 1–15.
- Takahashi, J. P. F., L. M. Feliciano, D. C. S. Santos, S. Ramos, R. A. Oliveira, *et al.*, 2020 Could fungicides lead to azole drug resistance in a cross-resistance manner among environmental cryptococcus strains? *Current Fungal Infection Reports* **14**: 9–14.
- Taylor-Mulneix, D. L., I. H. Soumana, B. Linz, and E. T. Harvill, 2017 Evolution of bordetellae from environmental microbes to human respiratory pathogens: Amoe-

- bae as a missing link. *Frontiers in Cellular and Infection Microbiology* **7**: 1–7.
- Tejero, M. E., V. S. Voruganti, J. M. Proffitt, J. E. Curran, H. H. Göring, *et al.*, 2008 Cross-species replication of a resistin mrna qtl, but not qtls for circulating levels of resistin, in human and baboon. *Heredity* **101**: 60–66.
- Tso, G. H. W., J. A. Reales-Calderon, A. S. M. Tan, X. H. Sem, G. T. T. Le, *et al.*, 2018 Experimental evolution of a fungal pathogen into a gut symbiont. *Science* **362**: 589–595.
- Tóth, R., V. Cabral, E. Thuer, F. Bohner, T. Németh, *et al.*, 2018 Investigation of candida parapsilosis virulence regulatory factors during host-pathogen interaction. *Scientific Reports* **8**: 1–14.
- Valdes, I. D., J. V. D. Berg, A. Haagsman, N. Escobar, J. F. Meis, *et al.*, 2018 Comparative genotyping and phenotyping of aspergillus fumigatus isolates from humans, dogs and the environment. *BMC Microbiology* **18**: 1–11.
- Virtanen, P., R. Gommers, T. E. Oliphant, M. Haberland, T. Reddy, *et al.*, 2020 Scipy 1.0: fundamental algorithms for scientific computing in python. *Nature Methods* **17**: 261–272.
- Visscher, P. M., R. Thompson, and C. S. Haley, 1996 Confidence intervals in qtl mapping by bootstrapping. *Genetics* **143**: 1013–1020.
- Voelz, K. and R. C. May, 2010 Cryptococcal interactions with the host immune system. *Eukaryotic Cell* **9**: 835–846.
- Waeyenberghe, L. V., J. Baré, F. Pasmans, M. Claeys, W. Bert, *et al.*, 2013 Interaction of *Aspergillus fumigatus* conidia with *Acanthamoeba castellanii* parallels macrophage-fungus interactions. *Environmental Microbiology Reports* **5**: 819–824.
- Wang, L., B. Zhai, and X. Lin, 2012 The link between morphotype transition and virulence in *Cryptococcus neoformans*. *PLoS Pathogens* **8**.
- Wang, Y., P. Aisen, and A. Casadevall, 1995 *Cryptococcus neoformans* melanin and virulence: Mechanism of action. *Infection and Immunity* **63**: 3131–3136.
- Wang, Z., Q. Qi, Y. Lin, Y. Guo, Y. Liu, *et al.*, 2019 Qtl analysis reveals genomic variants linked to high-temperature fermentation performance in the industrial yeast. *Biotechnology for Biofuels* **12**: 1–18.
- Warringer, J., E. Zörgö, F. A. Cubillos, A. Zia, A. Gjuvsland, *et al.*, 2011 Trait variation in yeast is defined by population history. *PLoS Genetics* **7**.

- Watkins, R., J. King, and S. Johnston, 2017 Nutritional requirements and their importance for virulence of pathogenic cryptococcus species. *Microorganisms* **5**: 65.
- Watkins, R. A., A. Andrews, C. Wynn, C. Barisch, J. S. King, *et al.*, 2018 *Cryptococcus neoformans* escape from dictyostelium amoeba by both wash-mediated constitutive exocytosis and vomocytosis. *Frontiers in Cellular and Infection Microbiology* **8**: 1–11.
- Winski, C. J., Y. Qian, S. Mobashery, and F. H. Santiago-Tirado, 2022 An atypical abc transporter is involved in antifungal resistance and host interactions in the pathogenic fungus *Cryptococcus neoformans*. *mBio* **13**: 1–20.
- Winsor, C. P., 1932 The gompertz curve as a growth curve. *Proceedings of the National Academy of Sciences* **18**: 1–8.
- Xu, J., 2004 Genotype-environment interactions of spontaneous mutations for vegetative fitness in the human pathogenic fungus *Cryptococcus neoformans*. *Genetics* **168**: 1177–1188.
- Xu, Q., P. Vandenkoornhuyse, L. Li, J. Guo, C. Zhu, *et al.*, 2022 Microbial generalists and specialists differently contribute to the community diversity in farmland soils. *Journal of Advanced Research* **40**: 17–27.
- Xu, X., 1987 The biological foundation of the gompertz model. *International Journal of Bio-Medical Computing* **20**: 35–39.
- Xu, Z., F. Takizawa, E. Casadei, Y. Shibasaki, Y. Ding, *et al.*, 2020 Specialization of mucosal immunoglobulins in pathogen control and microbiota homeostasis occurred early in vertebrate evolution. *Science Immunology* **5**: 1–18.
- Xue, C., T. Liu, L. Chen, W. Li, I. Liu, *et al.*, 2010 Role of an expanded inositol transporter repertoire in *Cryptococcus neoformans* sexual reproduction and virulence. *mBio* **1**: 1–14.
- Yan, L., R. L. Cerny, and J. D. Cirillo, 2004 Evidence that hsp90 is involved in the altered interactions of *Acanthamoeba castellanii* variants with bacteria. *Eukaryotic Cell* **3**: 567–578.
- Yang, D. H., K. W. Jung, S. Bang, J. W. Lee, M. H. Song, *et al.*, 2017 *Rewiring of signaling networks modulating thermotolerance in the human pathogen Cryptococcus neoformans*, volume 205.
- Yang, M. L., J. Uhrig, K. Vu, A. Singapuri, M. Dennis, *et al.*, 2016 Fluconazole susceptibility in *cryptococcus gattii* is dependent on the abc transporter pdr11. *Antimicrobial Agents and Chemotherapy* **60**: 1202–1207.

- Yoshihara, T., N. D. Miller, F. A. Rabanal, H. Myles, I. Y. Kwak, *et al.*, 2022 Leveraging orthology within maize and *Arabidopsis* qtl to identify genes affecting natural variation in gravitropism. *Proceedings of the National Academy of Sciences of the United States of America* **119**.
- Yu, C. H., Y. Chen, C. A. Desjardins, J. L. Tenor, D. L. Toffaletti, *et al.*, 2020 Landscape of gene expression variation of natural isolates of *Cryptococcus neoformans* in response to biologically relevant stresses. *Microbial Genomics* **6**.
- Zaragoza, O., C. J. Chrisman, M. V. Castelli, S. Frases, M. Cuenca-Estrella, *et al.*, 2008 Capsule enlargement in *Cryptococcus neoformans* confers resistance to oxidative stress suggesting a mechanism for intracellular survival. *Cellular Microbiology* **10**: 2043–2057.
- Zhu, X. and P. R. Williamson, 2004 Role of laccase in the biology and virulence of *Cryptococcus neoformans*. *FEMS Yeast Research* **5**: 1–10.

## Biography

Thomas John C Sauters graduated from the University of New Mexico in 2016 with B.S in Biochemistry with a minor in Psychology. During his tenure there, he earned the New Mexico Lottery Scholarship and was accepted into the Initiative to Maximize Student Development training program run by Dr. Maggie Werner-Washburne. Through this program, he joined the lab of Dr. Irene Salinas in 2014 studying the effects of chronic stress and IgA depletion on the microbiome of *Oncorhynchus mykiss* (Xu *et al.*, 2020). He also worked under Dr. Samuel Miller in the 2015 University of Washington Genome Sciences Summer Scholar program studying genes involved with cell wall rearrangements independent of the PhoP-PhoQ system of Salmonella.

Following graduation, Thomas, began his doctoral studies at Duke University in the Program in Genetics and Genomics. During his time at Duke University, he presented his research at the Evolution meeting, the Fungal Genetics Conference, and the South-Eastern Regional Yeast Meeting (SERYM). He was awarded the TriCEM graduate RFP in 2019 to fund his work (detailed in chapter four) experimentally evolving *Cryptococcus*.